Pro-oxidative and Pro-inflammatory Mechanisms of Brain Injury in Experimental Animal and 3D Cell Culture Model Systems

Hyung Joon Cho

Dissertation submitted to the Faculty of the
Virginia Polytechnic Institute and State University
in partial fulfillment of the requirement for the degree of

Doctor of Philosophy
In
Biomedical Engineering

Yong Woo Lee, Chair
Pamela J. VandeVord
Scott S. Verbridge
John L. Robertson
Rafael V. Davalos

April 24, 2015
Blacksburg, VA

Keywords: Oxidative Stress, Inflammation, Blast-induced Brain Injury, Radiation-induced Brain Injury, *In Vitro* three-dimensional (3D) Model System

Pro-oxidative and Pro-inflammatory Mechanisms of Brain Injury in Experimental Animal and 3D Cell Culture Model Systems

Hyung Joon Cho

ABSTRACT

The pro-oxidative and pro-inflammatory mechanisms have been implicated in various human diseases including neurological and psychiatric disorders. However, there is only limited information available on the etiology in the progression of neurological damage to brain. The emergence of tissue engineering with the growing interest in mechanistic studies of brain injury now raises great opportunities to study complex physiological and pathophysiological process *in vitro*. Therefore, the prime goals of this study include: (1) Determination of the molecular and cellular mechanisms responsible for blast- and radiation-induced brain injuries and (2) Development of a three-dimensional (3D) model system in order to mimic *in vivo*-like microenvironments to further broaden our knowledge in pro-oxidative and pro-inflammatory mechanisms and their cellular responses within 3D constructs.

In the first study, we demonstrated that blast exposure induced specific molecular and cellular alterations in pro-oxidative and pro-inflammatory environments in the brain and neuronal loss with adverse behavioral outcome. The results provide evidence that pro-oxidative and pro-inflammatory environments in the brain could play a potential role in blast-induced neuronal loss and behavioral deficits.

In the second study, we investigated that fractionated whole-brain irradiation induced specific molecular and cellular alterations in pro-oxidative and pro-inflammatory environments in the brain along with elevation of reactive oxygen species (ROS)-generating protein (NOX-2) and microglial activation. Additionally, the contribution of NOX-2 in fractionated whole-brain radiation-induced oxidative stress was observed by dramatic amelioration of ROS generation after pharmacological inhibition of NOX-2. These results support that NOX-2 may play a pivotal role in fractionated whole-brain radiation-induced pro-oxidative and pro-inflammatory pathways in mouse brain.

In the third study, we developed an *in vitro* 3D experimental model of brain inflammation by encapsulating microglia in collagen hydrogel with computational analysis of 3D constructs. The results indicated that our newly developed *in vitro* 3D model system provides a more physiologically relevant environment to mimic *in vivo* responses.

In conclusion, these data may be beneficial in defining a cellular and molecular basis of pathophysiological mechanisms of brain injuries. Furthermore, it may provide new opportunities for preventive and therapeutic interventions for patients with brain injuries and associated neurological disorders.

ACKNOWLEDGMENTS

Standing at the end of this road and looking back of the journey, I clearly see the importance of having incalculable support and advice from numerous individuals around me. First and foremost, I would like to deeply express my sincere gratitude and respect to my advisor, Dr. Yong Woo Lee. Along with his professional guidance, charismatic mentorship, ceaseless support, and patience throughout my graduate studies, his dedication to accomplish excellence and his belief to be a constructive part of the whole have been instrumental to achieve my goals. I have been very fortunate to have Dr. Lee as my advisor. Thank you for everything you provided during my entire Ph.D. period.

I would like to acknowledge my committee members, Dr. Pamela J. VandeVord, Dr. Scott S. Verbridge, Dr. John L. Robertson, and Dr. Rafael V. Davalos, for providing their valuable suggestions and individual efforts in helping me through this process. It has been a true pleasure to work with these terrific mentors. Dr. Aaron S. Goldstein also provided significant guidance and support during the development of this dissertation. A special thanks goes to the help from our collaborator, Dr. William E. Sonntag, at University of Oklahoma Health Sciences Center.

I must also thank all my fellow lab members, Won Hee Lee, Anjali Hirani, Paul Kim, Katelyn Bittleman, Jamelle Simmons, and Min Ha Hwang for their constant support, encouragement, and kind friendship throughout my graduate career. They have truly made my time an enjoyable and memorable one in the lab.

Our graduate and department administrative staff, Tess Sentelle, Pam Stiff, Monika Lawless, and Kathy Creggar, will always have my thanks and good wishes for being helpful and cheerful along the way.

Most importantly, I am profoundly grateful to my parents, who have been a constant source of love, support, and encouragement at all times for longer than I can remember. I would like to especially thank my father, Dr. Seung Hwan Cho, for his unwavering belief in my ability over the years. Lastly, I have never been without a cheerleader throughout my life, thanks to my mother.

DECLARATION OF WORK PERFORMED

I declare that with the exception of the items indicated below, all work reported in this dissertation was performed by myself.

All *in vivo* blast exposure were tested by a custom-built blast simulator at the Center for Injury Biomechanics (CIB) at Virginia Tech. Dr. Pamela J. VandeVord supervised all blast exposure procedures. Blast exposure procedures and animal behavioral assessments of rats were performed by Dr. Sujith Sajja at CIB.

All *in vivo* irradiation procedures and collection of tissue samples were conducted at University of Oklahoma Health Sciences Center (OUHSC), Oklahoma City, OK. All animal protocols were approved by the Institutional Animal Care and Use Committees of OUHSC. Dr. William E. Sonntag supervised all irradiation procedures. Irradiation procedures, blood perfusion, and brain tissue collection from mice were performed by Dr. Junie P. Warrington, Dr. Han Yan, and Matthew Mitschelen at OUHSC.

Cell culture bioenergetic study was conducted at Virginia Tech Metabolic Phenotyping Core, Blacksburg, VA. Oxygen consumption rate of microglia (BV-2) was analyzed by Dr. Nabil Boutagy from Skeletal Muscle Metabolism Laboratory at Virginia Tech.

TABLE OF CONTENTS

LIST OF FIGURES AND TABLES

LIST OF ABBREVIATIONS

2D	:	Two-dimensional
3D	:	Three-dimensional
AD	:	Alzheimer's disease
AIF	:	Apoptosis inducing factor
ALS	:	Amyotrophic lateral sclerosis
Ang	:	Angiopoietin
ANOVA	:	Analysis of variance
AP-1	:	Activator protein-1
APO	:	Apocynin
BED	:	Biologically effective dose
BINT	:	Blast-induced neurotrauma
BOP	:	Blast overpressure
BSA	:	Bovine serum albumin
CBTRUS	:	Central brain tumor registry of the United States
CD68	:	Cluster of differentiation 68
CNS	:	Central nervous system
COX	:	Cyclooxygenase
CREB	:	cAMP-responsive element-binding protein
C_T	:	Threshold cycle
DCF	:	2',7'-dichlorofluorescein
DCX	:	Doublecortin
DHE	:	Dihydroethidium
DMEM	:	Dulbecco's modified eagle medium
DPI	:	Diphenyleneiodonium
ECM	:	Extracellular matrix
ELISA	:	Enzyme-linked immunosorbent assay
EMMPRIN	:	Extracellular matrix metalloproteinase inducer
FBS	:	Fetal bovine serum
FIR	:	Fractionated whole-brain irradiation
GAPDH	:	Glyceraldehyde-3-phosphate dehydrogenase
GFAP	:	Glial fibrillary acidic protein
GKS:	:	Gamma knife surgery
Gy	:	Gray
HA	:	Hyaluronic acid
HD	:	Huntington's disease
Iba1	:	Ionized calcium binding adaptor molecule 1
ICAM-1	:	Intercellular adhesion molecule-1

IFN-γ	:	Interferon-γ
IL-1β	:	Interleukin-1β
IL-6	:	Interleukin-6
iNOS	:	Inducible nitric oxide synthase
LPS	:	Lipopolysaccharide
MCP-1	:	Monocyte chemoattractant protein-1
MDA	:	Malondialdehyde
MIP	:	Monocyte inflammatory protein
MMP	:	Matrix metalloproteinase
MS	:	Multiple sclerosis
NeuN	:	Neuron-specific nuclear protein
NF-ϰB	:	Nuclear factor-ϰB
NG2	:	Chondroitin sulfate proteoglycan
NOR	:	Novel object recognition
NOX	:	NADPH oxidase
OEF	:	Operation Enduring Freedom
OIF	:	Operation Iraqi Freedom
p53	:	Tumor suppressor protein 53
PAI	:	Plasminogen activator inhibitor
PARP	:	Poly (ADP-ribose) polymerase
PBS	:	Phosphate buffered saline
PD	:	Parkinson's disease
PDMS	:	Polydimethylsiloxane
PTSD	:	Post-traumatic stress disorder
ROS	:	Reactive oxygen species
RT-PCR	:	Reverse transcriptase-polymerase chain reaction
SOD	:	Superoxide dismutase
STAT	:	Signal transducers and activators of transcription
TBI	:	Traumatic brain injury
Tie	:	Endothelial receptor tyrosine kinase
TIMP	:	Tissue inhibitor of metalloproteinases
TNF-α	:	Tumor necrosis factor-α
Tuj1	:	Neuron-specific class III β-tubulin
VCAM-1	:	Vascular cell adhesion molecule-1
VEGF	:	Vascular endothelial growth factor
γ-HA2X	:	Phosphorylated histone H2A

CHAPTER 1:

INTRODUCTION

1.1. **Significance and Hypothesis**

The pro-oxidative and pro-inflammatory environments in the brain have been implicated in the onset and progression of neurological and psychiatric disorders [1-8]. However, very limited information on the etiology of the progression of neurological damage to brain tissue is currently available. Additionally, the specific mechanisms by which mechanical or biochemical cues cause various brain injuries and diseases have not yet been fully understood. Therefore, a deeper understanding of pathophysiological mechanisms underlying these phenomena at the cellular and molecular levels could enable the development of more effective therapies to contribute to long-term disease suppression or even a cure.

Given the growing interest in mechanistic studies of brain injury and development of therapeutic approaches against chronic brain diseases, tissue engineering strategies employing biomaterials have made great improvement and progress during the last few decades and have widely applied to pre-clinical and clinical fields [9-12]. In particular, tissue-engineered three-dimensional (3D) constructs have shown several benefits over conventional two-dimensional (2D) *in vitro* experimental model systems, delivering an invaluable knowledge on subtle cellular responses under a controlled mechanical and biochemical microenvironment [11, 13, 14]. However, development of *in vitro* 3D model systems to mimic *in vivo* brain microenvironments remains to be further investigated.

Therefore, **we proposed to examine our hypothesis that pro-oxidative and pro-inflammatory pathways contribute to blast- and radiation-induced brain injuries. In addition, the present study aimed to develop a 3D cell culture system to create a brain inflammation model *in vitro*.** To fully address our hypothesis**,** we pursued the following three specific aims:

1. **To examine molecular and cellular mechanisms of pro-oxidative and pro-inflammatory environments in blast-induced brain injury *in vivo*.** We examined (i) effect of blast overpressure (BOP) on generation of oxidative stress in the brain, (ii) effect of BOP on induction of inflammation in the brain, (iii) effect of BOP on neuronal loss, (iv) effect of BOP on microglial activation, and (v) effect of BOP on behavioral changes.
2. **To examine molecular and cellular mechanisms of pro-oxidative and pro-inflammatory environments in radiation-induced brain injury *in vivo*.** We examined (i) effect of fractionated whole-brain irradiation on induction of inflammation in the brain, (ii) effect of

fractionated whole-brain irradiation on microglial activation, (iii) effect of fractionated whole-brain irradiation on generation of oxidative stress in the brain, and (iv) potential role of NADPH oxidase (NOX) on pro-oxidative and pro-inflammatory pathways in radiation-induced brain injury.

3. **To develop an *in vitro* 3D model system to mimic pro-oxidative and pro-inflammatory environments *in vivo*.** We (i) designed and constructed an *in vitro* 3D model system using collagen-based hydrogel, (ii) compared molecular interactions of three different culture systems (*in vitro* 2D/3D and *in vivo* model systems) under pro-oxidative and pro-inflammatory environments, and (iii) compared cellular responses of three different culture systems under pro-oxidative and pro-inflammatory environments.

1.2. Specific Aims and Justification

*1.2.1. **Specific Aim 1**: To examine molecular and cellular mechanisms of pro-oxidative and pro-inflammatory environments in blast-induced brain injury in vivo*

Pro-oxidative and pro-inflammatory environments in the brain have been implicated in the onset and progression of neurological disorders. However, molecular and cellular mechanisms of brain injury after exposure to BOP have not yet been fully understood. The present study hypothesizes that pro-oxidative and pro-inflammatory pathways in the brain may be responsible for neuronal loss and behavioral deficits following BOP exposure.

*1.2.2. **Specific Aim 2**: To examine molecular and cellular mechanisms of pro-oxidative and pro-inflammatory environments in radiation-induced brain injury in vivo*

The use of radiation therapy is limited by the risk of significant clinical side effects including progressive cognitive impairments in brain tumor patients. However, the cellular and molecular mechanisms by which irradiation induces damage to brain tissues remain largely unknown. The present study was designed to investigate our hypothesis that NADPH oxidase plays a crucial role in fractionated whole-brain irradiation-induced pro-oxidative and pro-inflammatory environments in the brain.

1.2.3. ***Specific Aim 3****: To develop an in vitro 3D model system to mimic pro-oxidative and pro-inflammatory environments in vivo*

The central nervous system (CNS) is a highly complex 3D environment that is regulated by dynamic interactions among a variety of different cell types including neurons, glial cells, and vascular endothelial cells. Therefore, it is often difficult to investigate specific molecular and cellular mechanisms *in vivo* due to the complexity of CNS microenvironment and numerous challenges involved in controlling variables and monitoring cellular level responses. Hydrogels have been widely employed as potential biomimetic scaffolds because of their 3D properties mimicking hydrated microenvironment of native extracellular matrix (ECM). In this study, we designed and constructed an *in vitro* 3D hydrogel model system to mimic more physiologically relevant environments in order to investigate specific cellular responses and molecular interactions of brain cells such as microglia.

CHAPTER 2:

BACKGROUND

2.1. Reactive Oxygen Species and Oxidative Stress

Reactive oxygen species (ROS), including superoxide anion ($O_2^{\cdot -}$), hydrogen peroxide (H_2O_2), peroxide ($O_2^{\cdot 2-}$), hydroxyl radical ($\cdot OH$), and hydroxyl ion (OH^-), are critical molecules that play a key role as messengers in normal cell signal transduction and cell cycling. These reactive molecules are generated through multiple mechanisms mainly in the mitochondria, peroxisomes, endoplasmic reticulum, and cell membranes [15-18]. The major endogenous source of ROS production is the mitochondrial electron transport chain by oxidative metabolism. Electrons are passed through the chain via oxidation-reduction reactions to the final destination of oxygen molecule for creating energy to fuel biological functions. However, electron leakage from mitochondrial electron transfer chain to molecular oxygen generates a steady flux of incomplete superoxide radical molecules, which in turn constitute the major site of cellular ROS production [19, 20]. Other oxygen metabolic enzymes including NADPH oxidase (NOX), lipoxygenase, cyclooxygenase, and xanthine oxidase also involve in ROS generation during catalytic metabolism [16].

In general, ROS generation is regarded as an essential and physiological process for maintaining normal function of mitochondria-rich organs including heart, brain, and liver. Particularly, a downstream of ROS modulates neuronal excitability, synaptic function, and neuronal network activity in the brain [16, 21-24]. A moderate increase of ROS may promote cell proliferation and differentiation, whereas excessive or accumulation of ROS may cause severe damage to lipids, proteins, and DNA as toxic by-products of metabolism. In addition, the cellular redox homeostasis is maintained by a delicate balance between ROS production and antioxidant system in order to protect against a potential damage from ROS. Therefore, severe disturbance in the balance through greatly overwhelmed pro-oxidant over antioxidant defense system may result in oxidative stress, leading to cellular damage [8, 16, 20].

According to the previous studies, oxidative stress has been implicated in the progression of various neurodegenerative diseases including Alzheimer's disease (AD), Parkinson's disease (PD), Huntington's disease (HD), amyotrophic lateral sclerosis (ALS), and multiple sclerosis (MS) [25-33]. Indeed, oxidative stress can induce expression of pro-inflammatory mediators, such as cytokines, chemokines, and adhesion molecules, via redox-responsive transcription factor(s)-mediated molecular signaling pathways. It is well known that expression of pro-

inflammatory genes is up-regulated by increased oxidative stress through activation of a variety of transcription factors, such as activator protein-1 (AP-1), nuclear factor-κB (NF-κB), cAMP-responsive element-binding protein (CREB), specificity protein-1 (SP-1), and signal transducers and activators of transcription (STAT) [34-46]. Thus, excessive ROS production interferes with cell signaling and regulation of important physiological conditions. Furthermore, pathophysiological conditions of oxidative stress via excessive ROS generation may cause cell death and degeneration by up-regulation of pro-inflammatory mediators leading to severe or prolonged inflammation [47-49].

2.2. Inflammation

Inflammation is an immediate response to damaged tissues and cells aiming elimination or neutralization of injurious stimuli to combat pathogenic intruders as a self-defense mechanism, and restoration of tissue integrity. However, inflammatory response has been characterized as a double-edged sword, resulting in favorable repairing process but leading to various disease conditions or aggravating an existing disease process.

In general, pro-inflammatory environment in response to injury is beneficial in neutralizing potential threats to the central nervous system (CNS) by diminishing cellular damage [2, 3, 5, 6]. Upon microenvironmental alterations by injuries, the presence of activated glial cells, such as microglia and astrocytes, contributes to the existence of a self-propagating toxic cycle and provides a rationale to prevent or delay neurodegeneration. However, despite the fact that the inflammatory response is critical in promoting and supporting tissue repair or regeneration at the site of injury and disease in the CNS, this may also compromise healthy tissues and exacerbate inflammation. Recent evidence suggested that a pro-inflammatory environment, in conjunction with the aforementioned oxidative stress, has been implicated in the pathophysiological process of brain injury and subsequent progression of neurological and psychiatric disorders [1-8, 50-53]. For example, interferon-γ (IFN-γ), interleukin-1β (IL-1β), and CD40 triggered by β-amyloid peptides contribute to pathogenesis in AD through an inflammatory cascade in the brain [54, 55]. In addition, inflammation in the brain has been actively involved in the neurodegenerative process of PD [56, 57] and other progressive neurodegenerative diseases including HD, ALS, and MS [58-64]. Furthermore, there is emerging

evidence that a sustained neuroinflammatory response can be detrimental due to neuronal damage, neuronal circuit impairments, and neurodegeneration [49, 65-67]. These findings provide robust evidence that an inflammatory process in the brain plays a significant role in the pathogenesis of CNS diseases.

2.3. Blast-induced Brain Injury

Over 80,000 cases of veterans returning from Operation Iraqi Freedom (OIF) and Operation Enduring Freedom (OEF) were diagnosed with mild or severe traumatic brain injury (TBI), suffering from closed head injuries due to blast overpressure (BOP) exposure [68, 69]. Additionally, the prevalence of civilians exposed to explosions has been increasing [70]. Previous studies often reported that BOP exposure may trigger various neurological problems associated with more than one symptom of traumatic injuries [71-76]. Furthermore, clinical reports stated that several psychiatric outcomes, including anxiety, attention deficit, memory issues and impaired problem solving skills, have been linked to individuals who have been exposed to BOP [69, 77-79]. Particularly, these clinical outcomes have indicated that BOP exposure is involved in dysfunction of various brain regions, most likely resulting from direct damage to the cognitive regions or indirectly through the circuits that connect them. Overlapping symptoms with other forms of trauma, such as impact-related TBI and post-traumatic stress disorder (PTSD), have confounding effects on differential diagnosis [77, 80-82].

The simplest form of blast wave generated from laboratory scale shock tubes has been described by the following equation of a Friedlander waveform, resembling free field shock wave profiles with no surfaces nearby with which it can interact: $P(t) = P_s e^{-t/t^*}\left(1 - t/t^*\right)$ where P_s is the peak overpressure and t^* is the duration of positive (overpressure) phase. According to the previous data from Department of Defense [83], the range of 5~15 psi (34.5~103.4 kPa) blast may damage eardrums and over 55 psi (379.2 kPa) may cause 99% fatalities.

A blast wave from explosion releases a massive amount of energy by converting chemical energy into other forms of energy, such as electromagnetic, thermal, kinetic, and acoustic energy, and induce a complex mix of blast injuries (primary, secondary, tertiary, and quaternary; Table. 2.1). Several theories have been hypothesized to explain these blast injuries

[73]. One theory postulates that the blast from a positive pressure wave can propagate through the body via major vessels, cerebrospinal fluid, and soft tissues. Therefore, air emboli created by the force of blast wave may circulate to the cerebral vasculature, become lodged within smaller microvessels, and result in microvascular occlusion and stroke. Additionally, the shock wave may enter orifices of the skull propagating through other tissues to reach the brain. Skull flexure, bulk acceleration of the head, and electromagnetic pulse from blast wave are also considered as possible causes of blast injury. However, limited studies are currently available to validate these mechanisms of blast injury due to experimental difficulties.

Animal models of blast injuries have been established to investigate injury mechanisms in blast-induced neurotrauma (BINT) and its subsequent neurological impairments. Several pre-clinical studies have suggested different mechanisms of brain damage associated with morbidity related to BINT [84-89]. Diverse approaches have been applied to reveal astrocyte activation, neurodegeneration and neurochemical changes following BOP exposure in core regions of brain [77, 86, 90-99]. Despite extensive studies investigating injury in various core regions of the brain, a detailed mechanism and prognosis of injury is poorly understood.

Few experimental studies have attempted to demonstrate the potential role of pro-oxidative and pro-inflammatory mechanisms in BINT. For example, pro-inflammatory cytokines, such as tumor necrosis factor-α (TNF-α), interleukin-6 (IL-6) and IFN-γ, have been observed following BOP exposure in core regions of the brain [93, 100-102]. In addition, ROS generation in the cortical region of the brain following BOP exposure was detected using electron paramagnetic resonance and nitroblue tetrazolium staining [103, 104]. **However, the role of pro-oxidative and pro-inflammatory pathways in BINT remains largely unknown and was investigated in the Specific Aim 1 of the proposed studies**.

Table 2.1. Classification of Blast Injury

Classification	Mechanisms of Blast Injury
Primary	Barotrauma (Injuries from exposure to overpressure shock wave propagation through organs/tissues)
Secondary	Penetrating Injury (Injuries from penetration by projectiles)
Tertiary	Crush/Blunt Injury (Injuries from acceleration and deceleration of the body and its impact with other objects)
Quaternary	Thermal/Respiratory Injury (Injuries from thermal burns and inhalation of toxic gases)

2.4. Radiation-induced Brain Injury

Brain tumors are one of the most aggressive and detrimental forms of cancer. Approximately 68,470 new cases of primary non-malignant brain, malignant brain and CNS tumors are expected to be diagnosed every year in the United States [105]. Treatment options for brain tumors are selected based on a number of different factors including tumor type, location and size of tumor, tumor grade, and age and general health of the patient. Radiation therapy has been commonly used as the standard treatment for brain tumors in addition to surgery and chemotherapy. However, the use of radiation therapy for treatment of brain tumors is limited by the risk of radiation-induced damage to the normal, healthy brain tissue that can subsequently lead to devastating functional deficits [106-108].

Radiation therapy uses controlled high-energy electromagnetic radiation, such as X-ray and γ-ray, to damage the DNA of cancerous tissue leading to cellular death and preventing cell proliferation. Radiation deposits energy as it traverses various types of biologic materials or media (e.g., soft tissue and bone) within the human body, by either directly striking the DNA molecule or ionizing water molecules to produce highly reactive free radicals and indirectly impair DNA molecules. According to the tumor type and normal tissue limitations, the appropriate total dose of radiation is typically delivered in fractionated protocols over a span of several weeks. The quantity associated with radiation measurement in radiation therapy is the absorbed dose and defined as $\Delta E_{ab} / \Delta m$, where ΔE_{ab} is the absorbed energy and Δm is the mass of medium. In general, the dose is measured in grays (Gy; 1 Gy = 1 J/kg) although an older unit, the rad, is still used; 1 rad = 0.01 J/kg = 100 erg/g. In addition, biologically effective dose (BED)[109], specified by the linear quadratic model of radiation effect by the following equation, is commonly used for isoeffective dose fractionation calculations; $BED = nd\left[1 + d/(\alpha/\beta)\right]$ where n: the number of fractions, d: the dose per fraction (Gy), and α and β: the model parameters that govern the linear and quadratic elements of the dose response. This parameter is regarded as a clinically useful tool to compare the biological effects of different fractionation schedules and different types of radiotherapy. Currently, a typical radiation therapy regimen in clinical use consists of daily fractions of 1.5 to 3 Gy given over several weeks [110].

Based on the time of clinical expression, radiation-induced brain injury is classified as acute, early delayed (subacute), or late delayed injury [111-113]. Although acute and early

delayed injuries may result in severe reactions, most of the symptoms are generally reversible and resolve spontaneously. On the contrary, late delayed injury, characterized by demyelination, vascular abnormalities, and ultimate white matter necrosis, is considered to be irreversible and progressive. In addition, there is a growing awareness that patients with late delayed injury may develop significant cognitive impairment, focal deficits, seizures, and increased cranial pressure even in cases with no detectable anatomic abnormalities, profoundly affecting quality of life.

Previously, various experimental attempts have been conducted to demonstrate that whole brain radiation may cause significant deterioration in learning and memory [114-131]. In addition, other brain injures, such as growth hormone deficiency and motor dysfunction, have been reported as consequences of whole brain radiation (Table 2.2) [120, 122, 127, 129]. Despite significant progress in understanding pathogenesis of radiation-mediated brain injury (Table 2.3), a detailed knowledge about the etiology of radiation-mediated damage to normal brain tissue is not yet clear.

Pro-oxidative and pro-inflammatory environments have been implicated in the pathophysiological process of radiation-induced brain injury [46, 107, 132-139]. A significant induction of pro-inflammatory mediators, including TNF-α, IL-1β, IL-6, inducible nitric oxide synthase (iNOS), intercellular adhesion molecule-1 (ICAM-1), and matrix metalloproteinase-9 (MMP-9), in response to radiation has been implicated in radiotherapy-associated brain damage [132, 135-137]. Additionally, irradiation enhanced expression of adhesion molecules, such as ICAM-1, vascular cell adhesion molecule-1 (VCAM-1) and E-selectin [46, 132, 133, 136, 138]. Furthermore, it has been suggested the potential contribution of microglia to the overexpression of pro-inflammatory mediators in irradiated brains, indicating that oxidative stress-mediated inflammation is one of the major consequences of whole brain radiation and plays a pivotal role in subsequent radiation-induced brain injury [46, 140].

These studies suggest the role of pro-oxidative and pro-inflammatory environments in life-threatening neurological complications in brain tumor patients after radiation therapy. **However, very limited information on the etiology of radiation-induced damage to normal brain tissue is currently available. The specific mechanism by which radiation causes normal brain injury has not yet been fully understood. Thus, molecular mechanisms responsible for radiation-induced brain injury were investigated in the Specific Aim 2 of the proposed studies.**

Table 2.2. Types of Radiation-induced Brain Injury

Type of injury	Test	Doses (Total / fractions)	Species	References
Cognitive impairment	• Morris water maze test	25 Gy/single	R	[119]
		10, 20, and 40 Gy/single	R	[126]
		20 Gy/4 and 40 Gy/8	R	[128]
	• Auditory verbal learning test, Medical College of Georgia Complex figures, Test for attentional performance, Multiple-choice test of vocabulary knowledge	40 Gy/20 and 36 Gy/18	H	[123]
	• Letter-digit substitution test, Concept-shifting test, Stroop color-word test, Visual verbal learning test, Memory comparison test, Categoric word fluency	56.6 ± 7.0 Gy/30.6 ± 3.9	H	[125]
	• Behavior tests (IntelliCage)	6 Gy/single	M	[131]
	• Barnes maze test	36 Gy/8	M	[130]
Growth hormone deficiency	• Insulin tolerance test, Growth hormone-releasing hormone-arginine stimulation test	53.5 ± 10.0 Gy (Biological effective dose)	H	[120]
	• Growth hormone-releasing hormone-arginine stimulation test	59.4 Gy (50.1~60)/29.7	H	[127]
		55.1 ± 5.0 Gy/29.1 ± 1.5	H	[129]
Motor dysfunction	• Spontaneous motor activity test	6 Gy/single	M	[122]

Gy: Gray, M: Mouse, R: Rat, H: Human. *Excerpt from Lee YW, **Cho HJ**, Lee WH, Sonntag WE. *Biomol. Ther. (Seoul)* 2012, 20**:**357-370, with permission from The Korean Society of Applied Pharmacology.

Table 2.3. Pathophysiological Mechanisms of Whole Brain Radiation-induced Cognitive Impairment

Mechanisms of action	Biomarker	Doses (Total / fractions)	Species	References
Oxidative stress	• MDA	10 Gy (single)	M	[141]
	• ROS, NF-ϰB, PAI-1, NOX4	1-10 Gy (single)	R	[142]
Inflammation	• COX-2, TNF-α, IL-1β, IL-6, iNOS, ICAM-1, MIP-2, MCP-1	5-35 Gy (single)	M	[135]
	• TNF-α, IL-1β, MCP-1	10 Gy (single)	R	[46]
	• c-Jun, TNF-α, IL-1β, IL-6, COX-2	10 Gy (single)	M	[143]
Extracellular matrix	• MMPs, TIMPs, Collagen type IV	10 Gy (single) and 40 Gy/8	R, M	[144]
	• EMMPRIN	GKS (Max. 75 Gy)	R	[145]
Physiological angiogenesis	• VEGF, Ang-1, Ang-2, Tie-2	10 Gy (single)	R	[146]
	• VEGF	GKS (Max. 75 Gy)	R	[145]
Stem/progenitor cell death	• Caspase 3, p53, Nitrotyrosine, AIF	8 Gy (single)	R	[147]
	• PARP, Annexin V, γ-HA2X	1,2, and 5 Gy (single)	H	[148]
Impaired neurogenesis	• NeuN, Tuj1, GFAP, NG2	10 Gy (single)	R	[149]
	• Ki-67, DCX, NeuN, GFAP, NG2, CD68	2-10 Gy (single)	M	[150]

MDA: Malondialdehyde, ROS: Reactive oxygen species, NF-ϰB: Nuclear factor-ϰB, PAI: Plasminogen activator inhibitor, NOX: NADPH oxidase, COX: Cyclooxygenase, TNF: Tumor necrosis factor, IL: Interleukin, iNOS: Inducible nitric oxide synthase, ICAM: Intercellular adhesion molecule, MIP: Monocyte inflammatory protein, MCP: Monocyte chemoattractant protein, MMP: Matrix metalloproteinase, TIMP: Tissue inhibitor of metalloproteinases, EMMPRIN: Extracellular matrix metalloproteinase inducer, VEGF: Vascular endothelial growth factor, Ang: Angiopoietin, Tie: Endothelial receptor tyrosine kinase, p53: Tumor suppressor protein 53, AIF: Apoptosis inducing factor, PARP: Poly (ADP-ribose) polymerase, γ-HA2X: Phosphorylated histone H2A, NeuN: Neuron-specific nuclear protein, Tuj1: Neuron-specific class III β-tubulin, GFAP: Glial fibrillary acidic protein, NG2: Chondroitin sulfate proteoglycan, DCX: Doublecortin, CD68: Cluster of differentiation 68, GKS: Gamma knife surgery, M: Mouse, R: Rat, H: Human. *Excerpt from Lee YW, **Cho HJ**, Lee WH, Sonntag WE. *Biomol. Ther. (Seoul)* 2012, 20**:**357-370, with permission from The Korean Society of Applied Pharmacology.

2.5. *In Vitro* 3D Model Systems to Mimic *In Vivo* Environments

In vitro model systems are invaluable tools for investigating cellular responses under highly controlled environment. However, the conventional 2D model systems limit the interpretation of a variety of cellular physiology based on cell morphology, migration, adhesions, and signaling. Thus, the novel *in vitro* 3D model systems have been proposed as more accurate representation of the *in vivo* environment rather than 2D model systems, providing various benefits including better understanding of cell-cell and cell-matrix interactions, cellular responses upon extracellular cues, and cellular morphology [11, 13, 14, 151-161].

Among biomimetic scaffolds, hydrogels have been widely studied as a highly attractive group of polymeric materials for developing extracellular matrix (ECM) as a result of their excellent cellular compatibility. Many different types of hydrogel system have been evaluated mimicking biochemical (e.g., proteins and peptides) and mechanical (e.g., modulus) properties of *in vivo* environment of ECM [162-169]. In particular, type I collagen hydrogel have been a frequently used substrate for cell culture and tissue engineering application in that collagen is a most abundant (25~35% of the whole body protein content) protein and natural polymer in mammals, playing a vital role in cell adhesion to ECM and providing self-assembling capability in physiological environments [156, 170-173].

Microglia are the primary immune cells in the CNS, playing a key role in the brain injury and disease [174-176]. In particular, microglia are sensitive to pathological alterations of the brain microenvironment, subsequently leading to CNS diseases or injuries [177, 178]. Previous *in vivo* studies have demonstrated that activation of microglia results in increase in oxidative stress and induction of inflammation in various neurodegenerative diseases [179-182]. **Therefore, in Specific Aim 3, we designed and constructed *in vitro* 3D model systems including microglia in order to mimic pro-oxidative and pro-inflammatory environments in the brain *in vivo*.**

CHAPTER 3:

BLAST INDUCES OXIDATIVE STRESS, INFLAMMATION, NEURONAL LOSS AND SUBSEQUENT SHORT-TERM MEMORY IMPAIRMENT IN RATS

*Reprinted from **Cho HJ**, Sajja VS, VandeVord PJ, Lee YW. Neuroscience, 253:9-20 (2013), with permission from Elsevier Publisher.

BLAST INDUCES OXIDATIVE STRESS, INFLAMMATION, NEURONAL LOSS AND SUBSEQUENT SHORT-TERM MEMORY IMPAIRMENT IN RATS

3.1. Abstract

Molecular and cellular mechanisms of brain injury after exposure to blast overpressure (BOP) are not clearly known. The present study hypothesizes that pro-oxidative and pro-inflammatory pathways in brain may be responsible for neuronal loss and behavioral deficits following BOP exposure. Male Sprague-Dawley rats were anesthetized and exposed to calibrated BOP of 129.23 ± 3.01 kPa while controls received only anesthesia. *In situ* dihydroethidium fluorescence staining revealed that BOP significantly increased the production of reactive oxygen species in the brain. In addition, real-time reverse transcriptase-polymerase chain reaction, immunofluorescence staining and enzyme-linked immunosorbent assay demonstrated a significant up-regulation of mRNA and protein expressions of pro-inflammatory mediators, such as interferon-γ and monocyte chemoattractant protein-1, in brains collected from BOP-exposed animals compared with the controls. Furthermore, immunoreactivity of neuronal nuclei in brains indicated that fewer neurons were present following BOP exposure. Moreover, novel object recognition paradigm showed a significant impairment in the short-term memory at 2 weeks following BOP exposure. These results suggest that pro-oxidative and pro-inflammatory environments in the brain could play a potential role in BOP-induced neuronal loss and behavioral deficits. It may provide a foundation for defining a molecular and cellular basis of the pathophysiology of blast-induced neurotrauma (BINT). It will also contribute to the development of new therapeutic approaches selectively targeting these pathways, which have great potential in the diagnosis and therapy for BINT.

Key words: blast-induced neurotrauma, oxidative stress, inflammation, neuronal loss, novel object recognition, short-term memory impairment.

3.2. Introduction

According to the Armed Forces Health Surveillance [68], over 80,000 cases of US Armed Forces service members diagnosed as mild or severe traumatic brain injury (TBI) during the surveillance period between 2000 and 2012 were Veterans returning from Operation Iraqi Freedom (OIF) and Operation Enduring Freedom (OEF). These individuals have suffered traumatic injuries due to blast overpressure (BOP) exposure [71, 77, 80-82, 183]. In addition, BOP exposure has been reported to cause polytrauma in the military population (e.g., OIF/OEF Veteran), indicating multiple traumatic injuries in other organs including the lungs, intestines, eyes, and ears [184-187]. Although blast-induced TBI is a notable military health issue, it is also a menace to civilians who experienced BOP by explosion without protective equipment, which possesses a high risk of blast-induced TBI [73, 80, 81, 183].

Blast-induced TBI is the second most common cause of injuries from BOP, next to amputations [70]. Pre-clinical and clinical reports have indicated the development of cognitive-associated disorders following BOP exposure. Majority of these disorders are associated with anxiety, attention deficits, memory issues and impairments in problem-solving skills [69, 73, 92, 183, 188]. Overlapping symptoms with other forms of trauma such as impact-related TBI and post-traumatic stress disorder has confounding effects on diagnosis [77, 80-82].

Animal models of blast injury are currently under investigation in order to understand the molecular and cellular mechanisms of blast-induced neurotrauma (BINT) leading to cognitive impairment. Many pre-clinical studies have proposed different mechanisms of injury associated with morbidity related to BINT [84-89]. Various approaches have been applied to elucidate astrocyte activation, neurodegeneration and neurochemical changes following BOP exposure in various regions of the brain such as hippocampus, cortical regions, amygdala and cerebellum [77, 86, 90-99]. However, a detailed mechanism and prognosis of injury is poorly understood yet.

Pro-oxidative and pro-inflammatory environments in the brain have been implicated in the onset and progression of neurological and psychiatric disorders [1-8]. Reactive oxygen species (ROS) is a significant contributor to neurotoxic consequences mediated by oxidative stress. ROS, such as hydrogen peroxide and superoxide anion, are small and reactive oxygen-derived molecules regarded as essential participants in neurotoxicity and neurodegeneration [19, 189]. Thus, excessive ROS production interferes with cell signaling and the regulation of

important physiological conditions. In addition, pathophysiologcal conditions involving ROS generation causes cell death and degeneration by up-regulation of pro-inflammatory mediators leading to severe or prolonged inflammation [47-49]. Few studies have shown the role of pro-inflammatory cytokines including tumor necrosis factor-α (TNF-α), interleukin-6 (IL-6) and interferon-γ (IFN-γ) in various regions of the brain including the ventral hippocampus and amygdala following BOP exposure [93, 100-102]. ROS generation following BOP exposure was also observed in previous studies [103, 104]. However, the role of pro-oxidative and pro-inflammatory pathways in BINT remains largely unknown.

In the present study, a time-course evaluation of hippocampal pro-oxidative/inflammatory environments with subsequent neuronal changes was examined at an acute stage following BOP exposure. In addition, behavioral assessment for short-term memory impairment was performed using novel object recognition (NOR) paradigm.

3.3. Materials and Methods

3.3.1. Animals and BOP Exposure

The Virginia Polytechnic Institute and State University (Virginia Tech) Institutional Animal Care and Use Committee approved experimental protocols described herein. Prior to all experiments, animals were acclimated for at least three days (12 h light/dark) and food and water provided *ad libitum*. Male Sprague-Dawley rats weighing approximately 250 g (n = 5 per group) were briefly anesthetized with isoflurane (3%) and positioned inside the shock tube with a rostral cephalic orientation toward the shock wave. The blast shock front and dynamic overpressure were generated by a custom-built blast simulator (ORA Inc., Fredericksburg, VA; Figure 3.1A) consisting of a driving compression chamber paired with a rectangular test section and end wave eliminator located at the Center for Injury Biomechanics at Virginia Tech. A peak static overpressure was produced with compressed helium and calibrated acetate sheets (Grafix Plastics, Cleveland, OH). The advanced blast simulator generated a single (free field) pressure insult. Animals were exposed to a peak overpressure of 129.23 ± 3.01 kPa (18.74 ± 0.44 psi) for 2.5 milliseconds duration; sham animals did not experience the overpressure. The applied intensity was based on previous studies due to the visible molecular alterations of brain injury

[98, 103, 190]. Figure 3.1B provides a representative pressure profile of the shock wave generated from the blast simulator. Time profile is determined with a piezoelectric sensor axial to the blast pressure source and recorded at 250 kHz (per channel) as described previously [97-99].

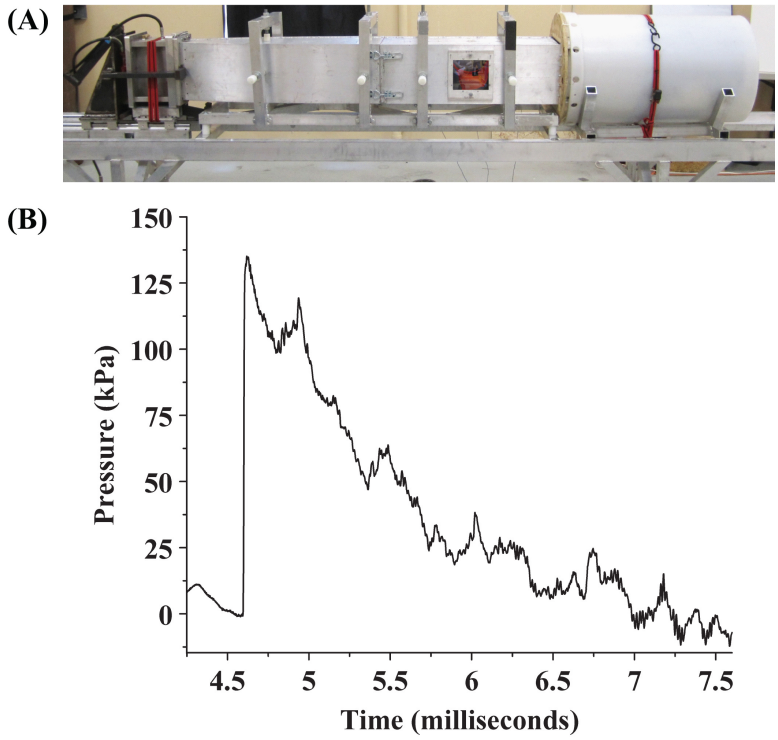

Figure 3.1. Blast Simulator and Pressure Profile of the Shock Wave. Pressure profile of a single (free field) overpressure was generated from the advanced blast simulator. (A) The advanced blast simulator located at Virginia Tech. (B) Representative pressure profile of the shock wave**.**

3.3.2. Tissue Collection and Preparation

Separate animals at 4, 24, 48 h and 2 weeks following BOP exposure (n = 5 per group) were briefly anesthetized with isoflurane (3%) and transcardially perfused with ice-cold phosphate-buffered saline (PBS) containing 6 units/ml heparin. Two hemispheres of brains were then dissected following the rapid whole brain removal, immediately frozen in dry ice, and stored at −80 °C until analysis; the hippocampi of the left hemispheres were dissected for real-time reverse transcriptase-polymerase chain reaction (RT-PCR) analysis and enzyme-linked immunosorbent assay (ELISA). The right hemispheres were cryopreserved in 30% sucrose solution for 24 h and processed in Tissue-Tek® optimal cutting temperature (O.C.T.) embedding

medium (Sakura Finetek USA, Inc., Torrance, CA). Serial 20-μm-thick sagittal sections were prepared for *in situ* ROS detection and immunofluorescence staining.

3.3.3. In Situ Detection of ROS

In situ levels of superoxide anion were measured by dihydroethidium (DHE) fluorescence staining. Briefly, brain sections were washed with PBS and incubated with 5 μM DHE solution in a light-protected humidified chamber at 37 ˚C for 30 min. After incubation, the slides were rinsed with PBS and imaged with an AxioCam MRc5 Digital Imaging System (Carl Zeiss MicroImaging, Inc., Thornwood, NY). Fluorescence intensity of acquired digital images was quantified by ImageJ software (NIH, Bethesda, MD).

3.3.4. Real-time RT-PCR

Quantitative real-time RT-PCR using TaqMan probes and primers (Applied Biosystems, Foster City, CA) were used for gene expression analyses as described previously [46]. Amplification of individual genes was performed with Applied Biosystems 7300 real-time PCR system using TaqMan Universal PCR Master Mix and a standard thermal cycler protocol. TaqMan Gene Expression Assay Reagents for rat IFN-γ, monocyte chemoattractant protein-1 (MCP-1), and glyceraldehyde-3-phosphate dehydrogenase (GAPDH) were used for specific probes and primers of PCR amplifications. The threshold cycle (C_T) was determined, and relative quantification was calculated by the comparative C_T method as described previously [46].

3.3.5. ELISA

Tissue homogenates from the rat brain were prepared using the method recommended by R&D Systems (Minneapolis, MN). Rat hippocampus was homogenized in 1 ml of ice-cold PBS and stored overnight at -80 ˚C. After three freeze-thaw cycles were performed, the homogenates were centrifuged for 5 min at 5000*g* at 4 ˚C. Supernatants were frozen immediately on dry ice and stored at -80 ˚C until analysis. Protein concentrations of brain tissue homogenates were determined as described by Bradford [191]. The protein expression levels of pro-inflammatory

mediators in brain tissue homogenates were determined by using Quantikine® Rat Immunoassay Kits for IFN-γ (R&D Systems, Minneapolis, MN) and Rat MCP-1 Immunoassay Kit (Biosource International, Camarillo, CA) following to the manufacturer's protocols.

3.3.6. Immunofluorescence Staining

Frozen brain sections (20 μm) were fixed in 4% (v/v) paraformaldehyde for 15 min at room temperature, rinsed with PBS, and incubated in 0.5% (v/v) Triton X-100 for 15 min. After being washed with PBS, nonspecific binding sites were blocked with 3% (w/v) bovine serum albumin (BSA) in PBS for 1 h at room temperature and incubated with the primary antibody, rabbit anti-IFN-γ (1:250, Abcam, Cambridge, MA), mouse anti-neuronal nuclei (NeuN) (1:250, Millipore, Billerica, MA), and rabbit anti-Iba1 (1:200, Biocare Medical, Concord, CA) diluted in 1% (w/v) BSA in PBS overnight at 4 ˚C. Sections were washed with PBS and incubated with secondary antibody, goat anti-rabbit IgG conjugated with Alexa Fluor 555 (Life Technologies, Grand Island, NY), goat anti-mouse IgG conjugated with Alexa Fluor 594, and goat anti-rabbit IgG conjugated with Alexa Fluor 488, respectively, 1:400 diluted in PBS in the dark for 1 h. After being washed with PBS, the sections were mounted in Vectashield® mounting medium with DAPI (Vector Labs., Inc., Burlingame, CA) and examined using a Leica DMI 6000 fluorescent microscope (Leica Microsystems Inc., Buffalo Grove, IL). Images were acquired with Leica DFC340 FX Digital FireWire Camera System and Leica Application Suite Advanced Fluorescence software. Fluorescence intensity of acquired digital images was quantified by ImageJ software.

3.3.7. NOR Test

The NOR test was used to measure chronic short-term memory, specifically object recognition [192]. Animals at 2 weeks following BOP exposure were tested. Testing occurred in three phases, including: acclimation = acclimate to novel environment (for the first two days), trial 1 (T1) = presentation of two similar objects, trial 2 (T2) = presentation of a novel and familiar object) (on the third day). In the first phase, rats were acclimated to a custom-made open-field testing chamber (79 × 79 × 35 cm) with lower light scale by allowing them to explore

the empty chamber for 5 min (time used in all phases) for three consecutive days prior to T1 and T2 testing. On the third day, rats underwent T1 where they were placed in the chamber with two identical objects residing in opposite corners. After another 20-min interval, object recognition was determined in T2. During T2, rats were returned to the testing chamber, where one of the familiar objects was substituted with a novel object. For T1 and T2 phases (5 min each), rats were placed in the chamber directed away from the objects. The rats were monitored for time spent exploring the familiar objects, which was defined as the nose-point of the animal being directed toward an object and also located within 1.5× radius of the object measured from the center of the object. Memory recognition behavior was quantified as the fraction of time spent exploring the novel object relative to the familiar object during T1 and T2 phases. An animal that spent 75% or more time in T1 exploring one of the objects was excluded from the study to avoid an initial object bias. The placement of objects within the chambers was counterbalanced among animals to reduce the potential of a place bias. Arena settings were set and behaviors were analyzed using Ethovision™ tracking software (Noldus Information Technology, Leesburg, VA). The testing chamber was located in a closed room and behavior was digitally recorded with a camera located above the chamber and linked to a computer outside the room. After placing an animal in the chamber, the experimenter exited the room and viewed the animal on the computer linked to the camera. Automated tracking and its scoring were verified by an independent assessor kept blind to the treatment conditions.

3.3.8. Statistical Analysis

Statistical analysis of data was completed using SigmaPlot version 11 software (SPSS, Chicago, IL). Effects of blast exposure were measured in separate experiments; 4, 24, 48 h and 2 weeks following BOP exposure. In each experiment, separate sham-treated animals served as respective comparison groups to control for unknown influences (e.g., residual effects of isoflurane). Results of *in situ* ROS detection, real-time RT-PCR, ELISA, and immunofluorescence staining were analyzed with a two-tailed student's *t*-test to compare sham and BOP-exposed rats. Behavioral test results were analyzed with a two-tailed repeated measured analysis of variance (ANOVA) to find the differences associated with learning in the

NOR paradigm. A statistical probability (p) value of <0.05 was considered statistically significant.

3.4. Results

3.4.1. BOP Increases ROS Generation in the Brain

In situ DHE fluorescence staining was performed to detect ROS generation. Significantly elevated levels of superoxide anion were observed at 4, 24, 48 h and 2 weeks following BOP exposure compared with the control hippocampus (Figure 3.2A to 3.2E). Quantitative analysis exhibited that BOP significantly increased ROS generation by 11.06-fold (4-h post-blast; $p < 0.05$), 17.16-fold (24-h post-blast; $p < 0.05$), 9.03-fold (48-h post-blast; $p < 0.05$), and 8.18-fold (2-weeks post-blast; $p < 0.05$), respectively (Figure 3.2F). These results suggest that BOP produces a constant response of pro-oxidative environment in the brain for up to 2 weeks following exposure.

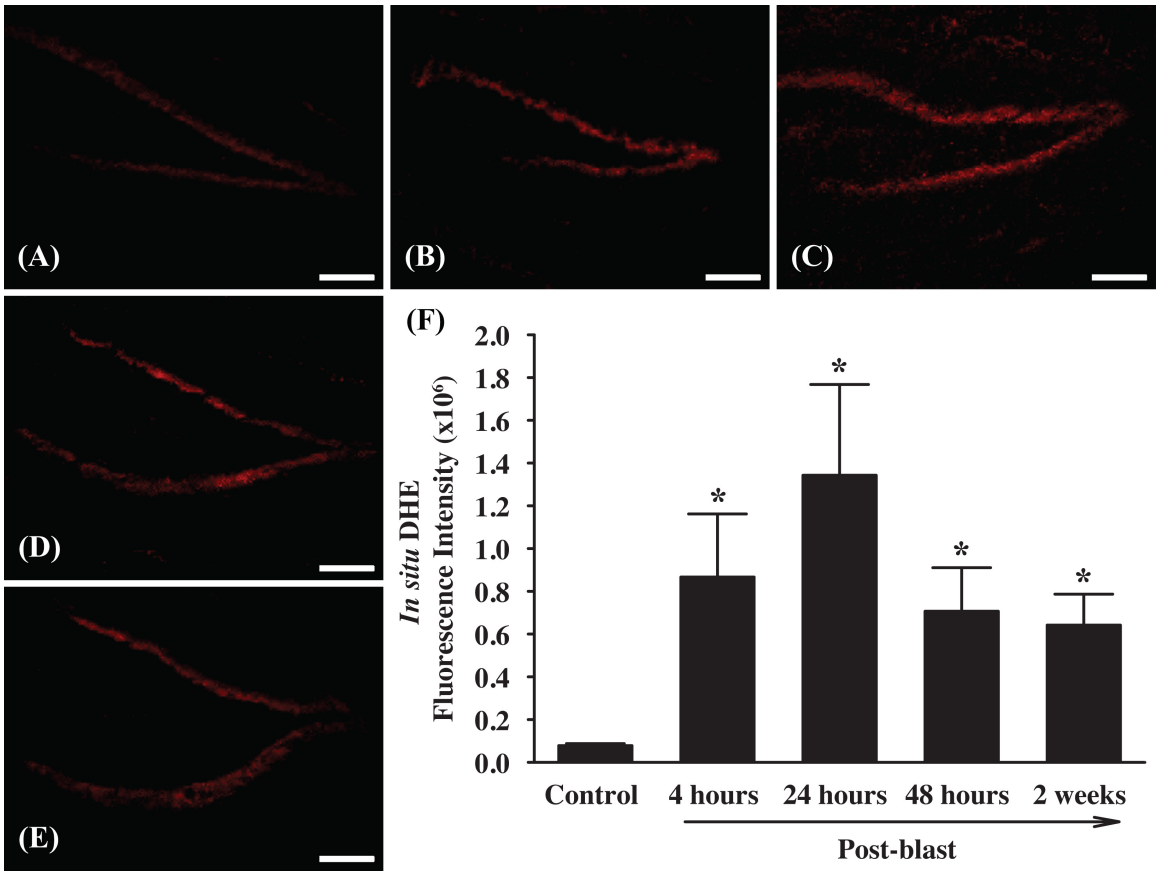

Figure 3.2. *In Situ* DHE Fluorescence Staining Following BOP Exposure. (A) Sham-blast (Control); (B) 4-h post-blast; (C) 24-h post-blast; (D) 48-h post-blast; (E) 2-weeks post-blast; (F) Quantitative analysis of fluorescence intensity. Data represent means ± SEM for each group (n = 5). *$p < 0.05$ vs. control. Scale bar = 100 μm.

3.4.2. BOP Up-regulates mRNA and Protein Expression of Pro-inflammatory Mediators in the Brain

To investigate whether BOP affects the pro-inflammatory pathways in the brain, mRNA expression levels of IFN-γ and MCP-1 were examined by quantitative real-time RT-PCR. Significant and marked up-regulation of IFN-γ and MCP-1 mRNA expressions was observed at 4-h post-blast (2.38- and 2.34-fold induction of IFN-γ and MCP-1, respectively, compared with the controls; Figure 3.3A and 3.4A). Expression of GAPDH (a housekeeping gene), however, was not affected by BOP (data not shown).

The quantitative sandwich enzyme immunoassay technique was employed to determine whether blast-mediated increases in mRNA levels of IFN-γ and MCP-1 translate to elevated protein expressions. Consistent with the gene expression data (Figure 3.3A and 3.4A), BOP resulted in a significant increase in IFN-γ and MCP-1 protein expression in the hippocampus at 24-h post-blast by 4.78- and 2.00-fold in blast group compared with the controls (IFN-γ: 50.44 ± 2.88 pg/mg vs. 10.55 ± 1.50 pg/mg; $p < 0.05$, MCP-1: 116.39 ± 8.06 pg/mg vs. 58.26 ± 3.48 pg/mg; $p < 0.05$), respectively (Figure 3.3C and 3.4B). In addition, both proteins were decreased at 48 h following BOP exposure but remained higher than the control group (IFN-γ: 23.98 ± 2.20 pg/mg; $p < 0.05$, MCP-1: 82.95 ± 4.33 pg/mg; $p < 0.05$, respectively) whereas both proteins returned to expression levels near control at 2 weeks following BOP exposure.

The blast-mediated overexpression of IFN-γ protein was also visualized and confirmed by immunofluorescence staining. A significant increase in immunoreactivity of IFN-γ was detected in the brain at 24 h following BOP exposure, whereas very little reactivity was observed in the control group (Figure 3.3I to 3.3M). In agreement with the results from ELISA (Figure 3.3C), quantitative analysis of fluorescence intensity demonstrated that BOP significantly increased immunoreactivity of IFN-γ in the brain and the maximal immunoreactivity of IFN-γ protein was detected at 24-h post-blast exposure by 31.68-fold (Figure 3.3B). These data demonstrate that BOP acutely produces IFN-γ- and MCP-1-mediated pro-inflammatory environment in the brain.

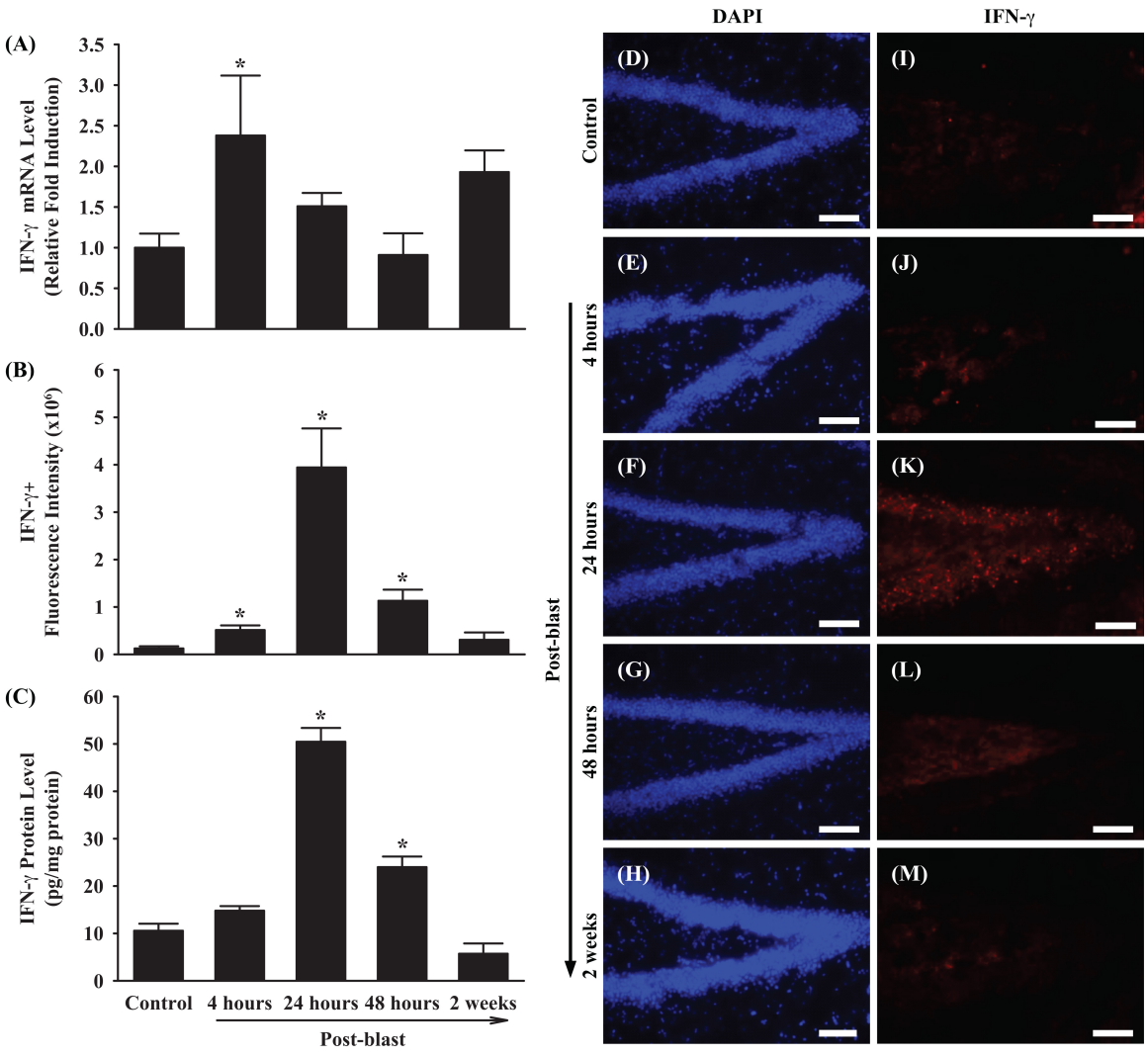

Figure 3.3. mRNA and Protein Expressions of IFN-γ in the Brain Following BOP Exposure. Nuclei were visualized with DAPI (D-H) and IFN-γ were significantly up-regulated following BOP exposure (I-M) in hippocampus. (A) Quantitative mRNA expression of IFN-γ by real-time RT-PCR; (B) Quantitative analysis of immunofluorescence intensity of IFN-γ; (C) Quantitative IFN-γ protein expression by ELISA; (D-M) Representative immunofluorescent photographs of DAPI and IFN-γ; (D and I) Sham-blast (Control); (E and J) 4-h post-blast; (F and K) 24-h post-blast; (G and L) 48-h post-blast; (H and M) 2-weeks post-blast. Data represent means ± SEM (Real-time RT-PCR: n = 5; Immunofluorescence staining: n = 4; ELISA: n = 5). *$p < 0.05$ vs. control. Scale bar = 100 μm.

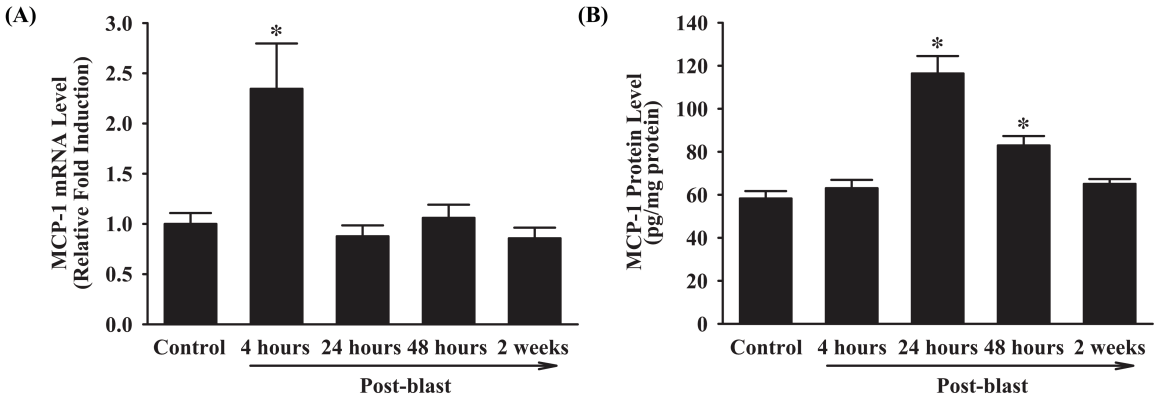

Figure 3.4. mRNA and Protein Expression of MCP-1 in the Brain Following BOP Exposure. (A) Quantitative mRNA expression of MCP-1 by real-time RT-PCR; (B) Quantitative MCP-1 protein expression by ELISA. Data represent means ± SEM for each group (n = 5). *$p < 0.05$ vs. control.

3.4.3. BOP Decreases Neuronal Density in the Brain

Protein levels of mature neuronal marker, NeuN, were assessed following BOP exposure by immunostaining. NeuN-immunopositive neurons in the hippocampus were significantly lower in the blast compared with the control group (Figure 3.5A to 3.5E). Quantitative analysis of fluorescence intensity demonstrated that BOP significantly reduced immunoreactivity of NeuN in rat hippocampus by 1.77-fold (4-h post-blast; $p < 0.05$; 24-h post-blast; $p < 0.05$), 2.75-fold (48-h post-blast; $p < 0.05$), and 2.40-fold (2-weeks post-blast; $p < 0.05$), respectively (Figure 3.5F). These results indicate that BOP provokes neuronal loss in the hippocampus.

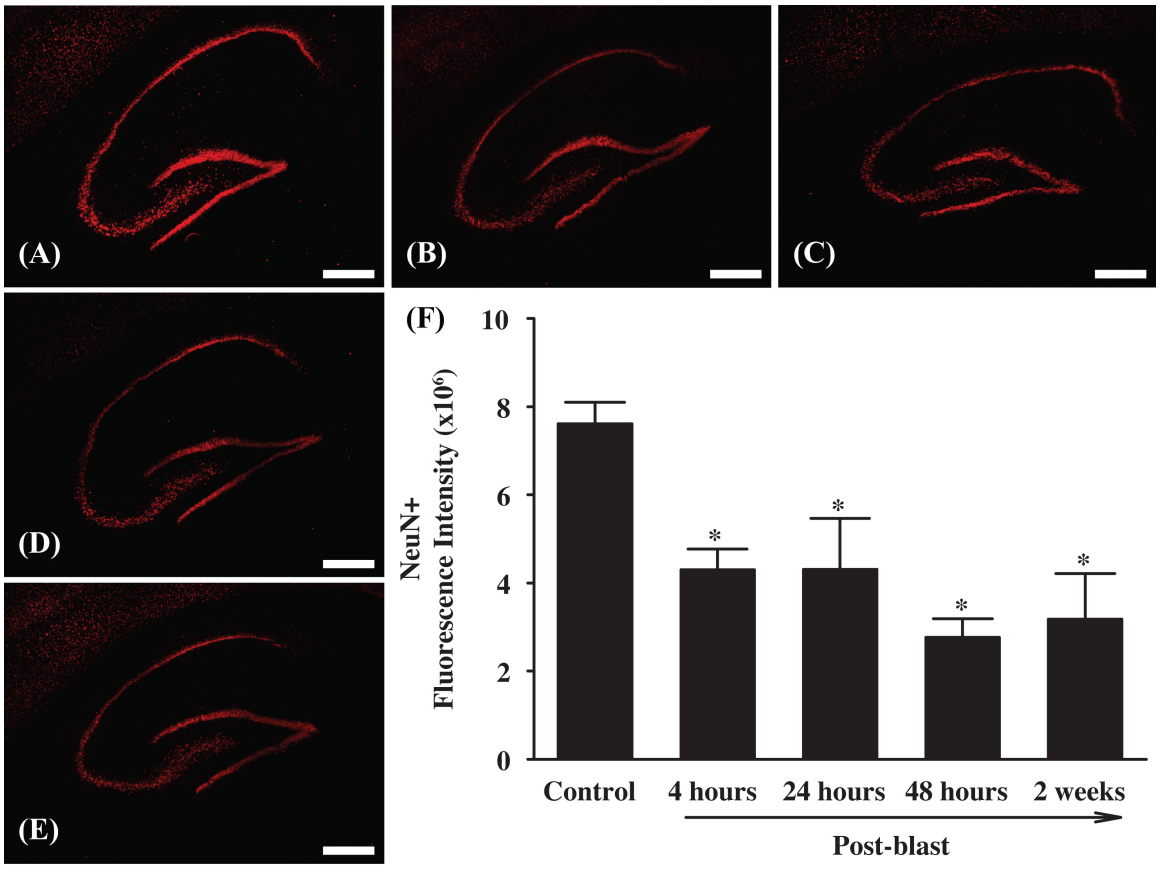

Figure 3.5. NeuN Protein Expression in the Brain Following BOP Exposure. (A) Sham-blast (Control); (B) 4-h post-blast; (C) 24-h post-blast; (D) 48-h post-blast; (E) 2-weeks post-blast; (F) Quantitative analysis of fluorescence intensity. Data represent means ± SEM for each group (n = 4). *$p < 0.05$ vs. control. Scale bar = 500 μm.

3.4.4. BOP Induces Late Microglial Activation

To determine whether BOP affects microglial activation, the protein expression levels of Iba1, a microglial activation marker, in rat brains were visualized by immunofluorescence staining. A strong Iba1-positive immunoreactivity was detected acutely at 2-weeks post-blast in rat brains compared with the control group while no significant immunoreactivity was detected at 4-, 24-, and 48-h post-blast (Figure 3.6A to 3.6E). Quantitative analysis of fluorescence intensity demonstrated that BOP significantly induced immunoreactivity of Iba1 in the rat hippocampus by 2.18-fold (2-weeks post-blast; $p < 0.05$, Figure 3.6F). These data demonstrate that BOP induces late activation of microglia in the hippocampus.

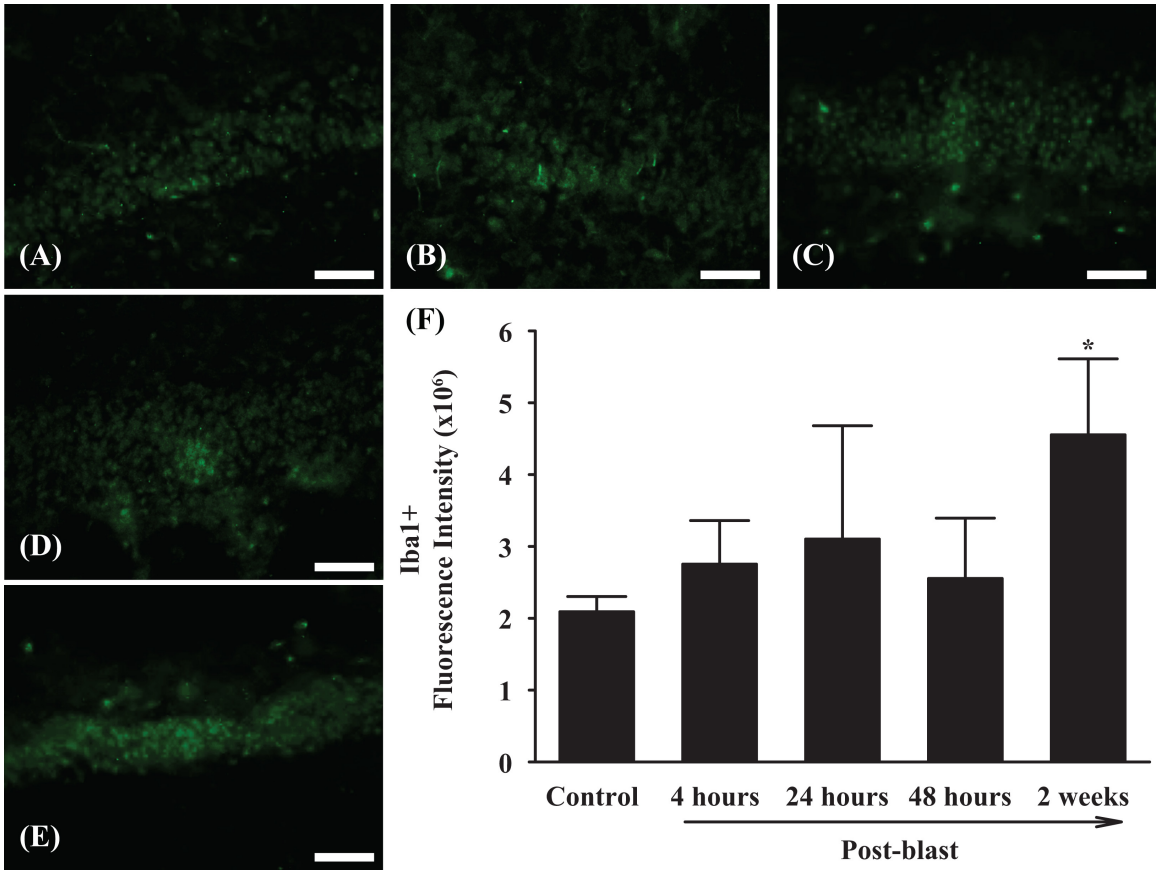

Figure 3.6. Late Microglial Activation Following BOP Exposure. (A) Sham-blast (Control); (B) 4-h post-blast; (C) 24-h post-blast; (D) 48-h post-blast; (E) 2-weeks post-blast; (F) Quantitative analysis of fluorescence intensity. Data represent means ± SEM for each group (n = 4). *$p < 0.05$ vs. control. Scale bar = 50 μm.

3.4.5. BOP Induces Behavioral Changes

A chronic assessment of short-term memory was performed using the NOR paradigm at 2 weeks following BOP exposure. Both BOP-exposed and control animals spent the same amount of time when presented with the two similar objects in T1, whereas the control group spent a significantly higher amount of time with the novel object compared to the familiar object in T2 at 2 weeks following BOP exposure. In addition, control animals spent more time learning the novel object compared with BOP-exposed animals (Figure 3.7A). Thus, NOR paradigm revealed a significant impairment in the short-term memory of BOP-exposed animals as compared to control animals at 2 weeks following BOP exposure ($p < 0.05$; Figure 3.7B).

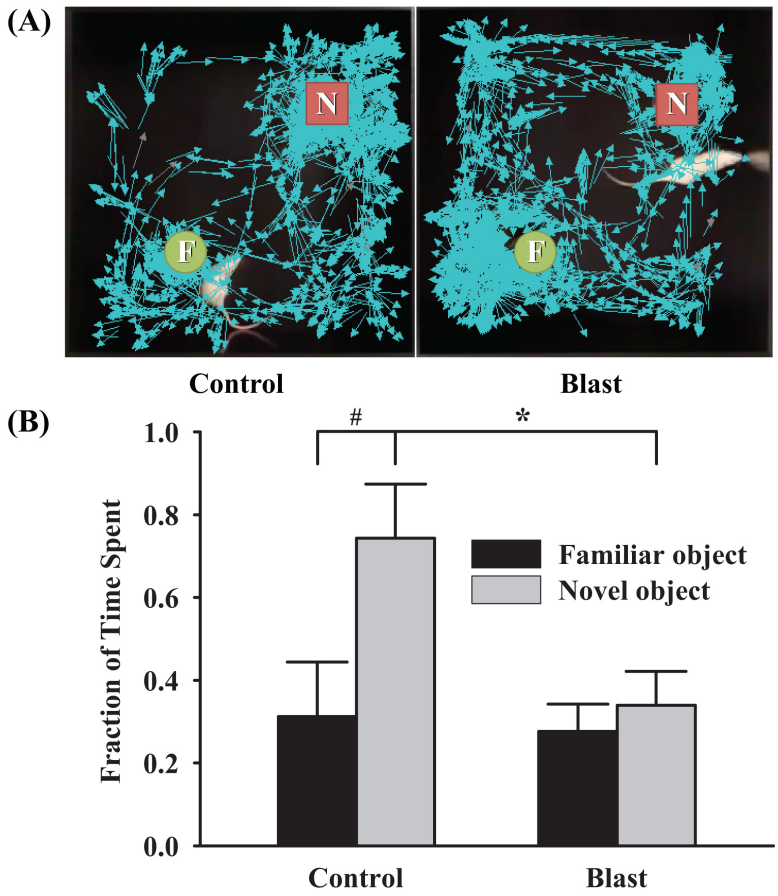

Figure 3.7. Behavioral Changes Following BOP Exposure. NOR test was performed to elucidate behavioral changes at 2-weeks post-blast. (A) Representative animal (head) orientation along the axis of arrows for both control and BOP-exposed groups in T2 during NOR test. N: novel object location, F: familiar object location; (B) Quantitative analysis of NOR paradigm. Data represent means ± SEM for each group (n = 5). #$p < 0.05$ vs. control (familiar object); *$p < 0.05$ vs. control (novel object).

3.5. Discussion

Recent clinical reports indicate that various cognitive regions are affected and involved in developing cognitive-communicative deficits. Damage to the cognitive cores of the brain can evoke stress-related responses, and high metabolic energy demands are required for repair mechanisms [193-195]. Therefore, acute neurochemical changes following BOP exposure are likely to initiate cellular or molecular mechanisms of pathological cascades, which may proceed into late-emerging clinical disorders without appreciable behavioral phenotypes, such as mood and anxiety disorders [80, 196, 197]. Pre-clinical studies have shown the pathological consequence of BOP-mediated damage to the hippocampus of the brain, which is directly involved in memory and learning. Indeed, BOP exposure results in significant delayed neurobehavioral sequelae including depression, increased anxiety and memory impairments [86, 91, 97-99, 102, 183, 198-202].

Recent evidence has identified oxidative stress with a concomitant neuroinflammation as one of the arising mechanistic pathways leading to blast-induced brain injury [91, 103, 198, 203]. However, the effects of blast on pro-oxidative and pro-inflammatory pathways in the brain remain largely unclear. Prognosis of injury by evaluating time-course of ROS induction in addition to analyses of gene and protein expression of pro-inflammatory cytokine/chemokine may contribute to understanding selective biochemical pathways to neurodegeneration following BOP exposure. The present study demonstrated a prognosis of oxidative stress and neuroinflammation in the hippocampus with subsequent neuronal loss and delayed cognitive behavioral abnormalities following BOP exposure.

The current study first observed significant acute changes of ROS generation in the brain following BOP. A significant and marked increase of ROS generation in the dentate granule cell layer of the hippocampus was observed after 4-h post-blast and the ROS levels were further increased at 24-h post-blast. In a previous study [97], markedly decreased levels of glutathione, a major anti-oxidant, was detected at 24- and 48-h post-blast, supporting the current study of pro-oxidative environment following BOP exposure. In addition, it has been reported that increased ROS-generating enzymes, including NADPH oxidase 1 and inducible nitric oxide synthase, and up-regulated oxidative/nitrosative damage markers, such as 4-hydroxynonenal and 3-nitrotyrosine, with significant blood-brain barrier breakdown were detected following BOP

exposure [103, 203]. Moreover, increased ROS was directly detected using 2',7'-dichlorofluorescein, another indicator of ROS generation, at 6-h post-blast [204]. Although more information on oxidative stress following BOP exposure is vital in the understanding of chronic effects following the blast, these data suggest that blast-mediated induction of oxidative stress plays a critical role in the cerebral damage following BOP exposure.

Enhanced expression of pro-inflammatory mediators (e.g.,cytokines, chemokines) facilitates the inflammatory process in an injured sites. Recent studies suggest that inflammatory mediators may serve as potential biomarkers of BINT [205, 206]. In the present study, IFN-γ, a pro-inflammatory cytokine and activator of macrophages, and MCP-1, a member of CC chemokine family playing a critical role in monocyte chemotaxsis and transmigration [45], were both significantly elevated in the hippocampus following BOP exposure. Previous pre-clinical studies have also demonstrated that IFN-γ and MCP-1 were significantly up-regulated in brains following BOP exposure [86, 93, 101, 200, 207]. Likewise, there are several other reports demonstrating that overexpression of various pro-inflammatory markers including C-reactive protein, TNF-α, IL-6 has been involved and associated with biomolecular changes in the brain following BOP exposure [100-102, 200, 208]. Therefore, these studies provide sufficient evidence demonstrating the potential contribution of pro-inflammatory environment to brain injury following BOP exposure. Our results further revealed that the peak mRNA expression of IFN-γ and MCP-1 occurred at 4-h post-blast. In addition, the concomitant peak protein expression of these pro-inflammatory mediators appeared at 24-h post-blast. These time-course analyses suggest that mRNA and protein expression levels of pro-inflammatory mediators at different time points may be critically associated with pathological prognosis of BINT. More importantly, the novel findings in this study are time-dependent ROS generation and concomitant inflammatory response. It is still unclear whether oxidative response precedes inflammatory event or *vice versa*; however, due to an early imbalance in the redox system observed at 4-h post-blast compared with the significant protein induction of inflammatory mediators (IFN-γ and MCP-1) at 24-h post-blast, it is possible that the blast-induced increase in oxidative stress may be responsible for the pro-inflammatory events.

In general, pro-inflammatory environment in response to injury is beneficial in neutralizing potential threats to the central nervous system by diminishing cellular damage [2, 3, 5, 6]. However, there is emerging evidence that a sustained neuroinflammatory response can be

detrimental due to neuronal damage, neuronal circuit impairments and neurodegeneration [49, 65-67, 207, 209]. Particularly, chronic release of pro-inflammatory mediators is likely to perpetuate innate inflammatory cycle, as well as activate supplemental microglia, and stimulate their proliferation. Microglial activation has been observed up to 2 weeks in the rat brain following BOP exposure and widespread gliosis including reactive astrogliosis occurred in the blast-exposed rat hippocampus [91, 97, 190, 198, 210, 211]. Although there is still ongoing investigation on the relationship among gliosis, neurodegeneration and/or neuroprotective effects, it has been frequently reported that reactive gliosis is strongly associated with neurodegeneration in other types of brain damages including TBI and neurodegenerative diseases [212-215]. The present study showed a significant neuronal loss following BOP exposure in the hippocampus. These results are in agreement with previous studies demonstrating neurodegeneration in the hippocampus evaluated by Fluoro-Jade B, a marker for degenerating neurons, in order to link cognitive impairments to neuronal injury [97, 98]. In addition, Dalle Lucca *et al*. [100] demonstrated that BOP induced neuronal loss and neurodegeneration in the rat hippocampus by hematoxylin and eosin staining.

According to our results, neuronal loss after BOP exposure was detected from 4-h post-blast whereas microglial activation demonstrated a delayed response being observed at 2-weeks post-blast. A possible explanation of acute neuronal loss after BOP exposure is a direct ROS damage to cells. Previously, Choi *et al*. [216] demonstrated that hydrogen peroxide induced cell death *via* mitochondrial dysfunction, suggesting a possible trigger of apoptotic cascade by excessive ROS. Subsequently, the damage of neurons may lead to the activation of reactive astrogliosis for the metabolic support and repair process [97, 217]. According to Sajja *et al*. [97], levels of glial fibrillary acidic protein, a marker of reactive astrogliosis, in the hippocampus were increased within 24-h post-blast, and subsided at 48-h post-blast. Moreover, there was a significant elevation of apoptotic markers, cleaved caspase-3 and Bcl-2-associated X protein, in the hippocampus at 48-h post-blast, indicating the initiation of active apoptotic process after 24-h post-blast. Consequently, an early event of reactive astrogliosis and elevated apoptotic markers may be responsible for apoptotic neuronal loss in combination with direct ROS-induced cell death. In addition to immediate neuronal loss after BOP exposure by ROS, ROS may also trigger the production of pro-inflammatory mediators including IFN-γ and MCP-1 to reflect active inflammation, resulting in microglial activation and recruitment at a late stage [47, 218, 219].

According to previous studies, IFN-γ may act as an endogenous activator of microglial activation in the case of central nervous system damage whereas neuronal MCP-1 may play a critical role in microglial recruitment [47, 220]. In summary, late activation of microglia following possible direct ROS damage and subsequent apoptotic cell death may contribute to a continuous neuronal loss up to 2 weeks after BOP exposure.

In the present study, NOR test was performed at sub-acute stage (2 week post-blast) to evaluate short-term learning and memory, which pertains to high-order memory function of short-term memory in object recognition, resulting in impaired short-term memory in the BOP-exposed group compared with the controls. In addition, a significant elevation of anxiety-like behavior (latency change) in BOP-exposed group at 48-h post-blast compared with the control group was observed (data not shown). In previous *in vivo* studies, chronic inflammation has been implicated in learning impairments [221-225]. In addition, Tweedie *et al*. [202] examined the indices of cognition and anxiety-like behavioral deficits in regard to hippocampal gene transcriptome of mice. Previous studies have demonstrated that, neuronal loss, particularly in the hippocampus, is critically involved in behavior/cognitive deficits. For example, Li *et al*. [226] observed that neuronal loss in the hippocampus was correlated with learning and memory deficits in mice. In addition, Hicks *et al*. [227] and Witgen *et al*. [228] showed a significant correlation between cognitive performance and neuronal loss after brain injury in rodent models. Moreover, Cechetti *et al*. [229] reported that neuronal damage along with reactive astrogliosis may be responsible for memory impairment. Therefore, our results demonstrating neuronal loss and cognitive deficit are in agreement with these previous studies. Overall, our finding may contribute to understanding of a series of pathophysiological events including oxidative stress, inflammatory gene/protein expression, and neuronal loss, which in turn induce behavioral deficits in BOP-exposed rats.

3.6. Conclusions

The present study demonstrated that a time-course of acute pro-oxidative and pro-inflammatory environments contributes to BOP-induced neuronal loss and behavioral deficits. However, more detailed analysis of BINT over an expanded time-course would be required for better knowledge of any changes in microglial and neuronal inflammatory states. Additionally,

this study should be broadened to other brain areas, particularly the prefrontal cortex and amygdala complex, since they mediate cognitive and anxiety control, respectively. Nevertheless, due to the fact that excessive oxidative damage and overproduction of inflammatory mediators in the brain are substantially involved in the onset and progression of neurological/neuropathological disorders, the current study provides a foundation for defining a molecular and cellular basis of pathophysiology of BINT. Furthermore, the current study in a time-course of responses to BOP exposure may contribute to the development of novel therapeutic approaches selectively targeting these pathways, which have great potential in protecting the brain from BOP-mediated damage.

CHAPTER 4:

POTENTIAL ROLE OF NADPH OXIDASE IN RADIATION-INDUCED PRO-OXIDATIVE AND PRO-INFLAMMATORY PATHWAYS IN MOUSE BRAIN

* **Cho HJ**, Lee WH, Hwang MH, Sonntag WE, Lee YW. Submitted to *Molecular and Cellular Neuroscience* (December 2014).

POTENTIAL ROLE OF NADPH OXIDASE IN RADIATION-INDUCED PRO-OXIDATIVE AND PRO-INFLAMMATORY PATHWAYS IN MOUSE BRAIN

4.1. Abstract

The use of radiation therapy is limited by the risk of significant clinical side effects including progressive cognitive impairments in brain tumor patients. Additionally, the cellular and molecular mechanisms by which irradiation induces damage to brain tissues remain largely unknown. The present study was designed to investigate our hypothesis that NADPH oxidase plays a crucial role in fractionated whole-brain irradiation-induced pro-oxidative and pro-inflammatory environments in the brain. C57BL/6 mice received either fractionated whole-brain irradiation or sham-irradiation, and were maintained for 4, 8, and 24 h following irradiation. The mRNA expression levels of pro-inflammatory mediators, such as tumor necrosis factor-α (TNF-α) and monocyte chemoattractant protein-1 (MCP-1), were determined by quantitative real-time reverse transcriptase-polymerase chain reaction (RT-PCR). The protein expression levels of TNF-α, MCP-1, NADPH oxidase-2 (NOX-2), superoxide dismutase 1 (SOD1), and ionized calcium binding adaptor molecule 1 (Iba1) were detected by immunofluorescence staining. The levels of reactive oxygen species (ROS) were visualized by *in situ* dihydroethidium (DHE) fluorescence staining. Real-time RT-PCR and immunofluorescence staining demonstrated a significant up-regulation of mRNA and protein expression levels of TNF-α and MCP-1 in irradiated mouse brain compared with sham-irradiated controls. Additionally, immunofluorescence staining of Iba1 showed a marked increase of microglial activation in mouse brain after irradiation. Moreover, *in situ* DHE fluorescence staining revealed that fractionated whole-brain irradiation significantly increased production of ROS. Furthermore, a significant increase in immunoreactivity of NOX-2 and SOD1 was detected in mouse brain after irradiation. On the other hand, an increase of ROS generation in mouse brain after fractionated whole-brain irradiation was markedly attenuated in the presence of NOX inhibitors or NOX-2 neutralizing antibody. The present study demonstrated that NOX-2 may play a pivotal role in

fractionated whole-brain irradiation-induced pro-oxidative and pro-inflammatory pathways in mouse brain.

Key words: Fractionated whole-brain irradiation, TNF-α, MCP-1, NOX-2, Iba1, ROS, Inflammation

4.2. Introduction

According to the Central Brain Tumor Registry of the United States (CBTRUS) [105], approximately 68,470 new cases of primary brain and central nervous system (CNS) tumors are expected to be diagnosed in 2015 and over 200,000 patients are treated with either partial large-field or whole brain radiation every year in the United States. Radiation therapy has been commonly used as a standard treatment modality for patients with brain tumors. However, the use of radiotherapy for brain tumors has been restricted by the risk of radiation-induced injury to normal brain tissue, which may subsequently lead to both anatomic and functional deficits [107, 108, 230-232].

Radiation-induced brain injury has traditionally been classified as acute, early delayed (subacute), and late delayed responses depending on its time of onset [111-113]. In general, most of the symptoms and signs of acute and early delayed injuries are reversible whereas late delayed injury is considered irreversible and progressive. In addition, there is a growing awareness that late delayed injury is largely responsible for cognitive impairment, focal deficits, seizures, and increased cranial pressure even in cases with no detectable anatomic abnormalities.

Previous studies have shown that whole brain radiation may cause a significant deterioration of learning and memory in human as well as in rodent [119, 121, 123-126, 128, 130, 131, 233]. In addition to cognitive impairment, whole brain radiation causes other brain injures including growth hormone deficiency and motor dysfunction [120, 122, 127, 129]. Although there have been significant progresses in understanding pathogenesis of radiation-mediated brain injury, limited information about the etiology of radiation-induced damage to normal brain tissue is currently available.

Recent evidence has identified that oxidative stress and inflammation are important pathways leading to radiation-induced brain injury [46, 107, 132-139]. For example, irradiation

augmented CNS inflammation through up-regulation of a variety of pro-inflammatory mediators including tumor necrosis factor-α (TNF-α), interleukin-1β (IL-1β), interleukin-6 (IL-6), monocyte chemoattractant protein-1 (MCP-1), inducible nitric oxide synthase (iNOS), intercellular adhesion molecule-1 (ICAM-1), vascular cell adhesion molecule-1 (VCAM-1), and E-selectin, which may contribute to the radiation-induced functional impairments in the brain [46, 132, 133, 135-138]. In addition, oxidative stress may be, at least in part, a significant contributor to disastrous neurotoxic consequences in radiation-induced brain injury [141, 142, 234-236]. Furthermore, among the enzymatic pro-oxidative systems, the family of NADPH oxidase (NOX), a multi-subunit enzyme complex consisting of NOX-1 to -5, has been predominantly perceived as an important source of ROS causing serious damage to a variety of biomolecules in the brain [142, 237-239].

In the present study, we examined the potential role of NOX-2 in radiation-induced pro-oxidative and pro-inflammatory pathways in mouse brain. Our results provide the first evidence to demonstrate that NOX-2 plays a pivotal role in radiation-induced oxidative stress and inflammation in mouse brain.

4.3. Materials and Methods

4.3.1. Animals

C57BL/6 male mice were purchased from Jackson Laboratory (Bar Harbor, ME). Animals were housed under a 12-h light:12-h dark cycle with food and water provided *ad libitum*. Animal care was conducted in accordance with the National Institutes of Health Guide for the Care and Use of Laboratory Animals, and this study was approved by the Institutional Animal Care and Use Committee.

4.3.2. Fractionated Whole-brain Irradiation and Tissue Sample Preparation

Fractionated whole-brain irradiation was performed in mice as described previously [144]. Briefly, mice were anesthetized with ketamine-xylazine (intraperitoneal injection, 100-15 mg/kg) and received a clinical fractionated dose of whole-brain irradiation (total cumulative dose

of 40 Gy in 8 fractions of 5 Gy each, twice per week for 4 weeks) using a ^{137}Cs γ irradiator. Mice in the control group were only anesthetized. The mice were maintained for 4, 8, and 24 h after the last fractionated dose of whole-brain irradiation. Mouse brain was rapidly removed after perfusion and hemisected at the midline. Mouse brain was then immediately frozen in liquid nitrogen.

4.3.3. Real-time RT-PCR

Quantitative real-time RT-PCR using TaqMan probes and primers (Applied Biosystems, Foster City, CA) were used for gene expression analyses as described previously [46]. Amplification of individual genes was performed with Applied Biosystems 7300 real-time PCR system using TaqMan Universal PCR Master Mix and a standard thermal cycler protocol. TaqMan Gene Expression Assay Reagents for mouse TNF-α, MCP-1, and glyceraldehydes-3-phosphate dehydrogenase (GAPDH) were used for specific probes and primers of PCR amplifications. The threshold cycle (C_T) was determined, and relative quantification was calculated by the comparative C_T method as described previously [46].

4.3.4. Immunofluorescence Staining

Frozen brain sections (20 μm) were fixed in 4% (v/v) paraformaldehyde for 15 min at room temperature, rinsed with PBS, and incubated in 0.5% (v/v) Triton X-100 for 15 min. After being washed with PBS, nonspecific binding sites were blocked with 3% (w/v) bovine serum albumin (BSA) in PBS for 1 h at room temperature and incubated with the primary antibody, rabbit anti-MCP-1 (1:50, Santa Cruz Biotechnology Inc., Santa Cruz, CA), rabbit anti-TNF-α (1:200, Abcam, Cambridge, MA), rabbit anti-Iba1 (1:200, Wako Chemicals USA Inc., Richmond, VA), mouse anti-NOX-2 (1:100, BD Biosciences, San Jose, CA), rabbit anti-superoxide dismutase 1 (SOD1) (1:500, Abcam, Cambridge, MA), diluted in 1% (w/v) BSA overnight at 4 ˚C. Sections were washed with PBS and incubated with secondary antibody, donkey anti-mouse IgG conjugated with Alexa Fluor 488, donkey anti-rabbit IgG conjugated with Alexa Fluor 488, or goat anti-rabbit IgG conjugated with Alexa Fluor 555, 1:400 diluted in PBS in the dark for 1 h. After being washed with PBS, the sections were mounted in

Vectashield® mounting medium (Vector Labs., Inc., Burlingame, CA) and examined using a Zeiss AXIO Imager A1m fluorescence microscope. Images were acquired with an AxioCam MRc5 Digital Imaging System (Carl Zeiss MicroImaging, Inc., Thornwood, NY). Fluorescence intensity of acquired digital images was quantified by ImageJ software (NIH, Bethesda, MD).

4.3.5. In Situ Detection of ROS

In situ levels of superoxide anion, the main species of ROS, were measured by *in situ* dihydroethidium (DHE) fluorescence staining. Briefly, brain sections were washed with PBS and incubated with 5 μM DHE solution in a light-protected humidified chamber at 37 ˚C for 30 min. After incubation, the slides were rinsed with PBS and imaged with a Zeiss AXIO Imager A1m fluorescence microscope. Fluorescence intensity of acquired digital images was quantified by ImageJ software.

4.3.6. Statistical Analysis

Statistical analysis of data was completed using SigmaPlot version 11 software (SPSS, Chicago, IL). A two-tailed student's t-test was applied to compare sham and irradiated mice. A statistical probability (p) value of <0.05 was considered significant.

4.4. Results

4.4.1. Fractionated Whole-brain Irradiation Up-regulates mRNA and Protein Expressions of TNF-α and MCP-1 in Mouse Brain

To investigate whether fractionated whole-brain irradiation affects the pro-inflammatory mediators in mouse brain, mRNA expression levels of TNF-α and MCP-1 were examined by quantitative real-time RT-PCR. As shown in Figure 4.1, a significant up-regulation of TNF-α and MCP-1 mRNA expressions was observed at 4 h post-irradiation (10.34-fold induction of TNF-α and 36.10-fold induction of MCP-1, respectively, compared to sham-irradiated control mice). Expression of GAPDH (a housekeeping gene), however, was not affected by irradiation

(data not shown). In addition, protein expression levels of TNF-α and MCP-1 in mouse brain were visualized by immunofluorescence staining. As illustrated in Figure 4.2, markedly increased immunoreactivities of TNF-α and MCP-1 were detected in mouse brain at 8 h after irradiation, whereas very little reactivity was observed in sham-irradiated control mouse brain (Figure 4.2A to 4.2D and 4.2F to 4.2I, respectively). Quantitative analysis of fluorescence intensity demonstrated that fractionated whole-brain irradiation significantly induced protein expressions of TNF-α and MCP-1 in mouse brain at 8 h post-irradiation by 18.43-fold increase in TNF-α and 5.76-fold increase in MCP-1, respectively (Figure 4.2E and 4.2J). These results suggest that fractionated whole-brain irradiation produces pro-inflammatory environments in mouse brain.

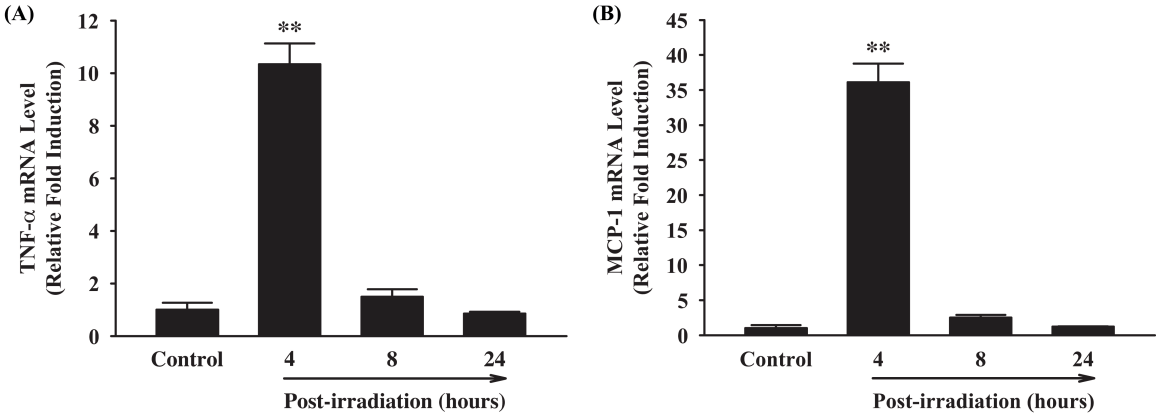

Figure 4.1. Effect of Fractionated Whole-brain Irradiation on mRNA Expression of TNF-α and MCP-1 in Mouse Brain. Compared with sham-irradiated controls, fractionated whole-brain irradiation significantly up-regulated mRNA expression levels of TNF-α (A) and MCP-1 (B) in mouse brain. Data represent mean ± SEM for each group (n=4). $^{**}p<0.001$ compared to control.

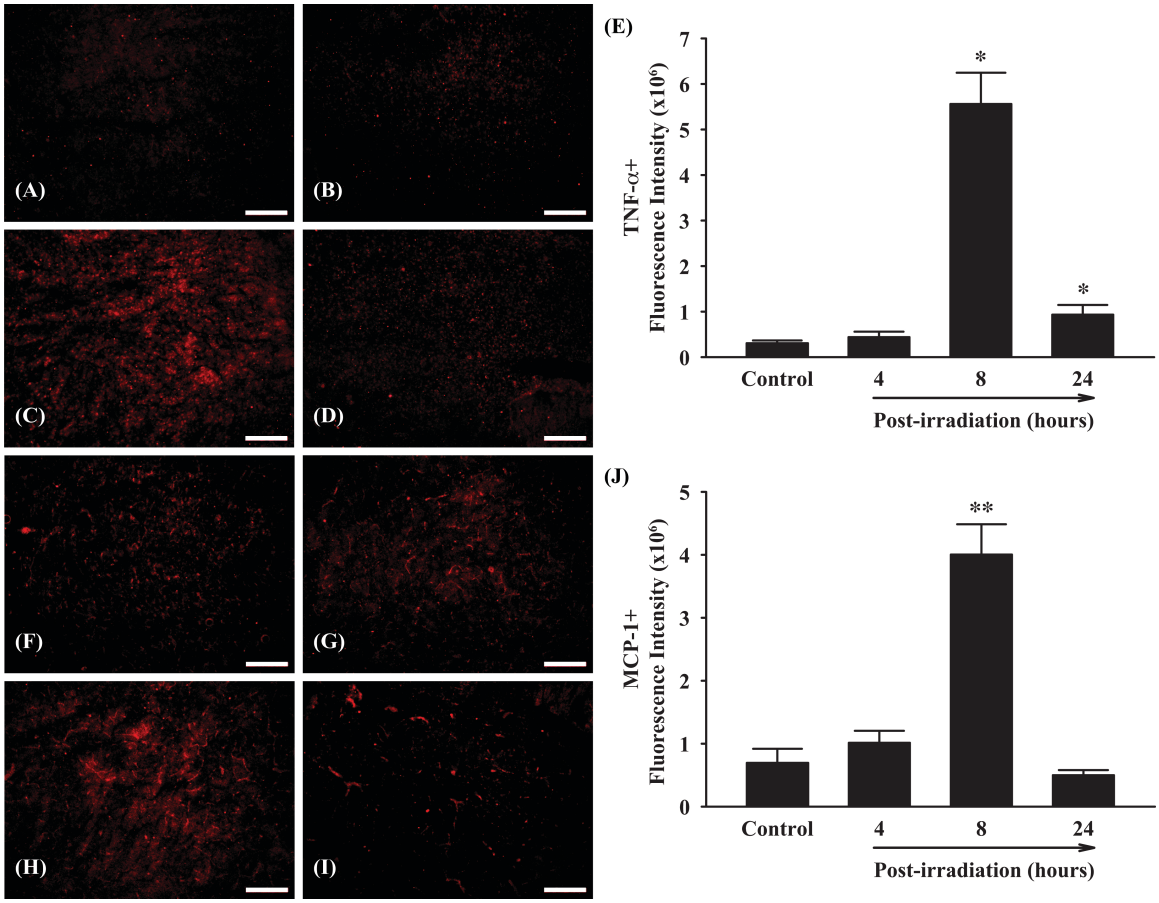

Figure 4.2. Effect of Fractionated Whole-brain Irradiation on Protein Expression of TNF-α and MCP-1 in Mouse Brain. Immunoreactivity of TNF-α (A-D) and MCP-1 (F-I) were visualized in mouse brain. Fractionated whole-brain irradiation significantly up-regulated protein expression levels of TNF-α and MCP-1 in mouse brain (E and J). (A and F) Sham-irradiation (Control); (B and G) 4 h post-irradiation; (C and H) 8 h post-irradiation; (D and I) 24 h post-irradiation; (E and J) Quantitative analysis of fluorescence intensity. Data represent mean ± SEM for each group (n=4). $^{*}p<0.05$; $^{**}p<0.001$ compared to control. Scale bar: 200 μm.

4.4.2. Fractionated Whole-brain Irradiation Increases Microglial Activation in Mouse Brain

To determine whether fractionated whole-brain irradiation affects microglial activation, the changes in protein expression levels of Iba1, a microglial activation marker, in mouse brains were visualized by immunofluorescence staining (Figure 4.3). A strong Iba1-positive immunoreactivity was detected at 4 h post-irradiation in mouse brains (16.96-fold increase) and reached to a maximum at 8 h post-irradiation (85.02-fold increase). These data demonstrate that fractionated whole-brain irradiation induces activation of microglia in mouse brain.

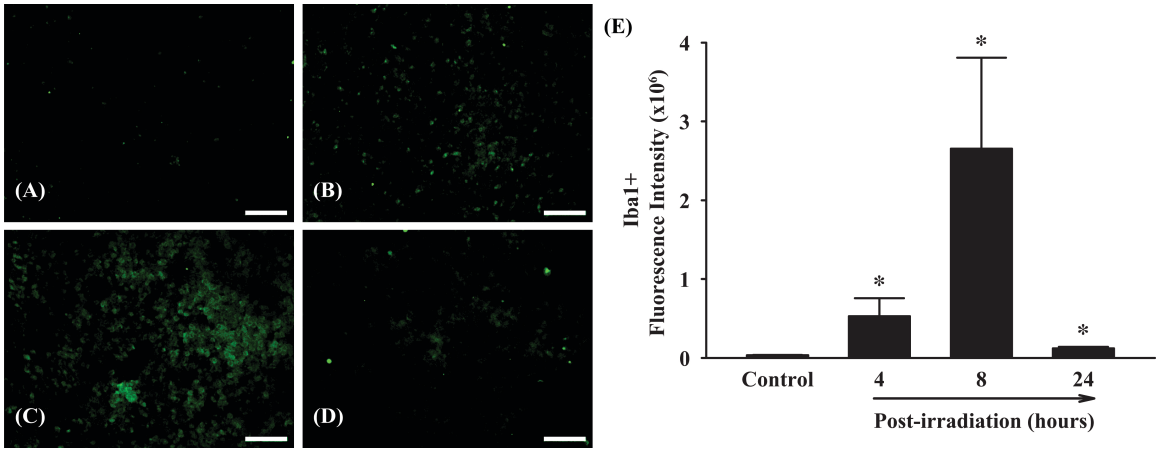

Figure 4.3. Effect of Fractionated Whole-brain Irradiation on Microglial Activation in Mouse Brain. Immunoreactivity of ionized calcium binding adaptor molecule 1 (Iba1) was visualized in mouse brain. Fractionated whole-brain irradiation significantly increased microglial activation in mouse brain (E). (A) Sham-irradiation (Control); (B) 4 h post-irradiation; (C) 8 h post-irradiation; (D) 24 h post-irradiation; (E) Quantitative analysis of fluorescence intensity. Data represent mean ± SEM for each group (n=4). $^{*}p<0.05$ compared to control. Scale bar: 100 μm.

4.4.3. Fractionated Whole-brain Irradiation Increases ROS Generation in Mouse Brain

To examine whether fractionated whole-brain irradiation affects ROS generation, *in situ* DHE fluorescence staining for superoxide anion was performed. As depicted in Figure 4.4, significantly elevated levels of superoxide anion were observed at 4, 8, and 24 h post-irradiation compared with sham-irradiated control mouse brain. Quantitative analysis exhibited that fractionated whole-brain irradiation significantly increased ROS generation by 6.32-fold (4 h post-irradiation), 2.61-fold (8 h post-irradiation) and 2.63-fold (24 h post-irradiation), respectively. These results suggest that fractionated whole-brain irradiation produces pro-oxidative environment in mouse brain.

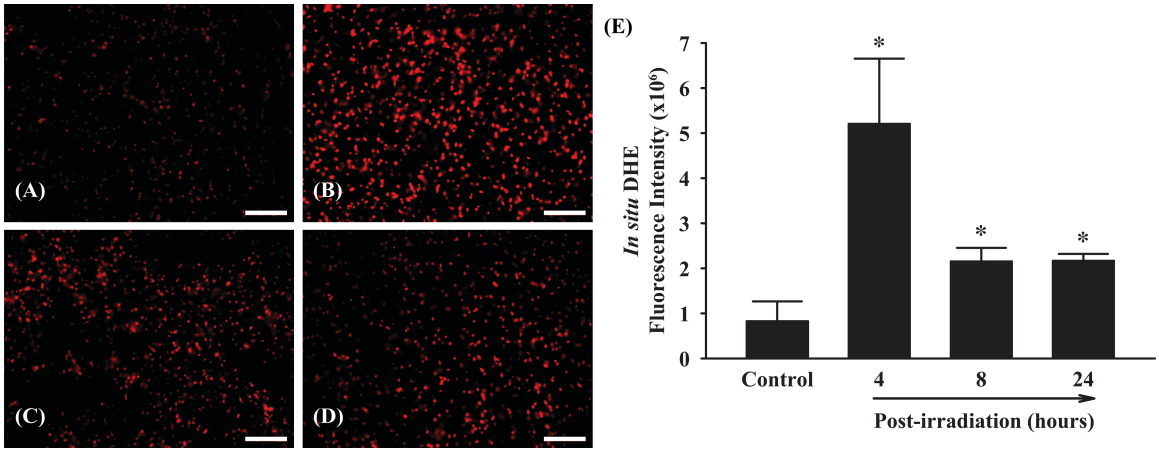

Figure 4.4. Effect of Fractionated Whole-brain Irradiation on Reactive Oxygen Species (ROS) Generation in Mouse Brain. The localization of red fluorescence demonstrates ROS generation in mouse brain (A-D). Fractionated whole-brain irradiation significantly increased superoxide anion formation in mouse brain (E). (A) Sham-irradiation (Control); (B) 4 h post-irradiation; (C) 8 h post-irradiation; (D) 24 h post-irradiation; (E) Quantitative analysis of fluorescence intensity. Data represent mean ± SEM for each group (n=4). $^{*}p<0.05$ compared to control. Scale bar: 100 μm.

4.4.4. Fractionated Whole-brain Irradiation Up-regulates Protein Expression Levels of NOX-2 and SOD1 in Mouse Brain

To elucidate the potential mechanisms of ROS generation, effects of fractionated whole-brain irradiation on protein expression levels of NOX-2, a ROS-generating enzyme, and SOD1, a ROS-scavenging enzyme, in mouse brain were examined. Significant increases in NOX-2-positive immunoreactivity were detected in mouse brain at 4 and 8 h post-irradiation (Figure 4.5A to 4.5D). Interestingly, strongly increased SOD1 expression was also observed at 8 h post-irradiation (Figure 4.5F to 4.5I). Quantitative analysis showed that fractionated whole-brain irradiation markedly up-regulated NOX-2 protein expression by 4.85-fold (4 h post-irradiation) and 14.68-fold (8 h post-irradiation) compared with sham-irradiated control mouse brain (Figure 4.5E). In contrast, SOD1 protein expression was significantly induced by 34.46-fold only at 8 h post-irradiation in mouse brain (Figure 4.5J). These data demonstrate that fractionated whole-brain irradiation differentially regulates protein expressions of NOX-2 and SOD1 in mouse brain.

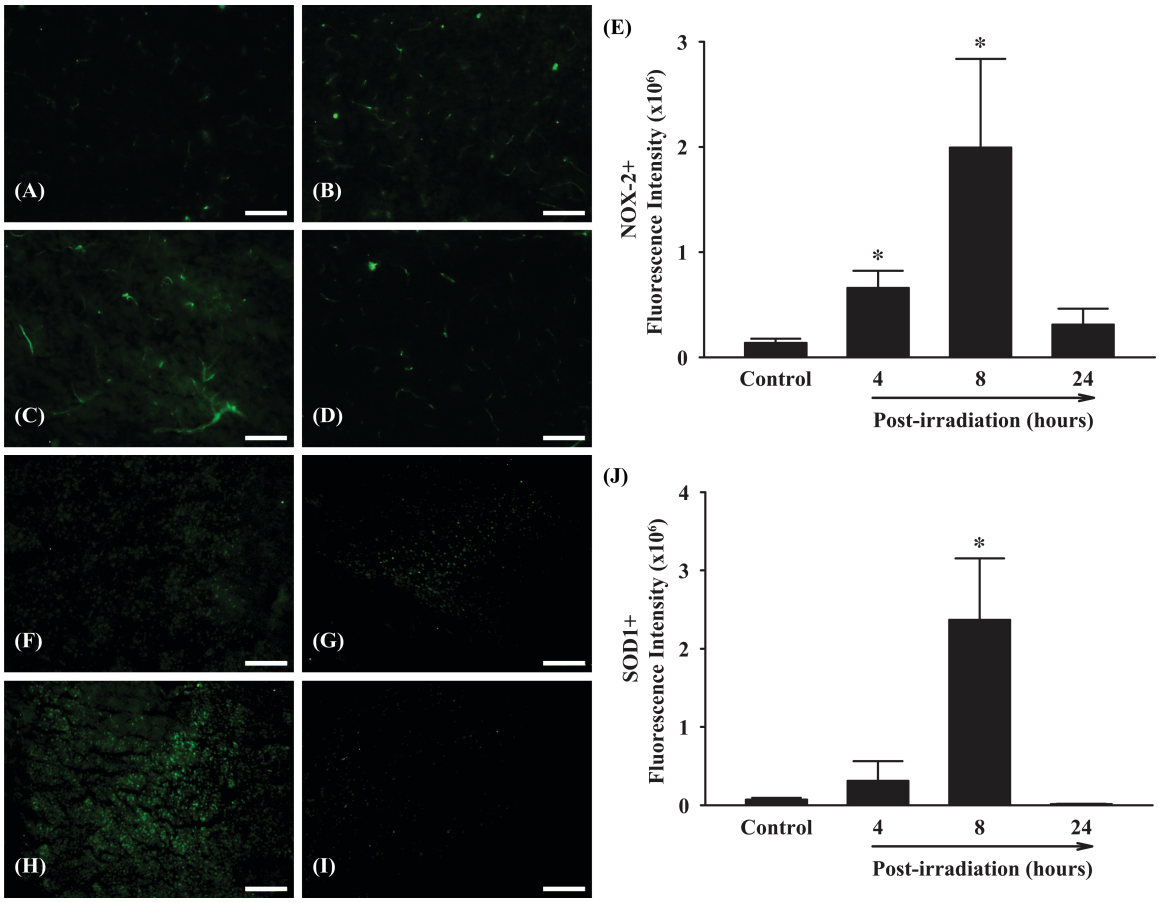

Figure 4.5. Effect of Fractionated Whole-brain Irradiation on NADPH Oxidase-2 (NOX-2) and Superoxide Dismutase 1 (SOD1) Expression in Mouse Brain. Immunoreactivities of NOX-2 (A-D) and SOD1 (F-I) were visualized in mouse brain. Fractionated whole-brain irradiation significantly up-regulated protein expression levels of NOX-2 and SOD1 in mouse brain (E and J). (A and F) Sham-irradiation (Control); (B and G) 4 h post-irradiation; (C and H) 8 h post-irradiation; (D and I) 24 h post-irradiation; (E and J) Quantitative analysis of fluorescence intensity. Data represent mean ± SEM for each group (n=4). $^{*}p<0.05$ compared to control. Scale bar: NOX-2 (100 μm) and SOD1 (200 μm).

4.4.5. NOX Inhibitors and NOX-2 Neutralizing Antibody Attenuate ROS Generation in Irradiated Mouse Brain

To further delineate the role of NOX-2, effects of NOX inhibitors, such as apocynin (APO) and diphenyleneiodonium (DPI), and NOX-2 neutralizing antibody on ROS generation in irradiated mouse brain were examined. As demonstrated in Figure 4.6A to 4.6E, both NOX inhibitors (APO and DPI) and NOX-2 neutralizing antibody (Anti-NOX-2) markedly decreased ROS generation compared with irradiated mouse brain (fractionated whole-brain irradiation:

FIR). Quantitative analysis demonstrated that fractionated whole-brain irradiation-induced ROS generation in mouse brain was significantly attenuated by APO (1.76-fold), DPI (4.16-fold), and anti-NOX-2 (4.37-fold), respectively (Figure 4.6F). These results indicate that NOX-2 may play a role in ROS-generating pathways induced by fractionated whole-brain irradiation.

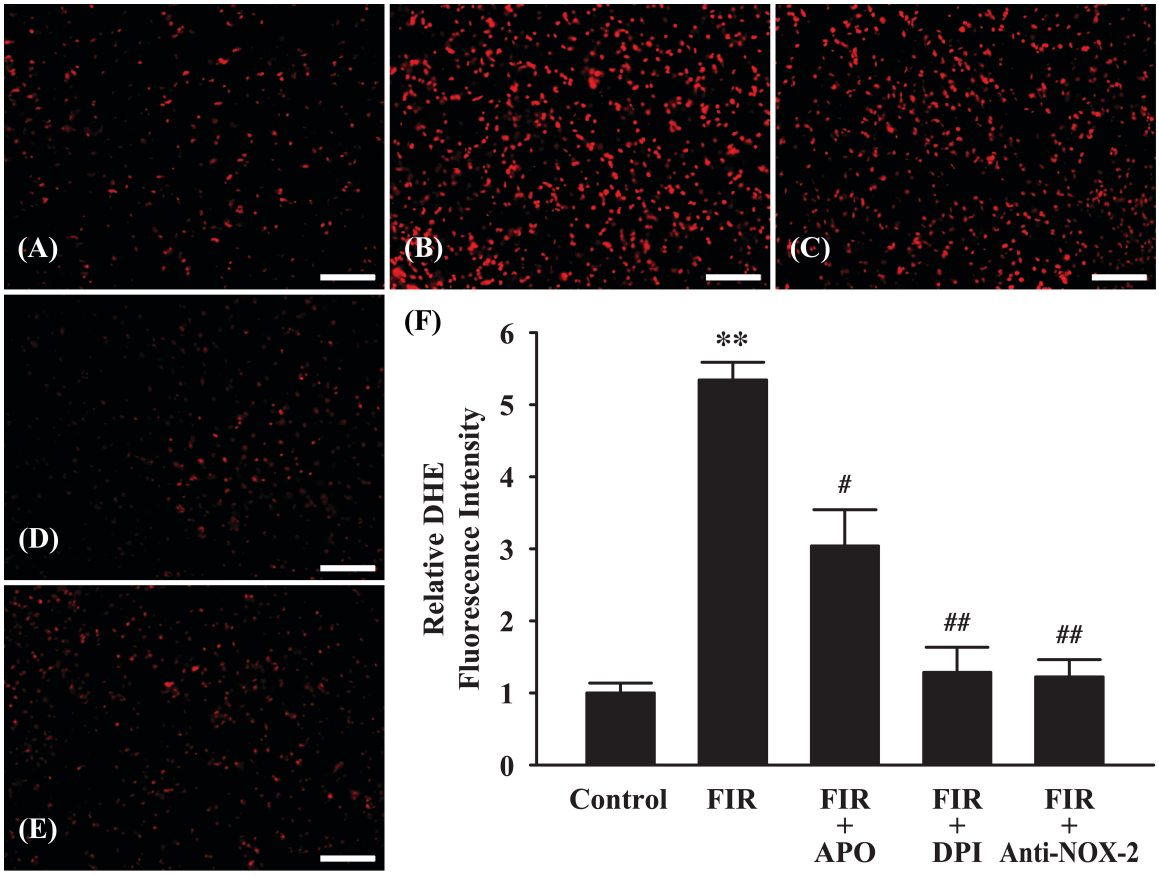

Figure 4.6. Effect of NADPH Oxidase (NOX) Inhibitors and NOX-2 Neutralizing Antibody on Radiation-induced ROS (Superoxide Anion) Generation in Mouse Brain. An increase in ROS generation in mouse brain 4 h after fractionated whole-brain irradiation (FIR) was markedly and significantly attenuated in the presence of NOX inhibitors (FIR + APO or FIR + DPI) or NOX-2 neutralizing antibody (FIR + anti-NOX-2). (A) Sham-irradiation (Control); (B) 4 h after fractioned whole-brain irradiation (FIR); (C) FIR + 1 mM apocynin (APO); (D) FIR + 20 μM diphenyleneiodonium (DPI); (E) FIR + anti-NOX-2 antibody; (F) Quantitative analysis of fluorescence intensity. Data represents mean ± SEM for each group (n=4). $^{**}p<0.001$ compared to control, $^{\#}p<0.05$; $^{\#\#}p<0.001$ compared to irradiated brain (FIR). Scale bar: 100 μm.

4.5. Discussion

The recent clinical findings associated with radiation exposure to brain tumor patients indicate that various primary cognitive regions are affected and may be even developed to cognitive-communicative deficits, which can significantly affect their quality of life [123-125, 240-245]. Progressive impairments in learning and memory, such as decreased verbal memory, spatial memory, attention, and novel problem solving ability, were observed in 40~50% of brain tumor patients as long-term consequences of radiation therapy. In addition, pre-clinical studies have shown the pathological consequence of radiation-induced hippocampal damage in animal models with severe neurobehavioral deficits [46, 117-119, 126, 128, 130, 131, 144, 150, 246-248]. At present, there are no successful therapies or effective prevention strategies for radiation-induced brain injury.

Recent studies have demonstrated that pro-oxidative and pro-inflammatory environments have been, at least in part, implicated in the radiation-induced brain injury [46, 107, 132-134, 136, 138, 140, 142]. However, details of specific molecular and cellular mechanisms of oxidative stress and inflammation in radiation-induced brain injury remain unclear. Prognosis of radiation-induced brain injury by evaluating time-course of ROS induction in addition to analyses of gene and protein expressions of pro-inflammatory mediators may contribute to understanding selective biochemical pathways leading to neurodegeneration in fractionated whole-brain irradiated brain. In the present study, we demonstrated that NADPH oxidase may contribute to molecular and cellular responses in radiation-induced oxidative stress and inflammation following fractionated whole-brain irradiation.

The present study first observed enhanced expression of pro-inflammatory mediators, such as cytokine and chemokine, in the brain following fractionated whole-brain irradiation. A significant increase of TNF-α, a pro-inflammatory cytokine and critical regulator of immune activation, and MCP-1, a member of CC chemokine family playing a critical role in monocyte chemotaxis and transmigration [45], was observed following fractionated whole-brain irradiation. In a previous study [46], mRNA and protein expression levels of TNF-α, IL-1β, and MCP-1 were significantly up-regulated in hippocampal and cortical regions isolated from rat brain irradiated with a single, large dose (10 Gy). In addition, there are several reports demonstrating up-regulation of a variety of other pro-inflammatory markers, including IL-6,

macrophage inflammatory protein 2 (MIP-2), ICAM-1, iNOS, and cyclooxygenase-2 (COX-2), may be associated with the molecular responses of the brain to a single, large dose (10, 25 or 35 Gy) of irradiation [132, 133, 135, 137, 249]. Therefore, these studies provide sufficient evidence demonstrating the potential contribution of pro-inflammatory environment to radiation-induced brain injury. Moreover, a clinically relevant fractionated radiation regimen in the current study may provide more reliable information of the events occurring after a clinical whole-brain irradiation compared with a single, large dose irradiation. According to the linear quadratic model [250] with an assumption of α/β ratio of 3 Gy for late responding effects in the brain, the biologically effective dose (BED) of fractionation regimen (a total of 40 Gy; 8 fractions of 5 Gy in 4 weeks resulting in 106.7 Gy) in this study is correspond to a typical regimen in the clinic, such as 30 fractions of 2 Gy (a total of 60 Gy) in 6 weeks resulting in 100.2 Gy. Therefore, biological effect under current fractionated whole-brain irradiation regimen may be more relevant to the clinical situation than those after a single, large dose of irradiation in the aforementioned previous studies. Our results further revealed that the peak mRNA and its concomitant protein expressions of TNF-α and MCP-1 occurred at 4 and 8 h post-irradiation, respectively (Figure 4.1 and 4.2). These time-course analyses suggest that mRNA and protein expression levels of pro-inflammatory mediators at different time points may be critically associated with pathological prognosis of radiation-induced brain injury.

Although the potential contribution of complex and dynamic multiple cell types within the brain to the overexpression of pro-inflammatory mediators after irradiation remains unclear, microglia, the primary immune effector cells in the CNS, are considered as a key causative player in this process [19]. In the present study, the results indicated that a significant increase in microglial activation was detected in irradiated brain (Figure 4.3). Previous *in vitro* studies [46, 135, 251, 252] suggested whole-brain irradiation-mediated pro-inflammatory environments in the brain may be mediated through activation of microglia that resulted in a significant up-regulation of mRNA and protein expressions of pro-inflammatory mediators including TNF-α, IL-1β, IL-6, COX-2, and MCP-1. In addition, *in vivo* studies support that an overexpression of pro-inflammatory mediators [46, 134, 135] and an increase in the number of activated microglia [140, 253, 254] were detected in the brain following irradiation. Our data also indicate that fractionated whole-brain irradiation significantly activated microglia at 4 h post-irradiation and the activation reached maximum at 8 h post-irradiation, suggesting that microglial activation is

responsible for acute inflammatory responses, such as up-regulation of TNF-α and MCP-1 expressions.

Recent evidence has identified oxidative stress as one of the mechanistic pathways leading to radiation-induced brain injury [112, 141, 142, 234-236, 255]. In the present study, ROS generation following fractionated whole-brain irradiation was observed by *in situ* DHE fluorescence staining in mouse brain. Interestingly, a significant increase of ROS generation was reached its peak at 4 h post-irradiation and maintained highly up to 24 h post-irradiation (Figure 4.4). In a previous *in vitro* study [141], levels of ROS were elevated in a dose-dependent manner from 6 h after exposure of X-rays in neural precursor cells. Another recent *in vitro* study [142] demonstrated that irradiation on brain endothelial cells caused a significant, dose-dependent increase in ROS generation using 2',7'-dichlorofluorescein (DCF) at 1 h post-irradiation. Therefore, these findings from other groups support that irradiation causes an acute response of redox system in the brain. More importantly, the novel findings in this study are time-dependent ROS generation and concomitant inflammatory response. It is still unclear whether oxidative response precedes inflammatory event or *vice versa*; however, due to an early imbalance in the redox system observed at 4 h post-irradiation compared with the significant protein induction of inflammatory mediators (TNF-α and MCP-1) at 8 h post-irradiation, it is possible that the radiation-induced increase in oxidative stress may be responsible for these pro-inflammatory events (Figure 4.1, 4.2 and 4.4). Although more information on oxidative stress following irradiation in the brain is vital in the understanding of chronic effects, these data suggest that radiation-mediated induction of oxidative stress plays a critical role in the cerebral damage following fractionated whole-brain irradiation.

To elucidate origin of ROS generation following fractionated whole-brain irradiation, we investigated expression levels of two different enzymes, NOX-2 and SOD1. NOX-2, the primary phagocytic oxidase [239, 256, 257], has been frequently studied and demonstrated its critical role of ROS formation in glial cells and neurons under neuropathological conditions, such as neurodegenerative diseases [237, 258-264]. In the present study, we demonstrated that NOX-2 expression was markedly elevated at 4 and 8 h post-irradiation (Figure 4.5A to 4.5E) and its pharmacological inhibitions (DPI, APO, and a neutralizing antibody) dramatically ameliorated the radiation-induced increase in the production of ROS (Figure 4.6), which strongly suggest NOX-2 contributes to radiation-induced oxidative stress. Furthermore, our investigation of

SOD1, one of the first line defense systems against excessive ROS in cells and tissues, revealed that its expression was significantly up-regulated at 8 h post-irradiation. Interestingly, our data indicated that a transiently less expression of SOD1 at 4 h post-irradiation, taken together with a significant up-regulation of NOX-2, may account for a cause of excessive ROS after 4 h post-irradiation (Figure 4.4) and play a major role in the redox imbalance status of brain after irradiation. Previous studies have observed specific markers in the redox system to investigate a primary cause of excessive ROS generation after irradiation [142, 235, 265, 266]. The time-course for the effects of irradiation on redox balance with concomitant differential changes in molecular and cellular responses, however, has not yet been explored. To our knowledge, this is the first report demonstrating that a time-dependent analysis of redox system in balance between pro-oxidant and antioxidant enzymes in irradiated brain. The detailed mechanism(s) underlying our observation is still unknown and needs to be further investigated.

4.6. Conclusions

The present study demonstrated the evidence that NOX-2 may play a potential role in fractionated whole-brain irradiation-mediated pro-oxidative and pro-inflammatory pathways in mouse brain. These findings may provide a foundation for defining cellular and molecular basis of radiation-induced brain injury that will lead to new opportunities for preventive and therapeutic interventions for brain tumor patients who receive radiation therapy.

4.7. Acknowledgments

The work was supported by Grant Number R01NS056218 from the National Institute of Neurological Disorders and Stroke.

CHAPTER 5:

DEVELOPMENT OF AN *IN VITRO* 3D BRAIN INFLAMMATION MODEL

* **Cho HJ**, Verbridge SS, Davalos RV, Lee YW. Tissue Engineering, Part A, 2015; In preparation.

5.1. Abstract

Given the growing interest in development of therapeutic approaches against brain diseases, there is an increasing demand for physiologically relevant experimental model systems *in vitro*. Hydrogels have been widely employed as potential biomimetic scaffolds because of their three-dimensional (3D) properties mimicking the hydrated microenvironment of native extracellular matrix (ECM). In the present study, we designed and constructed a 3D experimental model system to investigate cellular responses and molecular interactions of brain inflammation *in vitro*. Type I collagen containing the murine microglial cell line, BV-2, was used to develop an *in vitro* 3D brain inflammation model. The finite element modeling of oxygen diffusion and cellular oxygen consumption predicted the oxygen profile within 3D structures. Live/dead viability/cytotoxicity analyses of experimental 3D constructs supported the mathematical analysis and determined the optimal 3D construct with initial cell seeding density of 1×10^6 cells/ml and 72-h growth. Traditional two-dimensional (2D) cell culture and *in vivo* studies were used for comparison. To generate pro-oxidative and pro-inflammatory environments in *in vitro* 2D/3D and *in vivo* model systems, BV-2 cells and C57BL/6J mice were exposed to lipopolysaccharide (LPS). Real-time RT-PCR analyses and ELISA demonstrated a significant up-regulation of pro-inflammatory mediators, such as tumor necrosis factor-α (TNF-α), monocyte chemoattractant protein-1 (MCP-1), interleukin-6 (IL-6), and interleukin-1β (IL-1β), in LPS-stimulated *in vitro* 2D/3D and *in vivo* model systems. Interestingly, the levels of inflammatory responses from *in vitro* 3D model system were more similar to *in vivo* than *in vitro* 2D. Additionally, *in situ* DHE assays and immunofluorescence staining revealed that the levels of LPS-stimulated ROS generation and microglial activation from *in vitro* 3D model system were close to *in vivo* compared with *in vitro* 2D. These results demonstrated that an *in vitro* 3D model system, newly developed in the present study, provides more physiologically relevant pro-oxidative and pro-inflammatory environments in the brain than traditional *in vitro* 2D models.

Key words: 3D collagen hydrogel, LPS, ROS, Inflammation, TNF-α, MCP-1, IL-6, IL-1β, Microglial activation

5.2. Introduction

Providing a 3D support to cells may recapitulate temporal and spatial complexity of extracellular matrix (ECM) *in vivo* and allow careful study of cellular behaviors under physiologically relevant and *in vivo*-like environment. Specifically, a three-dimensional (3D) culture has been represented as more accurate experimental model of *in vivo* compared with a two-dimensional (2D) culture due to various benefits. For example, *in vitro* 3D model systems mimic *in vivo*-like cytostructures, delivering a better knowledge of cell-cell and cell-matrix interactions [11, 151-154]. In addition, *in vitro* 3D model systems provide a high surface area for cell growth and migration, which may promote cell survival and response upon extracellular cues [11, 14, 155-157]. Furthermore, *in vitro* 3D model systems may provide protection from environmental disturbances by physiologically stable structures [267]. Moreover, cells encapsulated within *in vitro* 3D model systems exhibit amoeboid shape, which is more physiologically relevant morphology, while cells growing in *in vitro* 2D model system yield only a flat and stretched shape [11, 13, 158-161].

Hydrogels have been broadly explored to provide a distinctive and attractive matrix for ECM development due to their excellent cellular compatibilities of mimicking biochemical (e.g., proteins and peptides) and mechanical (e.g., modulus) properties of *in vivo* microenvironments [162-169]. Particularly, hydrogels formed from type I collagen have been a popular 3D scaffold with several excellent properties. Collagen is a cytocompatible natural polymer in tissues and the most abundant (up to 35% of the whole body protein content) protein in mammals. In addition, collagen plays a key role in cell adhesion to ECM by presenting several integrin-binding sites, such as arginine-glycine-aspartic acid sequence, and provides self-assembling capability to construct a fibrillar structure in physiological environments [156, 170-173]. Furthermore, collagen hydrogels are useful for investigating the effects of physical activation triggers [268, 269].

Despite considerable progress in the development of *in vitro* 3D tissue engineering with biomimetic hydrogels, there remains a challenge of limited information linking nutrient transport and cellular distribution in the field of tissue-engineered 3D culture system. The interaction between 3D scaffold and metabolic demand (e.g., oxygen and glucose) is crucial to sustain functional cellular microenvironment in 3D culture system. In particular, oxygen is a crucial

participant in cell life for maintaining the existence of all multicellular organisms by its regulation of cellular metabolism, proliferation, migration, differentiation, and cell-cell interactions [270-272]. Failure to attain dynamic equilibrium of essential oxygen demand in time and space through tissue-engineered 3D constructs may result in non-functional tissues. Indeed, previous studies have emphasized that insufficient supply of nutrients including oxygen throughout the 3D system may lead to impairing engineered tissues [273-275].

Microglia, the primary immune cells in the central nervous system (CNS), play a crucial role in the brain injury and disease [174-176]. Although microglia had long been thought of as simply a stromal cell, recent studies have revealed that microglia are sensitive to pathological variations of the brain microenvironment, subsequently leading to CNS diseases or injuries [177, 178]. Previous *in vivo* studies have demonstrated that microglial activation intensely involves in increase in oxidative stress and induction of inflammation in various neurodegenerative diseases [179-182].

In the present study, we developed an *in vitro* 3D experimental model system containing microglia, investigated cellular responses and molecular interactions after treatment with pro-oxidative and pro-inflammatory stimulus, and compared the 3D system with conventional *in vitro* 2D and *in vivo* systems.

5.3. Materials and Methods

5.3.1. Cell Culture

The murine microglial cell line, BV-2 cells, was kindly provided from Dr. Michael E. Robbins (Wake Forest University Medical Center, Winston-Salem, NC) and cells were cultured in Dulbecco's modified eagle medium (DMEM; Hyclone Laboratories, Inc., Logan, UT) with 5% fetal bovine serum (FBS; Mediatech, Inc., Manassas, VA) containing 100 unit/ml of penicillin, and 100 μg/ml of streptomycin. Cells were cultured at 37 °C with 5% CO_2 and 95% air under a humid atmosphere. To stimulate microglia into an inflammatory phenotype, cells were incubated with 100 ng/ml of lipopolysaccharide (LPS; Sigma-Aldrich, St. Louis, MO) for 4 and 24 h to investigate molecular and cellular changes, respectively.

5.3.2. Preparation of an In Vitro 3D Collagen Hydrogel and 3D Cell Culture

Based on previous study [276], type I collagen extracted from rat tails was used to construct an *in vitro* 3D structure. Briefly, 0.1 ml of type I collagen stock (1.5% w/v in 0.1% v/v acetic acid) was neutralized with 0.002 ml of NaOH (Sigma-Aldrich) and 0.025 ml of 10× DMEM (Sigma-Aldrich) on ice. The appropriate volume of concentrated cell suspension containing microglia in 0.123 ml of 1× DMEM was then mixed into the neutralized collagen solution. The collagen solution with cells was then placed into 24 well-plate by polydimethylsiloxane (PDMS) wells, creating cylindrical collagen structures with 4 mm diameter and 2 mm thick, and allowed to polymerize at 37 °C with 5% CO_2 for 30 min (Figure 5.1). After polymerization, collagen hydrogel with cells were incubated with complete culture medium.

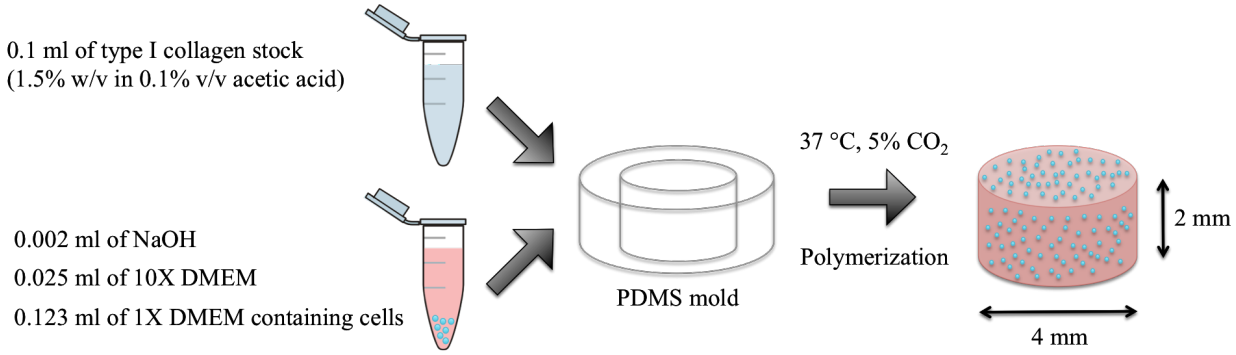

Figure 5.1. Preparation of an *In Vitro* 3D Model System Using Type I Collagen Hydrogel.

5.3.3. Animals

Eight-week-old male C57BL/6 mice were purchased from The Jackson Laboratory (Bar Harbor, ME). Animals were maintained under environmentally controlled conditions and subject to a 12-h light:12-h dark cycle with food and water *ad libitum*. All protocols in this study were approved by the Institutional Animal Care and Use Committee and were conducted in accordance with the National Institutes of Health Guide for the Care and Use of Laboratory Animals. To generate inflammation in the brain, mice were intraperitoneally injected with a single dose of LPS (0.5 mg/kg) in 0.2 ml of saline. Control groups only received 0.2 ml of saline.

5.3.4. Tissue Collection and Preparation

Animals at 4 and 24 h following LPS or saline exposure (n=5 per group) were briefly anesthetized with isoflurane (3%) and transcardially perfused with ice-cold phosphate phosphate-buffered saline (PBS) containing 6 unit/ml heparin. Two hemispheres of brains were then dissected following the rapid whole brain removal, immediately frozen in dry ice, and stored at −80 °C until analysis; the left hemispheres were dissected for real-time RT-PCR analysis and ELISA. The right hemispheres were cryopreserved in 30% sucrose solution for 24 h and processed in Tissue-Tek® optimal cutting temperature (O.C.T.) embedding medium (Sakura Finetek USA, Inc., Torrance, CA). Serial 20 μm-thick sagittal sections were prepared for *in situ* ROS detection and immunofluorescence staining.

5.3.5. Oxygen Consumption Rate and Finite Element Modeling

The basal BV-2 O_2 consumption was measured using a XF24 extracellular flux analyzer (Seahorse Bioscience, North Billerica, MA). Briefly, cells were seeded into 24-well plates (XF24 cell culture microplates) at 3×10^4 cells per well for 24 h in complete media. Prior to the assay, the culture medium was replaced with DMEM without sodium bicarbonate and phenol red and placed in an incubator without CO_2 for 1 h. The dissolved oxygen in the medium surrounding the cells was then measured by solid-state fluorescence sensors, and oxygen consumption rate of microglia was calculated. The oxygen concentration levels within 3D hydrogels were initially estimated using a mathematical model with an assumption of consumption kinetics as zeroth-order. Therefore, the oxygen consumption $\left[R\left(C_{O_2}\right);\ mol/m^3 \cdot s\right]$ of cells was treated depending on the spatial cell density $[\rho_{Cell};\ cells/ml]$ and oxygen consumption rate by cells $\left[R_{O_2,cell}\ ;\ mol/cell \cdot s\right]$ using the following simplified equation, $R\left(C_{O_2}\right) = \rho_{Cell} R_{O_2,cell}$. In addition, the population of cells over time was predicted by logistic cell growth.

$$N\ (t) = \rho_{cell} \cdot V_{3D\ construct} = \frac{KN_0}{N_0 + (K - N_0)e^{-rt}}$$

where $N\ (t)$ is the cell numbers as a function of time (t), $V_{3D\ construct}\ [m^3]$ is the 3D hydrogel volume, K is the carrying capacity, $N_0\ [cells]$ is the initial cell seeding numbers, and $r\ [h^{-1}]$ is the cell growth rate, respectively. Estimated parameters of logistic cell growth, K and r, were

experimentally predicted using MATLAB software (The MathWorks, Inc., Natick, MA). Along with consumption kinetics and logistic cell growth, the final cross-sectional oxygen profile of was computed by solving the following mass balance equation:

$$\frac{\partial C_{O_2}}{\partial t} = D\nabla^2 C_{O_2} - R\left(C_{O_2}\right)$$

where C_{O_2} $[mol/m^3]$ is the concentration of oxygen as a function of time (t) and position and D $[m^2/s]$ is the oxygen diffusion constant for water, respectively. The partial pressure of oxygen (P_{O_2}) was calculated by using Henry's law and approximating the solubility of oxygen in water; $P_{O_2} = HC_{O_2}$ where H is the Henry's law constant for oxygen in water at 37°C: $H = 584.6$ $[m^3 \cdot mmHg/mol]$. The solution for oxygen profile within the 3D structure over time was calculated with the finite element modeling using commercial software package Comsol Multiphysics (Comsol Inc., Burlington, MA), assuming a fixed boundary concentration at 21% O_2 $\left[C_{O_2,0} = 273\ \mu M\right]$.

5.3.6. Live/Dead Cell Viability/Cytotoxicity Assay

A LIVE/DEAD® viability/cytotoxicity kit (Molecular Probes, Eugene, OR) was used to determine viable/dead cell populations in 3D culture systems according to the protocol provided by the supplier. Briefly, after cell culture, 3D collagen hydrogels were rinsed with PBS twice and incubated in PBS containing calcein-AM (2 μM) and ethidium homodimer-1 (4 μM) at 37 °C in 5% CO_2 for 45 min. After washing with PBS twice, live and dead cells were imaged by fluorescence microscopy.

5.3.7. Real-time RT-PCR

Total RNA from *in vivo* and *in vitro* 3D model systems were isolated as described previously [277] while total RNA from *in vitro* 2D model system was isolated and purified using RNeasy Mini Kit (Qiagen, Valencia, CA) according to the protocol of the manufacturer. Quantitative real-time RT-PCR using TaqMan probes and primers were used for gene expression analyses and amplification of individual genes was performed with Applied Biosystems 7300 real-time PCR system using TaqMan Universal PCR Master Mix and a standard thermal cycler

protocol. TaqMan Gene Expression Assay Reagents for mouse pro-inflammatory genes, including tumor necrosis factor-α (TNF-α), monocyte chemoattractant protein-1 (MCP-1), interleukin-6 (IL-6), and interleukin-1β (IL-1β), and housekeeping gene (GAPDH) were used for specific probes and primers of PCR amplifications. The threshold cycle (C_T) was determined, and relative quantification was calculated by the comparative C_T method as described previously [46].

5.3.8. ELISA

Secreted proteins of 2D cell culture supernatants were collected after LPS stimulation while homogenates from mouse brains and *in vitro* 3D collagen hydrogels after LPS stimulation were prepared as described previously [278]. Protein concentrations of homogenates and cell culture supernatants were determined as described by Bradford [191]. The protein expression levels of pro-inflammatory mediators in collected samples were determined by using Quantikine® Mouse Immunoassay Kits for TNF-α, MCP-1, IL-6, and IL-1β (R&D Systems, Minneapolis, MN) following to the manufacturer's protocols.

5.3.9. Immunofluorescence Staining

Frozen brain tissue sections (20 μm) were analyzed by immunofluorescence staining as described previously [278]. The primary antibody, rabbit anti-Iba1 (1:200), and its corresponding secondary antibody, goat anti-rabbit IgG conjugated with Alexa Fluor 555 (1:400), was utilized to detect Iba1 protein expression. Samples were mounted with a mounting medium with DAPI, imaged and quantified as described previously [278].

5.3.10. In Situ Detection of ROS

In situ levels of superoxide anion, the main species of ROS, were measured by *in situ* dihydroethidium (DHE) fluorescence staining. Briefly, brain sections were washed with PBS and incubated with 5 μM DHE solution in a light-protected humidified chamber at 37 ˚C for 30 min. After incubation, the slides were rinsed with PBS and imaged with a Zeiss AXIO Imager A1m

fluorescence microscope. Fluorescence intensity of acquired digital images was quantified by ImageJ software.

5.3.11. Statistical Analysis

Statistical analysis of data was completed using SigmaPlot version 11 software (SPSS, Chicago, IL). A two-tailed student's t-test was applied to compare controls and experimental groups. A statistical probability (p) value of <0.05 was considered significant.

5.4. Results

5.4.1. Development of an In Vitro 3D Collagen Hydrogel With Microglia

To explore the contribution of spatial dimension on cellular and molecular responses of microglia, a 3D model comprised of BV-2-seeded 2 mm-thick type I collagen hydrogel was engineered. The basal oxygen consumption of BV-2 was measured by XF24 analyzer; $R_{O_2,cell} = 6.78 \times 10^{-17} mol/cell \cdot s$. With an assumption of uniformly distributed cells within the engineered 3D hydrogel, finite element modeling of the steady-state oxygen distribution within the 3D structure was performed with the values of initial cell seeding density, measured oxygen consumption $\left(R_{O_2,cell}\right)$, and oxygen diffusion coefficient (D) in water (Figure 5.2A). As shown in Figure 5.2B, three different oxygen concentration distributions at the point probe $(z = 0, r = 0)$ were uniformly maintained after 30 min depending on initial cell seeding densities; 20.2% at 5×10^5 $cells/ml$, 19.4% at 1×10^6 $cells/ml$, and 17.8% at 2×10^6 $cells/ml$, respectively. In addition, cross-sectional oxygen concentration distributions after 1 h were predicted according to the initial cell seeding densities (Figure 5.2D).

Moreover, oxygen concentration distribution with logistic cell growth over time was computed. In Figure 5.2C, three different profiles of partial pressure of O_2 (%) were predicted over 96 h depending on the initial cell seeding densities and corresponding estimated values of carrying capacity (K) and cell growth rate (r). After 96 h, partial pressure of O_2 (%) dramatically dropped below 0.32% in the 3D hydrogel of the initial cell seeding density with 2×10^6 $cells/ml$ while the hydrogels with the initial cell seeding density of 5×10^5 $cells/ml$

and $1 \times 10^6\ cells/ml$ remained above 5%. Furthermore, cross-sectional oxygen concentration distributions of different cell seeding densities demonstrated that higher cell density yielded a wider range of oxygen gradient within the 3D hydrogel matrix (Figure 5.2E).

In addition to mathematical analysis, cellular viability/cytotoxicity of *in vitro* 3D hydrogels with simulated cell densities $(5 \times 10^5, 1 \times 10^6, and\ 2 \times 10^6\ cells/ml)$ was employed to visualize the distribution of viable and dead cells within 3D constructs after 48, 72, and 96 h in culture (Figure 5.3A). Quantitative analysis of live and dead cells in fluorescence intensity demonstrated that the 3D construct with the initial cell seeding density of $1 \times 10^6\ cells/ml$ and 72-h growth showed the highest viability and lowest cell cytotoxicity compared to 48 and 96 h in culture (Figure 5.3B).

Based on mathematical modeling analyses and live/dead viability/cytotoxicity assay, the initial cell seeding density of $1 \times 10^6\ cells/ml$ and 72 h of growth were chosen to study physiologically relevant microglial responses within 2 mm-thick engineered 3D structures.

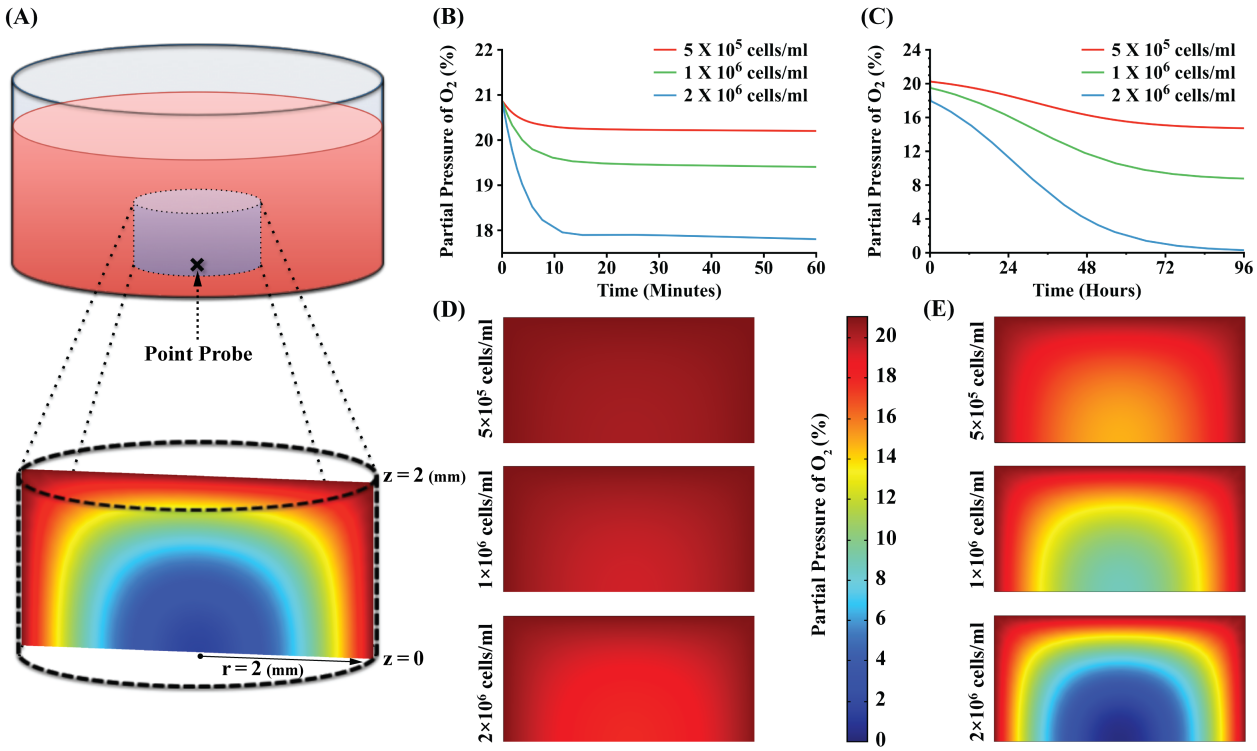

Figure 5.2. Mathematical Modeling of Oxygen Concentration Distribution Within 3D Hydrogels. Finite element model of oxygen consumption within 3D model was computationally calculated, assuming the zeroth-order consumption kinetics: $D = 2.76 \times 10^{-9} m^2/s$, $C_{O_2,0} = 273\ \mu M$, $R_{O_2,cell} = 6.78 \times 10^{-17} mol/cell \cdot s$. In these computations, boundary conditions of oxygen concentration were maintained at the surface of 3D structure $\left(C_{O_2\ @z=2\ or\ r=2} = C_{O_2,0}\right)$ and no-flux conditions were maintained at the bottom of surface $(z = 0)$. Three different cell seeding densities were applied for the calculation; $5 \times 10^5 cells/ml$, $1 \times 10^6 cells/ml$, and $2 \times 10^6 cells/ml$. (A) Schematic of *in vitro* 3D hydrogel; (B) Prediction of O_2 partial pressure (%) at the point probe during the first hour; (C) Prediction of O_2 partial pressure (%) at the point probe during 96 h with logistic cell growth; (D) Prediction of cross-sectional O_2 levels after 1 h; (E) Prediction of cross-sectional O_2 levels after 96 h.

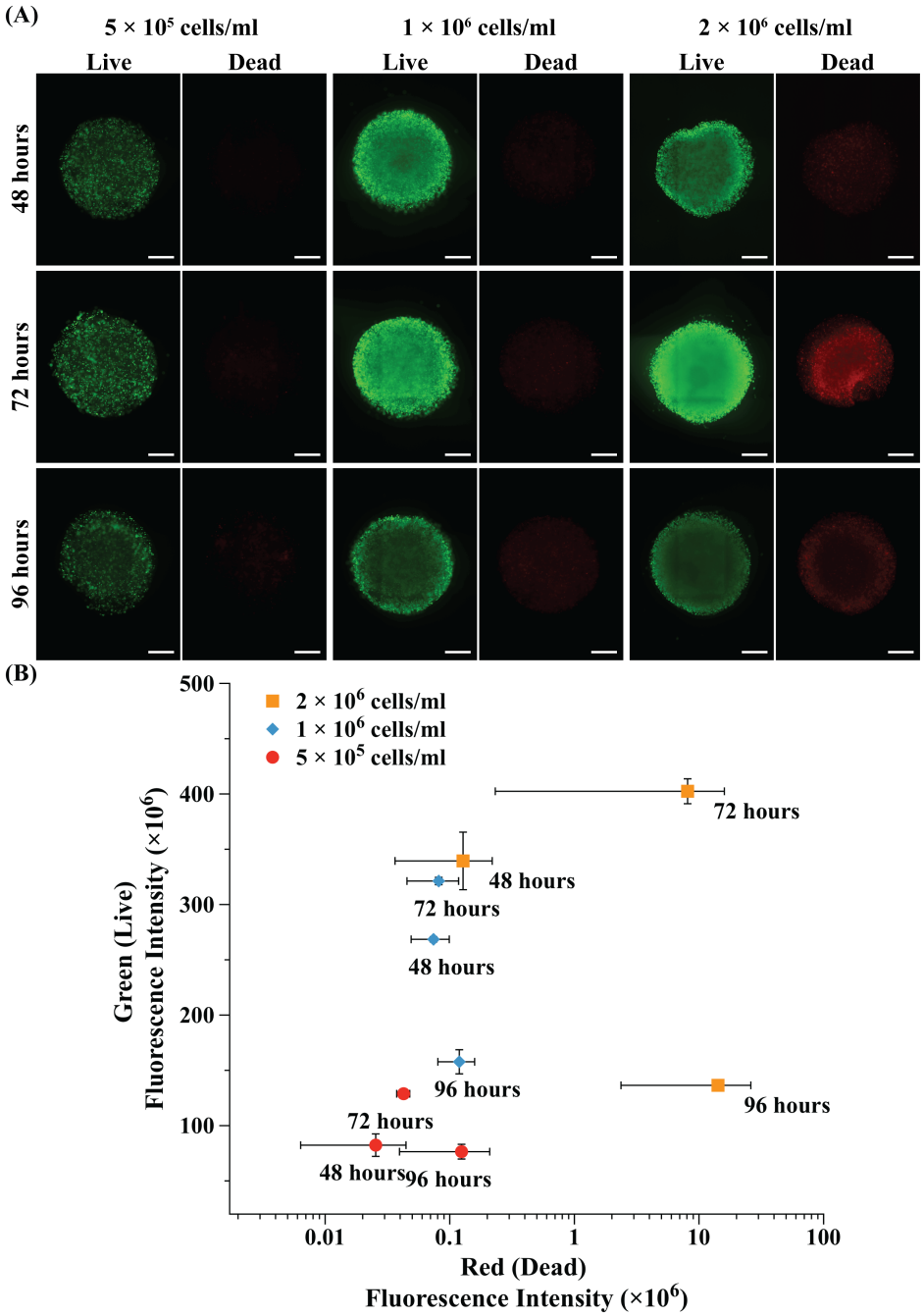

Figure 5.3. Live/Dead Cell Viability/Cytotoxicity Assay of *In Vitro* 3D Hydrogels by Fluorescence Microscopy. The fluorescence intensity of live and dead cells within the 3D hydrogel was visualized by LIVE/DEAD® viability/cytotoxicity assay kit. (A) Representative images of live and dead cells within 3D hydrogels at 1 mm-depth varying cell densities and culture times. (B) Quantitative analysis of live and dead cells within 3D hydrogels by fluorescence intensity. Data represent mean ± SEM for each group (n=3). Scale bar: 1000 μm.

5.4.2. Pro-inflammatory Responses of In Vitro 3D System After LPS Stimulation

To investigate the pro-inflammatory responses of *in vitro* 2D/3D and *in vivo* model systems, mRNA expression levels of pro-inflammatory mediators, such as TNF-α, MCP-1, IL-6, and IL-1β, were examined by quantitative real-time RT-PCR after 4 h of LPS treatment (*in vitro* 2D/3D: 100 ng/ml; *in vivo*: 0.5 mg/kg). As shown in Figure 5.4, a significant up-regulation of TNF-α, MCP-1, IL-6, and IL-1β expressions was observed in LPS-treated groups. Expression of GAPDH (a housekeeping gene), however, was not affected by LPS stimulation (data not shown). In particular, cells on *in vitro* 2D system exhibited highest responses to LPS treatment (41.02-fold induction of TNF-α, 50-fold induction of MCP-1, 43,158-fold induction of IL-6, and 2,198-fold induction of IL-1β; $p<0.05$) compared with LPS-treated cells within *in vitro* 3D system (24-fold induction of TNF-α, 35-fold induction of MCP-1, 721-fold induction of IL-6, and 237-fold induction of IL-1β; $p<0.05$) and *in vivo* system (9-fold induction of TNF-α, 12-fold induction of MCP-1, 3.92-fold induction of IL-6, and 17-fold induction of IL-1β; $p<0.05$).

In addition, protein expression levels of TNF-α, MCP-1, IL-6 and IL-1β after LPS stimulation were quantified by ELISA (Figure 5.5). Similar to mRNA expression, highest inflammatory protein responses of cells on *in vitro* 2D system by LPS stimulation were observed compared with cells within *in vitro* 3D system and *in vivo* system. As illustrated in Figure 5.5 (5.5A to 5.5C), a remarkable induction of pro-inflammatory proteins after LPS stimulation was detected in *in vitro* 2D system (64-fold induction of TNF-α, 22-fold induction of MCP-1, and 99-fold induction of IL-6; $p<0.05$) compared with LPS-treated cells within *in vitro* 3D system (7.1-fold induction of TNF-α, 10-fold induction of MCP-1, and 46-fold induction of IL-6; $p<0.05$) and *in vivo* system (4.7-fold induction of TNF-α, 3.9-fold induction of MCP-1, and 11-fold induction of IL-6; $p<0.05$). Interestingly, IL-1β induction after LPS stimulation were lower (8.4-fold induction of *in vitro* 2D, 7.8-fold induction of *in vitro* 3D, and 5.5-fold induction of *in vivo*, respectively; $p<0.05$) than other pro-inflammatory proteins but its induction of *in vitro* 3D system was lower than that of *in vitro* 2D system (Figure 5.5D). Overall, the pro-inflammatory responses of *in vitro* 3D system after LPS stimulation are lower than those of *in vitro* 2D system but closer to *in vivo* system. These results suggest that the pro-inflammatory responses of *in vitro* 3D model system closely reflect *in vivo* responses.

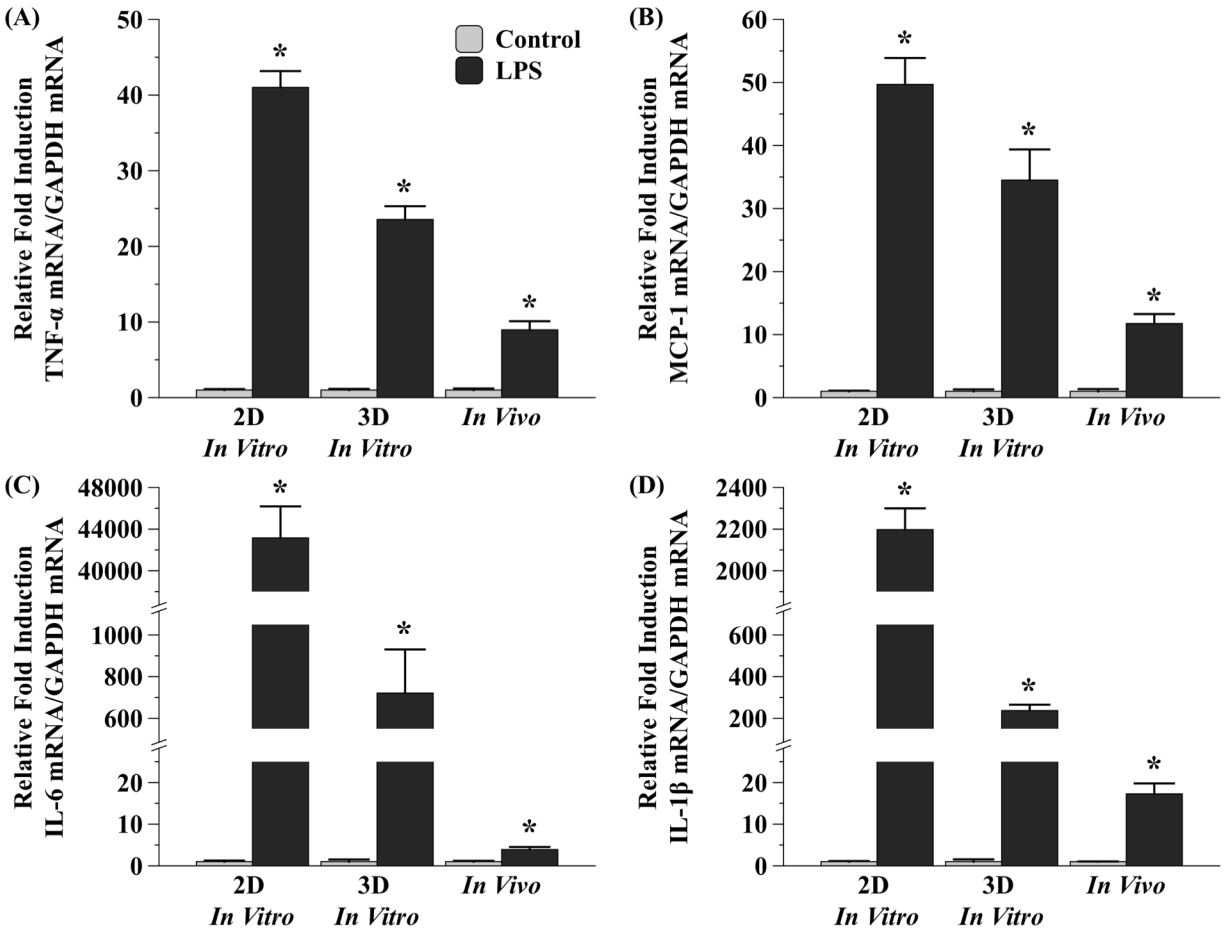

Figure 5.4. Comparison of Pro-inflammatory Gene Expression Among *In Vitro* 2D/3D and *In Vivo* Model Systems After LPS Stimulation. The mRNA expression levels of TNF-α (A), MCP-1 (B), IL-6 (C), and IL-1β (D) after LPS stimulation were measured by quantitative real-time RT-PCR. Data represent mean ± SEM for each group (n=4). *p<0.05 compared to each control group.

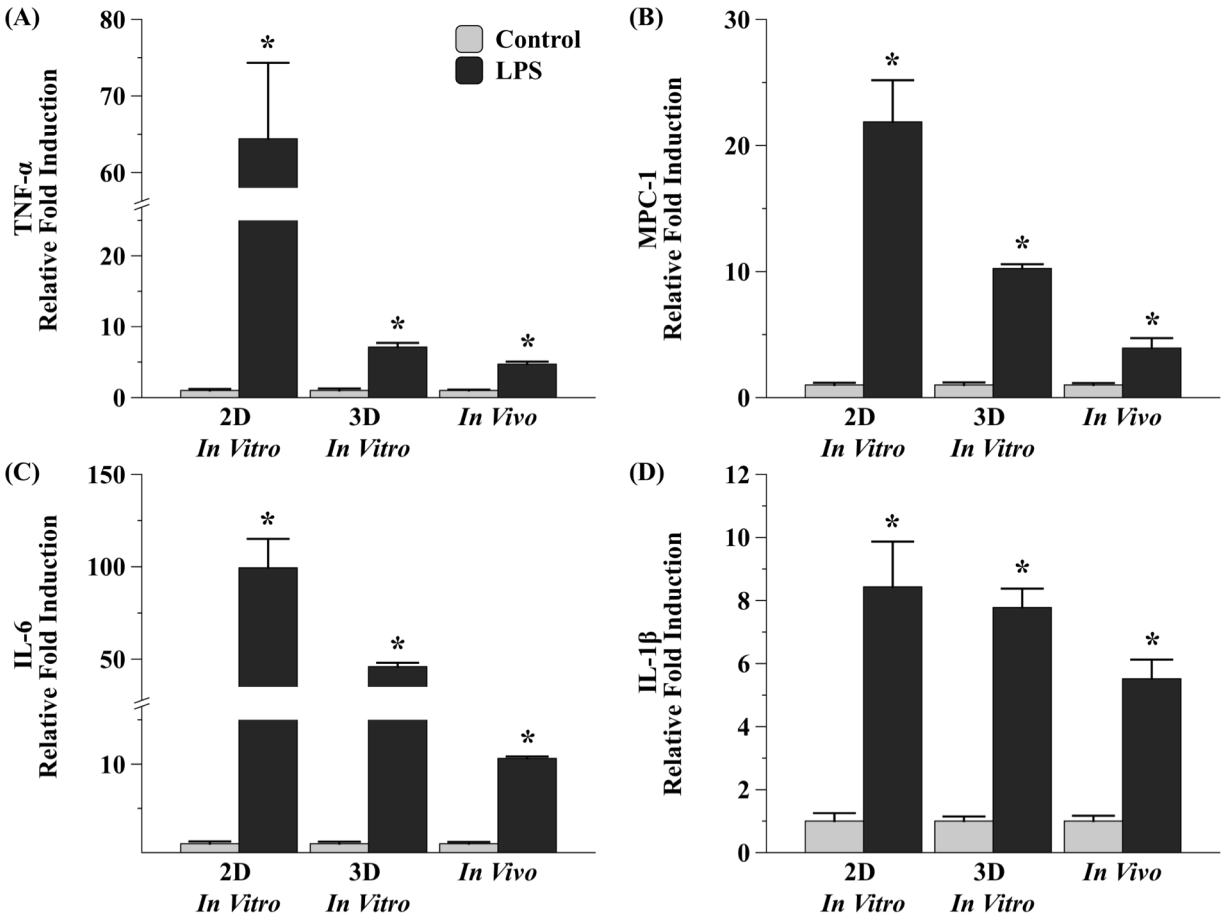

Figure 5.5. Comparison of Pro-inflammatory Protein Expression Among *In Vitro* 2D/3D and *In Vivo* Model Systems After LPS Stimulation. The protein expression levels of TNF-α (A), MCP-1 (B), IL-6 (C), and IL-1β (D) after LPS stimulation were quantified by ELISA. Data represent mean ± SEM for each group (*in vitro* 2D/3D: n=6; *in vivo*: n=5). *p<0.05 compared to each control group.

5.4.3. Pro-oxidative Responses of In Vitro 3D System After LPS Stimulation

To elucidate the pro-oxidative responses of *in vitro* 2D/3D and *in vivo* model systems, *in situ* DHE fluorescence staining was performed to detect ROS generation after 4 h of LPS stimulation (*in vitro* 2D/3D: 100 ng/ml; *in vivo*: 0.5 mg/kg). A marked increase of superoxide anion in LPS-treated groups was examined compared to each control group (Figure 5.6A to 5.6F). Quantitative analysis of relative fold induction in fluorescence intensity exhibited that LPS treatment significantly increased ROS generation by 24-fold (*in vitro* 2D; $p<0.05$), 7.8-fold (*in vitro* 3D; $p<0.05$), and 14-fold (*in vivo*; $p<0.05$). In addition, ROS-generating responses of *in vitro* 2D system by LPS stimulation was higher than those observed in *in vitro* 3D system and *in vivo* system while *in vitro* 3D system demonstrated less responses of ROS generation to LPS treatment, rather close to *in vivo* responses. These results suggest that pro-oxidative responses of *in vitro* 3D system after LPS stimulation resemble the profile of *in vivo* responses.

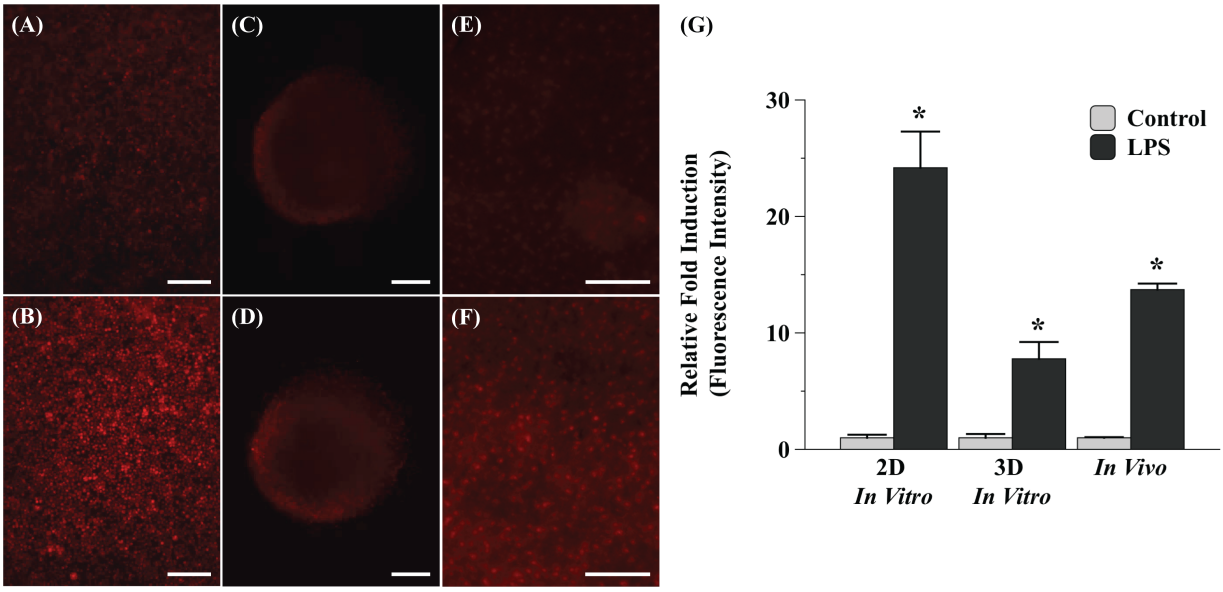

Figure 5.6. Comparison of ROS Generation Among *In Vitro* 2D/3D and *In Vivo* Model Systems After LPS Stimulation. The fluorescence intensity of superoxide anion formation after LPS stimulation was visualized by *in situ* DHE fluorescence staining. (A) Control (*in vitro* 2D); (B) LPS stimulation (*in vitro* 2D); (C) Control (*in vitro* 3D); (D) LPS stimulation (*in vitro* 3D); (E) Control (*in vivo*); (F) LPS stimulation (*in vivo*); (G) Quantitative analysis of fluorescence intensity by relative fold induction. Data represent mean ± SEM for each group (*in vitro* 2D/3D: n=6; *in vivo*: n=5). *$p<0.05$ compared to each control group. Scale bar: (A) and (B), 200 μm; (C) and (D), 1000 μm; (E) and (F), 100 μm.

5.4.4. Microglial Activation of In Vitro 3D System After LPS Stimulation

To compare microglial activation among *in vitro* 2D/3D and *in vivo* model systems after 24 h of LPS treatment (*in vitro* 2D/3D: 100 ng/ml; *in vivo*: 0.5 mg/kg), the protein expression levels of Iba1, a microglial activation marker, were visualized by immunofluorescence staining. A significantly increased number of Iba1-immunopositive cells was detected in LPS-treated groups compared to each control group (Figure 5.7A to 5.7F). Quantitative analysis of microglial activation demonstrated that LPS treatment markedly increased ROS generation by 9.1-fold (*in vitro* 2D; $p<0.05$), 1.7-fold (*in vitro* 3D; $p<0.05$), and 2.4-fold (*in vivo*; $p<0.05$). Highest levels of microglial activation were observed in *in vitro* 2D system after LPS stimulation while *in vitro* 3D system showed less microglial activation that was closer to *in vivo* responses. These results suggest that microglial activation of *in vitro* 3D system provides closer prediction of *in vivo* responses upon LPS than that of *in vitro* 2D system.

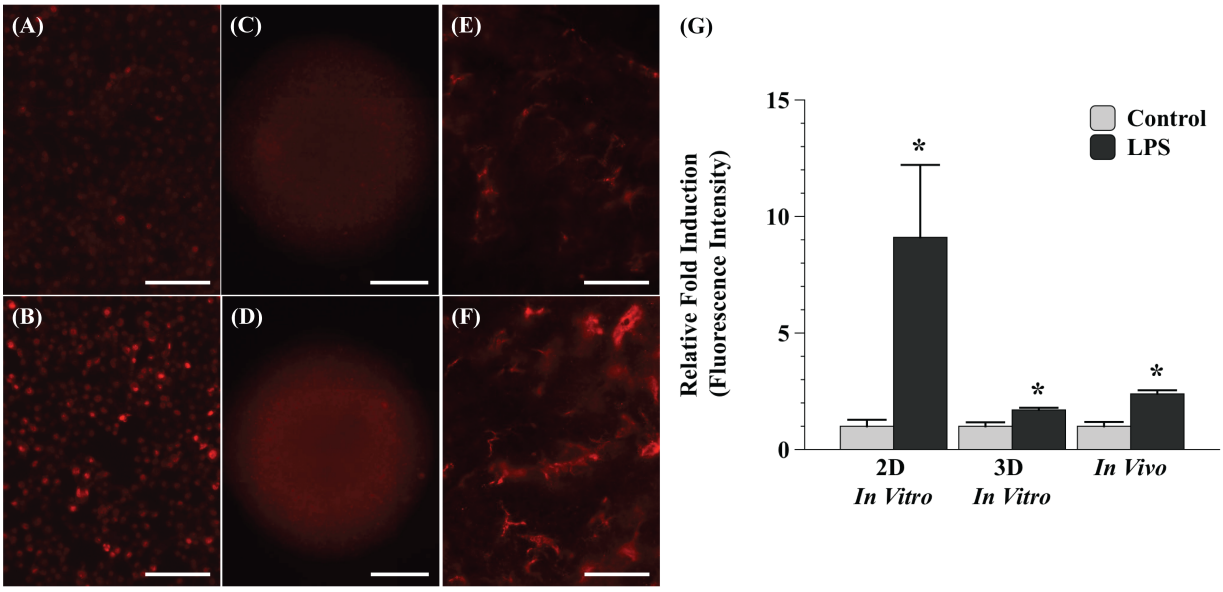

Figure 5.7. Comparison of Microglial Activation Among *In Vitro* 2D/3D and *In Vivo* Model Systems After LPS Stimulation. Activated microglia by LPS stimulation was visualized by Iba1-positive immunofluorescence staining. (A) Control (*in vitro* 2D); (B) LPS stimulation (*in vitro* 2D); (C) Control (*in vitro* 3D); (D) LPS stimulation (*in vitro* 3D); (E) Control (*in vivo*); (F) LPS stimulation (*in vivo*); (G) Quantitative analysis of fluorescence intensity by relative fold induction. Data represent mean ± SEM for each group (*in vitro* 2D: n=4; *in vitro* 3D and *in vivo*: n=5). *$p<0.05$ compared to each control group. Scale bar: (A) and (B), 100 μm; (C) and (D), 1000 μm; (E) and (F), 50 μm.

5.5. Discussion

The rapid progress in tissue engineering and emerging biotechnologies has raised new strategies to investigate complex physiological and pathophysiological processes of cells. A variety of tools for harvesting cells in 3D space have been expanded over the past decade to create functional *in vitro* 3D experimental models and the application of *in vitro* 3D models has become diverse. Previous researchers have demonstrated that *in vitro* 3D models have the potential to improve understanding of more relevant cellular physiology and pathology than the traditional 2D model systems can achieve [13, 275, 279]. For example, 3D culture systems mimic physiologically relevant microenvironments to provide mechanical properties (stiffness) and molecular composition of the ECM, delivering information of cell-cell/matrix interactions and cellular behavior/response regulations [11, 152, 153, 161, 280]. Due to the fact that cell-cell/matrix interactions are of pivotal for cell growth, differentiation, and migration, promoting cell survival and dynamic responses upon external cues, there is an increasing demand for *in vitro* 3D models to develop new therapeutic strategies and predictive toxicological investigations by studying normal cell/tissue functions and disease progression [281-283]. In the present study, we developed an *in vitro* 3D model system to investigate cellular responses and molecular interactions of microglia under pro-oxidative and pro-inflammatory environments and compared the *in vitro* 3D system with traditional *in vitro* 2D and *in vivo* systems.

A main challenge of designing a 3D cell culture system is the limited information associating nutrient delivery and cellular distribution for maintaining cellular function and cell viability. Particularly, oxygen is normally considered to be limiting factor due to its low solubility in culture medium while gradients in glucose and amino acids are almost negligible. Compared with conventional 2D culture systems, *in vitro* 3D systems may result in differentially proliferating regions of cells, significantly due to the oxygen gradients (diffusion) within the 3D constructs. In addition, cell density linked to the temporal oxygen gradients may determine cells' fate in the 3D structures according to metabolic oxygen consumption of cells. Previous studies have emphasized that understanding of the spatial oxygen gradient established in 3D constructs depending on cell densities is crucial to balance oxygen diffusion and cellular metabolism (oxygen consumption) [284-289].

The present study first investigated the magnitude of oxygen concentration distribution throughout the 3D construct using a mathematical analysis in terms of diffusion (oxygen diffusion) and reaction (oxygen consumption). Computational simulations predicted the oxygen diffusion through a 3D cylindrical collagen structure and oxygen consumption by seeded cells. In addition, experimentally obtained logistic cell growth of microglia was integrated into the mathematical model to further estimate oxygen distribution profile within the construct depending on cellular growth over time, adding the part of oxygen consumption according to cellular proliferation. Our results showed that, according to initial cell seeding densities, oxygen concentration within the construct fell towards each approximate equilibrium and remained with relatively high partial pressure of $O_2(\%)$ ranging from 17 to 20 after the first half an hour of the simulation (Figure 5.2B and 5.2D). However, oxygen distribution dramatically dropped as the cells proliferate afterwards within the 3D constructs with the highest cell density, which may result in oxygen depletion (Figure 5.2C and 5.2E).

The oxygen concentrations in tissues are much lower than the atmospheric oxygen concentrations (about 21% partial pressure of O_2); a range of 2 to 10% is frequently observed in mammalian tissues. In particular, previous *in vivo* and clinical studies measuring oxygen concentration in brain tissue indicated that the partial pressure of oxygen in brain tissue above 5% is a normoxic condition in the brain [290-295]. In contrast, pathological hypoxia with values below 1% resulted in compromised cellular metabolism *in vivo* [296]. In the present study, the initial cell seeding density of $5 \times 10^5\ cells/ml$ and $1 \times 10^6\ cells/ml$ remained above 5% partial pressure of O_2 throughout the 3D constructs after 72-h growth while the construct with the initial cell seeding density of $2 \times 10^6\ cells/ml$ underwent pathological hypoxia condition. To further optimize *in vitro* 3D system culturing conditions, live/dead viability/cytotoxicity assay of experimental 3D constructs was conducted to support the mathematical analyses. As shown in Figure 5.3, the results demonstrated the 3D construct with initial cell seeding density of 1×10^6 cells/ml and 72-h growth exhibited the highest viability and lowest cytotoxicity within *in vitro* 3D systems. Therefore, these conditions were used for further experiments to investigate better molecular and cellular responses upon extracellular cue.

To investigate molecular interactions and cellular responses of our developed *in vitro* 3D model system, LPS stimulation was employed to create pro-oxidative and pro-inflammatory environments in microglia. LPS has been widely used to trigger pro-oxidative/inflammatory

responses and microglial responses to LPS have been well characterized [19, 189]. In the current study, significantly up-regulated mRNA and protein expression levels of pro-inflammatory mediators, such as TNF-α, MCP-1, IL-6, and IL-1β, were observed after LPS stimulation (Figure 5.4 and 5.5). Moreover, the pro-inflammatory responses to LPS stimulation of *in vitro* 2D system were greater than those of *in vitro* 3D system. Similar to pro-inflammatory responses, markedly elevated levels of superoxide anion were detected after LPS stimulation and the pro-oxidative responses to LPS stimulation of *in vitro* 2D system were higher than those of *in vitro* 3D system (Figure 5.6). In both responses, an *in vitro* 3D model system demonstrated resembling profile of *in vivo* responses upon LPS stimulation. Furthermore, the microglial activation response of *in vitro* 3D system demonstrated closer prediction of *in vivo* responses upon LPS stimulation compared with *in vitro* 2D system (Figure 5.7). Particularly, the present study demonstrated that molecular and cellular responses of *in vitro* 3D and *in vivo* model systems after LPS stimulation were much lower than those observed in *in vitro* 2D system. These results imply that oxygen diffusion may be limited *in vitro* 3D and *in vivo* systems compared with *in vitro* 2D system due to the presence of oxygen diffusion barrier, such as hydrogels and tissues. Interestingly, pro-oxidative responses and microglial activation of *in vivo* system upon LPS stimulation were higher than those of *in vitro* 3D system. This result may be due to the presence of vasculature *in vivo* to continuously provide oxygen into tissues. In addition, the responses of microglial activation of *in vitro* 2D/3D and *in vivo* model systems showed a similar trend in the pro-oxidative responses, demonstrating ROS generation may be associated with microglial activation. Previously, Haw *et al*. [297] observed specific microglial responses upon LPS in a 3D collagen construct to characterize microglia in 3D, supporting that an *in vitro* 3D system may provide a useful tool to investigate physiologically relevant cellular responses. Engineering analysis of 3D constructs by estimating oxygen diffusion and consumption, however, has not yet been explored. It is essential to establish the precise oxygen diffusion and consumption dynamics within the construct, in relation to local cellular responses over prolonged periods. To our knowledge, this is the first report demonstrating that comparing molecular and cellular responses of *in vitro* 2D/3D and *in vivo* systems to create a physiologically relevant *in vitro* brain inflammation model system. The detailed mechanism(s) underlying our observation, however, needs to be further investigated.

5.6. Conclusions

In summary, we have developed an *in vitro* 3D brain inflammation model system by encapsulating microglia within a collagen hydrogel matrix based on mathematical analyses to integrate two major defining features to construct a 3D experimental model system, oxygen diffusion and consumption. In addition, the present study demonstrated that our engineered *in vitro* 3D brain inflammation model system provides a more physiologically relevant environment to accurately reflect the characteristic of *in vivo* responses. Given the limitations of existing 2D approaches to represent *in vivo*, these findings may provide a foundation for further defining cellular and molecular analysis in various neurological diseases by a simple *in vitro* system.

5.7. Acknowledgments

The authors are thankful to Nabil Boutagy, Ph.D., Department of Human Nutrition, Foods, and Exercise, Virginia Tech, for his vital assistance with the Seahorse XF24 analyzer.

CHAPTER 6:

CONCLUSIONS AND FUTURE WORK

6.1 Conclusions

Oxidative stress and inflammation have been implicated in various disease processes including neurological and psychiatric disorders [1-8]. However, very limited information on the etiology of the progression of neurological damage to brain tissue is currently available. In addition, the molecular and cellular mechanisms in the pathophysiology of brain injuries have not yet been fully understood.

The emergence of tissue engineering have promoted great improvement and progress over the last few decades and raises great opportunities to study complex physiological and pathophysiological processes *in vitro*. Despite of various available tools to create tissue-engineered 3D models *in vitro*, recreating biochemical and mechanical cues in 3D model systems to mimic *in vivo* brain microenvironments remains to be further investigated.

Therefore, the prime goals of the present work were to examine the molecular and cellular mechanisms responsible for blast- and radiation-induced brain injuries, and to develop a 3D cell culture system mimicking *in vivo*-like microenvironments to further expand our knowledge in pro-oxidative and pro-inflammatory molecular interactions and cellular responses within 3D constructs. Therefore, the following main conclusions have been achieved:

1. The effect of blast exposure on pro-oxidative and pro-inflammatory pathways in rat brain and behavioral impairment were examined. This study demonstrated that blast exposure induces specific molecular and cellular alterations in pro-oxidative and pro-inflammatory environments in the brain, through excessive ROS generation, overexpression of pro-inflammatory mediators (e.g., IFN-γ and MCP-1), and neuronal loss, and subsequently results in short-term memory loss. These results suggest that pro-oxidative and pro-inflammatory environments in the brain could play a potential role in blast-induced neuronal loss and behavioral deficits.

2. The pivotal role of NADPH oxidase in fractionated whole-brain radiation-induced pro-oxidative and pro-inflammatory pathways in mouse brain was examined. This study revealed that fractionated whole-brain irradiation induces specific molecular and cellular alterations in pro-oxidative and pro-inflammatory environments in the brain through excessive ROS generation, overexpression of pro-inflammatory mediators (e.g., TNF-α

and MCP-1), elevation of ROS-generating protein (NOX-2), and microglial activation. In addition, the contribution of NOX-2 in fractionated whole-brain radiation-induced oxidative stress was observed by dramatic amelioration of ROS generation after pharmacological inhibitions of NOX-2. These results suggest that NOX-2 may play a critical role in fractionated whole-brain radiation-induced pro-oxidative and pro-inflammatory pathways in mouse brain.

3. An *in vitro* 3D brain inflammation model was designed and constructed by encapsulating microglia in collagen hydrogel matrix after engineering analyses of oxygen diffusion and consumption within 3D constructs using mathematical modeling. The molecular and cellular responses of *in vitro* 3D constructs containing microglia were compared with conventional *in vitro* 2D and *in vivo* systems. The results indicated that our developed *in vitro* 3D model provides a more physiologically relevant environment to mimic *in vivo* responses.

These findings may contribute to defining a new cellular and molecular basis for different types of brain injuries. Furthermore, this work may lead to new opportunities for preventive and therapeutic interventions for patients with brain injuries and associated neurological/ neurodegenerative disorders.

6.2 Future Work

The ultimate goal of my work is to elucidate the etiology of different types of brain injuries, which may share molecular and cellular mechanisms during disease processes. In order to improve understanding the pathophysiological mechanisms responsible for brain injuries and successfully develop novel strategies for prevention and treatment of associated brain diseases, there are several areas of study that need to be further explored. The following research areas are of considerable research interest for future work:

1. ***Expanded time-course observation of microglial and neuronal inflammatory states and broadened exploration of other brain areas in blast-induced brain injury***

It was demonstrated in Chapter 3 that acute pro-oxidative and pro-inflammatory environments contribute to BOP-induced neuronal loss and behavioral deficits. However, more detailed analysis of BINT over an expanded time-course would be required for better knowledge of any changes in microglial and neuronal inflammatory states. In addition, this study should be broadened to other brain areas, particularly prefrontal cortex and amygdala complex, since they mediates cognitive and anxiety control, respectively.

2. ***Role of NOX-2 in radiation-induced brain injury***

It was demonstrated in Chapter 4 that NOX inhibitors were able to scavenge ROS generation in irradiated mouse brain by *in situ* tissue ROS detection assay. However, the mechanistic study of NOX-2 inhibition *ex vivo* remains unclear and needs to be further investigated. Selective NOX-2 inhibitors and NOX-2 knockout mice could be employed as in-depth pharmacological and genetic approaches. Moreover, examining co-localization of NOX-2 and Iba1 may provide essential information about the source of microglia activation in radiation-induced brain injury. In addition to the proposed experiment to examine the effect of fractionated whole-brain irradiation on neurons, possibilities of progressive loss of neuronal structure and function in radiation-induced brain injury by using an immunohistochemistry method with a neurodegeneration marker (Fluoro-Jade B) may deliver long term effect of radiation on neurodegeneration.

3. ***Investigation of primary microglia responses in an in vitro 3D brain inflammation model***

In the proposed study of Chapter 5, immortalized cell lines (BV-2 cell line) were used for *in vitro* studies rather than primary cells. However, encapsulating primary microglia within 3D constructs may be required to represent *in vitro* 3D brain inflammation model and their responses under pro-oxidative and pro-inflammatory environments after LPS stimulation remain to be further investigated.

Furthermore, hydrogels composed of hyaluronic acid (HA) may be developed to test more physiologically relevant, *in vivo*-like 3D environments compared with the proposed type I collagen material due to fact that HA is the main structure of brain ECM [298].

REFERENCES

1. Najjar S, Pearlman DM, Alper K, Najjar A, Devinsky O. **Neuroinflammation and psychiatric illness.** *J Neuroinflammation* 2013, **10:**43.
2. Allan SM, Rothwell NJ. **Inflammation in central nervous system injury.** *Philos Trans R Soc Lond B Biol Sci* 2003, **358:**1669-1677.
3. Amor S, Puentes F, Baker D, van der Valk P. **Inflammation in neurodegenerative diseases.** *Immunology* 2010, **129:**154-169.
4. Glass CK, Saijo K, Winner B, Marchetto MC, Gage FH. **Mechanisms underlying inflammation in neurodegeneration.** *Cell* 2010, **140:**918-934.
5. Lucas SM, Rothwell NJ, Gibson RM. **The role of inflammation in CNS injury and disease.** *Br J Pharmacol* 2006, **147 Suppl 1:**S232-240.
6. Martino G, Adorini L, Rieckmann P, Hillert J, Kallmann B, Comi G, Filippi M. **Inflammation in multiple sclerosis: the good, the bad, and the complex.** *Lancet Neurol* 2002, **1:**499-509.
7. Tansey MG, Goldberg MS. **Neuroinflammation in Parkinson's disease: Its role in neuronal death and implications for therapeutic intervention.** *Neurobiol Dis* 2010, **37:**510-518.
8. Uttara B, Singh AV, Zamboni P, Mahajan RT. **Oxidative stress and neurodegenerative diseases: A review of upstream and downstream antioxidant therapeutic options.** *Curr Neuropharmacol* 2009, **7:**65-74.
9. Atala A, Bauer SB, Soker S, Yoo JJ, Retik AB. **Tissue-engineered autologous bladders for patients needing cystoplasty.** *Lancet* 2006, **367:**1241-1246.
10. Macchiarini P, Jungebluth P, Go T, Asnaghi MA, Rees LE, Cogan TA, Dodson A, Martorell J, Bellini S, Parnigotto PP, Dickinson SC, Hollander AP, Mantero S, Conconi MT, Birchall MA. **Clinical transplantation of a tissue-engineered airway.** *Lancet* 2008, **372:**2023-2030.
11. Geckil H, Xu F, Zhang X, Moon S, Demirci U. **Engineering hydrogels as extracellular matrix mimics.** *Nanomedicine (Lond)* 2010, **5:**469-484.
12. Langer R. **The evolution of biomaterials. Interview by Alison Stoddart and Victoria Cleave.** *Nat Mater* 2009, **8:**444-445.
13. Tibbitt MW, Anseth KS. **Hydrogels as extracellular matrix mimics for 3D cell culture.** *Biotechnol Bioeng* 2009, **103:**655-663.

14. Xu T, Molnar P, Gregory C, Das M, Boland T, Hickman JJ. **Electrophysiological characterization of embryonic hippocampal neurons cultured in a 3D collagen hydrogel.** *Biomaterials* 2009, **30:**4377-4383.

15. Bergamini CM, Gambetti S, Dondi A, Cervellati C. **Oxygen, reactive oxygen species and tissue damage.** *Curr Pharm Des* 2004, **10:**1611-1626.

16. Dröge W. **Free radicals in the physiological control of cell function.** *Physiol Rev* 2002, **82:**47-95.

17. Malhotra JD, Kaufman RJ. **Endoplasmic reticulum stress and oxidative stress: A vicious cycle or a double-edged sword?** *Antioxid Redox Signal* 2007, **9:**2277-2293.

18. Fisher AB. **Redox signaling across cell membranes.** *Antioxid Redox Signal* 2009, **11:**1349-1356.

19. Block ML, Zecca L, Hong JS. **Microglia-mediated neurotoxicity: Uncovering the molecular mechanisms.** *Nat Rev Neurosci* 2007, **8:**57-69.

20. Turrens JF. **Mitochondrial formation of reactive oxygen species.** *J Physiol* 2003, **552:**335-344.

21. Gerich FJ, Funke F, Hildebrandt B, Fasshauer M, Müller M. **H_2O_2-mediated modulation of cytosolic signaling and organelle function in rat hippocampus.** *Pflugers Arch* 2009, **458:**937-952.

22. Hepp S, Gerich FJ, Müller M. **Sulfhydryl oxidation reduces hippocampal susceptibility to hypoxia-induced spreading depression by activating BK channels.** *J Neurophysiol* 2005, **94:**1091-1103.

23. Huchzermeyer C, Albus K, Gabriel HJ, Otáhal J, Taubenberger N, Heinemann U, Kovács R, Kann O. **Gamma oscillations and spontaneous network activity in the hippocampus are highly sensitive to decreases in pO_2 and concomitant changes in mitochondrial redox state.** *J Neurosci* 2008, **28:**1153-1162.

24. Kietzmann T, Fandrey J, Acker H. **Oxygen radicals as messengers in oxygen-dependent gene expression.** *News Physiol Sci* 2000, **15:**202-208.

25. Cadet JL. **Free radical mechanisms in the central nervous system: An overview.** *Int J Neurosci* 1988, **40:**13-18.

26. Demopoulos HB, Flamm ES, Pietronigro DD, Seligman ML. **The free radical pathology and the microcirculation in the major central nervous system disorders.** *Acta Physiol Scand Suppl* 1980, **492:**91-119.

27. Nunomura A, Perry G, Aliev G, Hirai K, Takeda A, Balraj EK, Jones PK, Ghanbari H, Wataya T, Shimohama S, Chiba S, Atwood CS, Petersen RB, Smith MA. **Oxidative damage is the earliest event in Alzheimer disease.** *J Neuropathol Exp Neurol* 2001, **60:**759-767.

28. Praticò D, Uryu K, Leight S, Trojanowswki JQ, Lee VMY. **Increased lipid peroxidation precedes amyloid plaque formation in an animal model of Alzheimer amyloidosis.** *J Neurosci* 2001, **21:**4183-4187.

29. Sultana R, Boyd-Kimball D, Poon HF, Cai J, Pierce WM, Klein JB, Markesbery WR, Zhou XZ, Lu KP, Butterfield DA. **Oxidative modification and down-regulation of Pin1 in Alzheimer's disease hippocampus: A redox proteomics analysis.** *Neurobiol Aging* 2006, **27:**918-925.

30. Manczak M, Anekonda TS, Henson E, Park BS, Quinn J, Reddy PH. **Mitochondria are a direct site of Aβ accumulation in Alzheimer's disease neurons: Implications for free radical generation and oxidative damage in disease progression.** *Hum Mol Genet* 2006, **15:**1437-1449.

31. Kong J, Xu Z. **Massive mitochondrial degeneration in motor neurons triggers the onset of amyotrophic lateral sclerosis in mice expressing a mutant SOD1.** *J Neurosci* 1998, **18:**3241-3250.

32. Takeuchi H, Kobayashi Y, Ishigaki S, Doyu M, Sobue G. **Mitochondrial localization of mutant superoxide dismutase 1 triggers caspase-dependent cell death in a cellular model of familial amyotrophic lateral sclerosis.** *J Biol Chem* 2002, **277:**50966-50972.

33. Palacino JJ, Sagi D, Goldberg MS, Krauss S, Motz C, Wacker M, Klose J, Shen J. **Mitochondrial dysfunction and oxidative damage in parkin-deficient mice.** *J Biol Chem* 2004, **279:**18614-18622.

34. Wung BS, Cheng JJ, Hsieh HJ, Shyy YJ, Wang DL. **Cyclic strain-induced monocyte chemotactic protein-1 gene expression in endothelial cells involves reactive oxygen species activation of activator protein 1.** *Circ Res* 1997, **81:**1-7.

35. Verhasselt V, Goldman M, Willems F. **Oxidative stress up-regulates IL-8 and TNF-α synthesis by human dendritic cells.** *Eur J Immunol* 1998, **28:**3886-3890.

36. Lakshminarayanan V, Drab-Weiss EA, Roebuck KA. **H_2O_2 and tumor necrosis factor-α induce differential binding of the redox-responsive transcription factors AP-1 and NF-κB to the interleukin-8 promoter in endothelial and epithelial cells.** *J Biol Chem* 1998, **273:**32670-32678.

37. Simon AR, Rai U, Fanburg BL, Cochran BH. **Activation of the JAK-STAT pathway by reactive oxygen species.** *Am J Physiol* 1998, **275:**C1640-1652.

38. Bouloumie A, Marumo T, Lafontan M, Busse R. **Leptin induces oxidative stress in human endothelial cells.** *FASEB J* 1999, **13:**1231-1238.

39. Grösch S, Kaina B. **Transcriptional activation of apurinic/apyrimidinic endonuclease (Ape, Ref-1) by oxidative stress requires CREB.** *Biochem Biophys Res Commun* 1999, **261:**859-863.

40. Park HJ, Lee YW, Hennig B, Toborek M. **Linoleic acid-induced VCAM-1 expression in human microvascular endothelial cells is mediated by the NF-κB-dependent pathway.** *Nutr Cancer* 2001, **41:**126-134.

41. Lee YW, Hennig B, Fiala M, Kim KS, Toborek M. **Cocaine activates redox-regulated transcription factors and induces TNF-α expression in human brain endothelial cells.** *Brain Res* 2001, **920:**125-133.

42. Lee YW, Hennig B, Yao J, Toborek M. **Methamphetamine induces AP-1 and NF-κB binding and transactivation in human brain endothelial cells.** *J Neurosci Res* 2001, **66:**583-591.

43. Lee YW, Kühn H, Hennig B, Neish AS, Toborek M. **IL-4-induced oxidative stress upregulates VCAM-1 gene expression in human endothelial cells.** *J Mol Cell Cardiol* 2001, **33:**83-94.

44. Lee YW, Park HJ, Hennig B, Toborek M. **Linoleic acid induces MCP-1 gene expression in human microvascular endothelial cells through an oxidative mechanism.** *J Nutr Biochem* 2001, **12:**648-654.

45. Lee YW, Hennig B, Toborek M. **Redox-regulated mechanisms of IL-4-induced MCP-1 expression in human vascular endothelial cells.** *Am J Physiol Heart Circ Physiol* 2003, **284:**H185-192.

46. Lee WH, Sonntag WE, Mitschelen M, Yan H, Lee YW. **Irradiation induces regionally specific alterations in pro-inflammatory environments in rat brain.** *Int J Radiat Biol* 2010, **86:**132-144.

47. Yang G, Meng Y, Li W, Yong Y, Fan Z, Ding H, Wei Y, Luo J, Ke ZJ. **Neuronal MCP-1 mediates microglia recruitment and neurodegeneration induced by the mild impairment of oxidative metabolism.** *Brain Pathol* 2011, **21:**279-297.

48. Salim S, Chugh G, Asghar M. **Chapter one - Inflammation in anxiety.** In: Donev R (Ed.). *Adv Protein Chem Struct Biol*, *San Diego: Academic Press* 2012, **88:**1-25.

49. Block ML, Hong JS. **Chronic microglial activation and progressive dopaminergic neurotoxicity.** *Biochem Soc Trans* 2007, **35:**1127-1132.

50. McGeer PL, McGeer EG. **The inflammatory response system of brain: implications for therapy of Alzheimer and other neurodegenerative diseases.** *Brain Res Brain Res Rev* 1995, **21:**195-218.

51. Dheen ST, Kaur C, Ling EA. **Microglial activation and its implications in the brain diseases.** *Curr Med Chem* 2007, **14:**1189-1197.

52. Theoharides TC, Zhang B, Conti P. **Decreased mitochondrial function and increased brain inflammation in bipolar disorder and other neuropsychiatric diseases.** *J Clin Psychopharmacol* 2011, **31:**685-687.

53. Hagberg H, Gressens P, Mallard C. **Inflammation during fetal and neonatal life: Implications for neurologic and neuropsychiatric disease in children and adults.** *Ann Neurol* 2012, **71:**444-457.

54. Akiyama H, Barger S, Barnum S, Bradt B, Bauer J, Cole GM, Cooper NR, Eikelenboom P, Emmerling M, Fiebich BL, Finch CE, Frautschy S, Griffin WS, Hampel H, Hull M, Landreth G, Lue L, Mrak R, Mackenzie IR, McGeer PL, O'Banion MK, Pachter J, Pasinetti G, Plata-Salaman C, Rogers J, Rydel R, Shen Y, Streit W, Strohmeyer R, Tooyoma I, Van Muiswinkel FL, Veerhuis R, Walker D, Webster S, Wegrzyniak B, Wenk G, Wyss-Coray T. **Inflammation and Alzheimer's disease.** *Neurobiol Aging* 2000, **21:**383-421.

55. Suo Z, Tan J, Placzek A, Crawford F, Fang C, Mullan M. **Alzheimer's β-amyloid peptides induce inflammatory cascade in human vascular cells: The roles of cytokines and CD40.** *Brain Res* 1998, **807:**110-117.

56. McGeer PL, Yasojima K, McGeer EG. **Inflammation in Parkinson's disease.** *Adv Neurol* 2001, **86:**83-89.

57. Schulz JB, Falkenburger BH. **Neuronal pathology in Parkinson's disease.** *Cell Tissue Res* 2004, **318:**135-147.

58. Möller T. **Neuroinflammation in Huntington's disease.** *J Neural Transm* 2010, **117:**1001-1008.

59. Hsiao HY, Chen YC, Chen HM, Tu PH, Chern Y. **A critical role of astrocyte-mediated nuclear factor-κB-dependent inflammation in Huntington's disease.** *Hum Mol Genet* 2013, **22:**1826-1842.

60. Graves MC, Fiala M, Dinglasan LAV, Liu NQ, Sayre J, Chiappelli F, van Kooten C, Vinters HV. **Inflammation in amyotrophic lateral sclerosis spinal cord and brain is mediated by activated macrophages, mast cells and T cells.** *Amyotroph Lateral Scler Other Motor Neuron Disord* 2004, **5:**213-219.

61. McCombe PA, Henderson RD. **The role of immune and inflammatory mechanisms in ALS.** *Curr Mol Med* 2011, **11:**246-254.

62. Philips T, Robberecht W. **Neuroinflammation in amyotrophic lateral sclerosis: Role of glial activation in motor neuron disease.** *Lancet Neurol* 2011, **10:**253-263.

63. Vogel DYS, Vereyken EJF, Glim JE, Heijnen PDAM, Moeton M, van der Valk P, Amor S, Teunissen CE, van Horssen J, Dijkstra CD. **Macrophages in inflammatory multiple sclerosis lesions have an intermediate activation status.** *J Neuroinflammation* 2013, **10:**35.

64. Soulet D, Cicchetti F. **The role of immunity in Huntington's disease.** *Mol Psychiatry* 2011, **16:**889-902.

65. Little AR, Benkovic SA, Miller DB, O'Callaghan JP. **Chemically induced neuronal damage and gliosis: Enhanced expression of the proinflammatory chemokine, monocyte chemoattractant protein (MCP)-1, without a corresponding increase in proinflammatory cytokines.** *Neuroscience* 2002, **115:**307-320.

66. Gao HM, Zhou H, Zhang F, Wilson BC, Kam W, Hong JS. **HMGB1 acts on microglia Mac1 to mediate chronic neuroinflammation that drives progressive neurodegeneration.** *J Neurosci* 2011, **31:**1081-1092.

67. Zhang D, Sun L, Zhu H, Wang L, Wu W, Xie J, Gu J. **Microglial LOX-1 reacts with extracellular HSP60 to bridge neuroinflammation and neurotoxicity.** *Neurochem Int* 2012, **61:**1021-1035.

68. Armed Forces Health Surveillance Center. **Incident diagnoses of common symptoms ("sequelae") following traumatic brain injury, active component, U.S. Armed Forces, 2000-2012.** *MSMR* 2013, **20:**9-13.

69. Rosenfeld JV, Ford NL. **Bomb blast, mild traumatic brain injury and psychiatric morbidity: A review.** *Injury* 2010, **41:**437-443.

70. Rauh MJ, Aralis HJ, Melcer T, Macera CA, Sessoms P, Bartlett J, Galarneau MR. **Effect of traumatic brain injury among U.S. servicemembers with amputation.** *J Rehabil Res Dev* 2013, **50:**161-172.

71. Bazarian JJ, Cernak I, Noble-Haeusslein L, Potolicchio S, Temkin N. **Long-term neurologic outcomes after traumatic brain injury.** *J Head Trauma Rehabil* 2009, **24:**439-451.

72. Warden DL, French LM, Shupenko L, Fargus J, Riedy G, Erickson ME, Jaffee MS, Moore DF. **Case report of a soldier with primary blast brain injury.** *Neuroimage* 2009, **47 Suppl 2:**T152-153.

73. Hicks RR, Fertig SJ, Desrocher RE, Koroshetz WJ, Pancrazio JJ. **Neurological effects of blast injury.** *J Trauma* 2010, **68:**1257-1263.

74. McAllister TW, Stein MB. **Effects of psychological and biomechanical trauma on brain and behavior.** *Ann N Y Acad Sci* 2010, **1208:**46-57.

75. Helfer TM, Jordan NN, Lee RB, Pietrusiak P, Cave K, Schairer K. **Noise-Induced Hearing Injury and Comorbidities Among Postdeployment U.S. Army Soldiers: April 2003-June 2009.** *Am J Audiol* 2011, **20:**33-41.

76. Mao JC, Pace E, Pierozynski P, Kou Z, Shen Y, VandeVord PJ, Haacke EM, Zhang X, Zhang J. **Blast-induced tinnitus and hearing loss in rats: behavioral and imaging assays.** *J Neurotrauma* 2012, **29:**430-444.

77. Hoge CW, McGurk D, Thomas JL, Cox AL, Engel CC, Castro CA. **Mild traumatic brain injury in U.S. Soldiers returning from Iraq.** *N Engl J Med* 2008, **358:**453-463.

78. Thompson JM, Scott KC, Dubinsky L. **Battlefield brain: unexplained symptoms and blast-related mild traumatic brain injury.** *Can Fam Physician* 2008, **54:**1549-1551.

79. Dobscha SK, Clark ME, Morasco BJ, Freeman M, Campbell R, Helfand M. **Systematic review of the literature on pain in patients with polytrauma including traumatic brain injury.** *Pain Med* 2009, **10:**1200-1217.

80. Elder GA, Mitsis EM, Ahlers ST, Cristian A. **Blast-induced mild traumatic brain injury.** *Psychiatr Clin North Am* 2010, **33:**757-781.

81. Nampiaparampil DE. **Prevalence of chronic pain after traumatic brain injury: a systematic review.** *JAMA* 2008, **300:**711-719.

82. Warden D. **Military TBI during the Iraq and Afghanistan wars.** *J Head Trauma Rehabil* 2006, **21:**398-402.

83. Glasstone S, Dolan PJ (Eds.) **The effects of nuclear weapons**. 3rd ed. *Washington, DC: U. S. Department of Defense and the Energy Research and Development Administration* 1977:548-553.

84. Belanger HG, Kretzmer T, Yoash-Gantz R, Pickett T, Tupler LA. **Cognitive sequelae of blast-related versus other mechanisms of brain trauma.** *J Int Neuropsychol Soc* 2009, **15:**1-8.

85. Bhattacharjee Y. **Neuroscience. Shell shock revisited: Solving the puzzle of blast trauma.** *Science* 2008, **319:**406-408.

86. Cernak I, Merkle AC, Koliatsos VE, Bilik JM, Luong QT, Mahota TM, Xu L, Slack N, Windle D, Ahmed FA. **The pathobiology of blast injuries and blast-induced neurotrauma as identified using a new experimental model of injury in mice.** *Neurobiol Dis* 2011, **41:**538-551.

87. Säljö A, Bolouri H, Mayorga M, Svensson B, Hamberger A. **Low-level blast raises intracranial pressure and impairs cognitive function in rats: Prophylaxis with processed cereal feed.** *J Neurotrauma* 2010, **27:**383-389.

88. Leonardi AD, Bir CA, Ritzel DV, VandeVord PJ. **Intracranial pressure increases during exposure to a shock wave.** *J Neurotrauma* 2011, **28:**85-94.

89. Bolander R, Mathie B, Bir C, Ritzel D, VandeVord P. **Skull flexure as a contributing factor in the mechanism of injury in the rat when exposed to a shock wave.** *Ann Biomed Eng* 2011, **39:**2550-2559.

90. Aarabi B, Simard JM. **Traumatic brain injury.** *Curr Opin Crit Care* 2009, **15:**548-553.

91. Cernak I, Wang Z, Jiang J, Bian X, Savic J. **Ultrastructural and functional characteristics of blast injury-induced neurotrauma.** *J Trauma* 2001, **50:**695-706.

92. Elder GA, Cristian A. **Blast-related mild traumatic brain injury: Mechanisms of injury and impact on clinical care.** *Mt Sinai J Med* 2009, **76:**111-118.

93. Kamnaksh A, Kovesdi E, Kwon SK, Wingo D, Ahmed F, Grunberg NE, Long J, Agoston DV. **Factors affecting blast traumatic brain injury.** *J Neurotrauma* 2011, **28:**2145-2153.

94. Kocsis JD, Tessler A. **Pathology of blast-related brain injury.** *J Rehabil Res Dev* 2009, **46:**667-672.

95. Luethcke CA, Bryan CJ, Morrow CE, Isler WC. **Comparison of concussive symptoms, cognitive performance, and psychological symptoms between acute blast-versus nonblast-induced mild traumatic brain injury.** *J Int Neuropsychol Soc* 2011, **17:**36-45.

96. Risling M, Plantman S, Angeria M, Rostami E, Bellander BM, Kirkegaard M, Arborelius U, Davidsson J. **Mechanisms of blast induced brain injuries, experimental studies in rats.** *Neuroimage* 2011, **54 Suppl 1:**S89-97.

97. Sajja VS, Galloway MP, Ghoddoussi F, Thiruthalinathan D, Kepsel A, Hay K, Bir CA, VandeVord PJ. **Blast-induced neurotrauma leads to neurochemical changes and neuronal degeneration in the rat hippocampus.** *NMR Biomed* 2012, **25:**1331-1339.

98. Vandevord PJ, Bolander R, Sajja VS, Hay K, Bir CA. **Mild neurotrauma indicates a range-specific pressure response to low level shock wave exposure.** *Ann Biomed Eng* 2012, **40:**227-236.

99. Sajja VS, Galloway M, Ghoddoussi F, Kepsel A, VandeVord P. **Effects of blast-induced neurotrauma on the nucleus accumbens.** *J Neurosci Res* 2013, **91:**593-601.

100. Dalle Lucca JJ, Chavko M, Dubick MA, Adeeb S, Falabella MJ, Slack JL, McCarron R, Li Y. **Blast-induced moderate neurotrauma (BINT) elicits early complement activation and tumor necrosis factor alpha (TNFα) release in a rat brain.** *J Neurol Sci* 2012, **318:**146-154.

101. Kovesdi E, Gyorgy AB, Kwon SK, Wingo DL, Kamnaksh A, Long JB, Kasper CE, Agoston DV. **The effect of enriched environment on the outcome of traumatic brain injury; a behavioral, proteomics, and histological study.** *Front Neurosci* 2011, **5:**42.

102. Kwon SK, Kovesdi E, Gyorgy AB, Wingo D, Kamnaksh A, Walker J, Long JB, Agoston DV. **Stress and traumatic brain injury: A behavioral, proteomics, and histological study.** *Front Neurol* 2011, **2:**12.

103. Abdul-Muneer PM, Schuetz H, Wang F, Skotak M, Jones J, Gorantla S, Zimmerman MC, Chandra N, Haorah J. **Induction of oxidative and nitrosative damage leads to cerebrovascular inflammation in an animal model of mild traumatic brain injury induced by primary blast.** *Free Radic Biol Med* 2013, **60:**282-291.

104. Cernak I, Savic VJ, Kotur J, Prokic V, Veljovic M, Grbovic D. **Characterization of plasma magnesium concentration and oxidative stress following graded traumatic brain injury in humans.** *J Neurotrauma* 2000, **17:**53-68.

105. Ostrom QT, Gittleman H, Liao P, Rouse C, Chen Y, Dowling J, Wolinsky Y, Kruchko C, Barnholtz-Sloan J. **CBTRUS statistical report: primary brain and central nervous system tumors diagnosed in the United States in 2007-2011.** *Neuro Oncol* 2014, **16 Suppl 4:**iv1-63.

106. Sheline GE, Wara WM, Smith V. **Therapeutic irradiation and brain injury.** *Int J Radiat Oncol Biol Phys* 1980, **6:**1215-1228.

107. Denham JW, Hauer-Jensen M. **The radiotherapeutic injury - a complex 'wound'.** *Radiother Oncol* 2002, **63:**129-145.

108. Moulder JE, Cohen EP. **Future strategies for mitigation and treatment of chronic radiation-induced normal tissue injury.** *Semin Radiat Oncol* 2007, **17:**141-148.

109. Jones B, Dale RG, Deehan C, Hopkins KI, Morgan DA. **The role of biologically effective dose (BED) in clinical oncology.** *Clin Oncol (R Coll Radiol)* 2001, **13:**71-81.

110. Bernier J. **Alteration of radiotherapy fractionation and concurrent chemotherapy: a new frontier in head and neck oncology?** *Nat Clin Pract Oncol* 2005, **2:**305-314.

111. Tofilon PJ, Fike JR. **The radioresponse of the central nervous system: A dynamic process.** *Radiat Res* 2000, **153:**357-370.

112. Kim JH, Brown SL, Jenrow KA, Ryu S. **Mechanisms of radiation-induced brain toxicity and implications for future clinical trials.** *J Neurooncol* 2008, **87:**279-286.

113. Ramanan S, Zhao W, Riddle DR, Robbins ME. **Role of PPARs in radiation-induced brain injury.** *PPAR Res* 2010, **2010:**234975.

114. Maire JP, Coudin B, Guérin J, Caudry M. **Neuropsychologic impairment in adults with brain tumors.** *Am J Clin Oncol* 1987, **10:**156-162.

115. Asai A, Matsutani M, Kohno T, Nakamura O, Tanaka H, Fujimaki T, Funada N, Matsuda T, Nagata K, Takakura K. **Subacute brain atrophy after radiation therapy for malignant brain tumor.** *Cancer* 1989, **63:**1962-1974.

116. Imperato JP, Paleologos NA, Vick NA. **Effects of treatment on long-term survivors with malignant astrocytomas.** *Ann Neurol* 1990, **28:**818-822.

117. Lamproglou I, Chen QM, Boisserie G, Mazeron JJ, Poisson M, Baillet F, Le Poncin M, Delattre JY. **Radiation-induced cognitive dysfunction: An experimental model in the old rat.** *Int J Radiat Oncol Biol Phys* 1995, **31:**65-70.

118. Yoneoka Y, Satoh M, Akiyama K, Sano K, Fujii Y, Tanaka R. **An experimental study of radiation-induced cognitive dysfunction in an adult rat model.** *Br J Radiol* 1999, **72:**1196-1201.

119. Akiyama K, Tanaka R, Sato M, Takeda N. **Cognitive dysfunction and histological findings in adult rats one year after whole brain irradiation.** *Neurol Med Chir (Tokyo)* 2001, **41:**590-598.

120. Darzy KH, Pezzoli SS, Thorner MO, Shalet SM. **The dynamics of growth hormone (GH) secretion in adult cancer survivors with severe GH deficiency acquired after brain irradiation in childhood for nonpituitary brain tumors: Evidence for preserved pulsatility and diurnal variation with increased secretory disorderliness.** *J Clin Endocrinol Metab* 2005, **90:**2794-2803.

121. Brown WR, Blair RM, Moody DM, Thore CR, Ahmed S, Robbins ME, Wheeler KT. **Capillary loss precedes the cognitive impairment induced by fractionated whole-brain irradiation: A potential rat model of vascular dementia.** *J Neurol Sci* 2007, **257:**67-71.

122. Manda K, Ueno M, Moritake T, Anzai K. **Radiation-induced cognitive dysfunction and cerebellar oxidative stress in mice: Protective effect of α-lipoic acid.** *Behav Brain Res* 2007, **177:**7-14.

123. Welzel G, Fleckenstein K, Schaefer J, Hermann B, Kraus-Tiefenbacher U, Mai SK, Wenz F. **Memory function before and after whole brain radiotherapy in patients with and without brain metastases.** *Int J Radiat Oncol* 2008, **72:**1311-1318.

124. Chang EL, Wefel JS, Hess KR, Allen PK, Lang FF, Kornguth DG, Arbuckle RB, Swint JM, Shiu AS, Maor MH, Meyers CA. **Neurocognition in patients with brain metastases treated with radiosurgery or radiosurgery plus whole-brain irradiation: A randomised controlled trial.** *Lancet Oncol* 2009, **10:**1037-1044.

125. Douw L, Klein M, Fagel SS, van den Heuvel J, Taphoorn MJ, Aaronson NK, Postma TJ, Vandertop WP, Mooij JJ, Boerman RH, Beute GN, Sluimer JD, Slotman BJ, Reijneveld JC, Heimans JJ. **Cognitive and radiological effects of radiotherapy in patients with low-grade glioma: Long-term follow-up.** *Lancet Neurol* 2009, **8:**810-818.

126. Liu Y, Xiao S, Liu J, Zhou H, Liu Z, Xin Y, Suo WZ. **An experimental study of acute radiation-induced cognitive dysfunction in a young rat model.** *AJNR Am J Neuroradiol* 2010, **31:**383-387.

127. Madaschi S, Fiorino C, Losa M, Lanzi R, Mazza E, Motta M, Perna L, Brioschi E, Scavini M, Reni M. **Time course of hypothalamic-pituitary deficiency in adults receiving cranial radiotherapy for primary extrasellar brain tumors.** *Radiother Oncol* 2011, **99:**23-28.

128. Zhou H, Liu Z, Liu J, Wang J, Zhou D, Zhao Z, Xiao S, Tao E, Suo WZ. **Fractionated radiation-induced acute encephalopathy in a young rat model: Cognitive dysfunction and histologic findings.** *AJNR Am J Neuroradiol* 2011, **32:**1795-1800.

129. Quik EH, Valk GD, Drent ML, Stalpers LJ, Kenemans JL, Koppeschaar HP, van Dam PS. **Reduced growth hormone secretion after cranial irradiation contributes to neurocognitive dysfunction.** *Growth Horm IGF Res* 2012, **22:**42-47.

130. Warrington JP, Csiszar A, Mitschelen M, Lee YW, Sonntag WE. **Whole brain radiation-induced impairments in learning and memory are time-sensitive and reversible by systemic hypoxia.** *PLoS One* 2012, **7:**e30444.

131. Barlind A, Karlsson N, Björk-Eriksson T, Isgaard J, Blomgren K. **Decreased cytogenesis in the granule cell layer of the hippocampus and impaired place learning after irradiation of the young mouse brain evaluated using the IntelliCage platform.** *Exp Brain Res* 2010, **201:**781-787.

132. Hong JH, Chiang CS, Campbell IL, Sun JR, Withers HR, McBride WH. **Induction of acute phase gene expression by brain irradiation.** *Int J Radiat Oncol Biol Phys* 1995, **33:**619-626.

133. Olschowka JA, Kyrkanides S, Harvey BK, O'Banion MK, Williams JP, Rubin P, Hansen JT. **ICAM-1 induction in the mouse CNS following irradiation.** *Brain Behav Immun* 1997, **11:**273-285.

134. Chiang CS, Hong JH, Stalder A, Sun JR, Withers HR, McBride WH. **Delayed molecular responses to brain irradiation.** *Int J Radiat Biol* 1997, **72:**45-53.

135. Kyrkanides S, Moore AH, Olschowka JA, Daeschner JC, Williams JP, Hansen JT, Kerry O'Banion M. **Cyclooxygenase-2 modulates brain inflammation-related gene expression in central nervous system radiation injury.** *Brain Res Mol Brain Res* 2002, **104:**159-169.

136. Gaber MW, Sabek OM, Fukatsu K, Wilcox HG, Kiani MF, Merchant TE. **Differences in ICAM-1 and TNF-α expression between large single fraction and fractionated irradiation in mouse brain.** *Int J Radiat Biol* 2003, **79:**359-366.

137. Moore AH, Olschowka JA, Williams JP, Okunieff P, O'Banion MK. **Regulation of prostaglandin E2 synthesis after brain irradiation.** *Int J Radiat Oncol Biol Phys* 2005, **62:**267-272.

138. Baluna RG, Eng TY, Thomas CR. **Adhesion molecules in radiotherapy.** *Radiat Res* 2006, **166:**819-831.

139. Lee YW, Cho HJ, Lee WH, Sonntag WE. **Whole brain radiation-induced cognitive impairment: Pathophysiological mechanisms and therapeutic targets.** *Biomol. Ther. (Seoul)* 2012, **20:**357-370.

140. Conner KR, Forbes ME, Lee WH, Lee YW, Riddle DR. **AT1 receptor antagonism does not influence early radiation-induced changes in microglial activation or neurogenesis in the normal rat brain.** *Radiat Res* 2011, **176:**71-83.

141. Limoli CL, Giedzinski E, Rola R, Otsuka S, Palmer TD, Fike JR. **Radiation response of neural precursor cells: Linking cellular sensitivity to cell cycle checkpoints, apoptosis and oxidative stress.** *Radiat Res* 2004, **161:**17-27.

142. Collins-Underwood JR, Zhao W, Sharpe JG, Robbins ME. **NADPH oxidase mediates radiation-induced oxidative stress in rat brain microvascular endothelial cells.** *Free Radic Biol Med* 2008, **45:**929-938.

143. Deng Z, Sui G, Rosa PM, Zhao W. **Radiation-Induced c-Jun Activation Depends on MEK1-ERK1/2 Signaling Pathway in Microglial Cells.** *PLoS One* 2012, **7:**e36739.

144. Lee WH, Warrington JP, Sonntag WE, Lee YW. **Irradiation alters MMP-2/TIMP-2 system and collagen type IV degradation in brain.** *Int J Radiat Oncol Biol Phys* 2012, **82:**1559-1566.

145. Wei M, Li H, Huang H, Xu D, Zhi D, Liu D, Zhang Y. **Increased expression of EMMPRIN and VEGF in the rat brain after gamma irradiation.** *J Korean Med Sci* 2012, **27:**291-299.

146. Lee WH, Cho HJ, Sonntag WE, Lee YW. **Radiation attenuates physiological angiogenesis by differential expression of VEGF, Ang-1, tie-2 and Ang-2 in rat brain.** *Radiat Res* 2011, **176:**753-760.

147. Fukuda A, Fukuda H, Jönsson M, Swanpalmer J, Hertzman S, Lannering B, Björk-Eriksson T, Marky I, Blomgren K. **Progenitor cell injury after irradiation to the developing brain can be modulated by mild hypothermia or hyperthermia.** *J Neurochem* 2005, **94:**1604-1619.

148. Acharya MM, Lan ML, Kan VH, Patel NH, Giedzinski E, Tseng BP, Limoli CL. **Consequences of ionizing radiation-induced damage in human neural stem cells.** *Free Radic Biol Med* 2010, **49:**1846-1855.

149. Monje ML, Toda H, Palmer TD. **Inflammatory blockade restores adult hippocampal neurogenesis.** *Science* 2003, **302:**1760-1765.

150. Rola R, Raber J, Rizk A, Otsuka S, VandenBerg SR, Morhardt DR, Fike JR. **Radiation-induced impairment of hippocampal neurogenesis is associated with cognitive deficits in young mice.** *Exp Neurol* 2004, **188:**316-330.

151. Hoffman RM. **To do tissue culture in two or three dimensions? That is the question.** *Stem Cells* 1993, **11:**105-111.

152. Cukierman E, Pankov R, Stevens DR, Yamada KM. **Taking cell-matrix adhesions to the third dimension.** *Science* 2001, **294:**1708-1712.

153. Cukierman E, Pankov R, Yamada KM. **Cell interactions with three-dimensional matrices.** *Curr Opin Cell Biol* 2002, **14:**633-639.

154. Schmeichel KL, Bissell MJ. **Modeling tissue-specific signaling and organ function in three dimensions.** *J Cell Sci* 2003, **116:**2377-2388.

155. Phillips MJ, Otteson DC. **Differential expression of neuronal genes in Müller glia in two- and three-dimensional cultures.** *Invest Ophthalmol Vis Sci* 2011, **52:**1439-1449.

156. O'Connor SM, Stenger DA, Shaffer KM, Maric D, Barker JL, Ma W. **Primary neural precursor cell expansion, differentiation and cytosolic Ca^{2+} response in three-dimensional collagen gel.** *J Neurosci Methods* 2000, **102:**187-195.

157. Myers TA, Nickerson CA, Kaushal D, Ott CM, Höner zu Bentrup K, Ramamurthy R, Nelman-Gonzalez M, Pierson DL, Philipp MT. **Closing the phenotypic gap between transformed neuronal cell lines in culture and untransformed neurons.** *J Neurosci Methods* 2008, **174:**31-41.

158. Hakkinen KM, Harunaga JS, Doyle AD, Yamada KM. **Direct comparisons of the morphology, migration, cell adhesions, and actin cytoskeleton of fibroblasts in four different three-dimensional extracellular matrices.** *Tissue Eng Part A* 2011, **17:**713-724.

159. Gurski LA, Jha AK, Zhang C, Jia X, Farach-Carson MC. **Hyaluronic acid-based hydrogels as 3D matrices for *in vitro* evaluation of chemotherapeutic drugs using poorly adherent prostate cancer cells.** *Biomaterials* 2009, **30:**6076-6085.

160. Naito H, Yoshimura M, Mizuno T, Takasawa S, Tojo T, Taniguchi S. **The advantages of three-dimensional culture in a collagen hydrogel for stem cell differentiation.** *J Biomed Mater Res A* 2013, **101:**2838-2845.

161. Pöttler M, Zierler S, Kerschbaum HH. **An artificial three-dimensional matrix promotes ramification in the microglial cell-line, BV-2.** *Neurosci Lett* 2006, **410:**137-140.

162. Seidlits SK, Khaing ZZ, Petersen RR, Nickels JD, Vanscoy JE, Shear JB, Schmidt CE. **The effects of hyaluronic acid hydrogels with tunable mechanical properties on neural progenitor cell differentiation.** *Biomaterials* 2010, **31:**3930-3940.

163. Sundararaghavan HG, Monteiro GA, Firestein BL, Shreiber DI. **Neurite growth in 3D collagen gels with gradients of mechanical properties.** *Biotechnol Bioeng* 2009, **102:**632-643.

164. Willits RK, Skornia SL. **Effect of collagen gel stiffness on neurite extension.** *J Biomater Sci Polym Ed* 2004, **15:**1521-1531.

165. Banerjee A, Arha M, Choudhary S, Ashton RS, Bhatia SR, Schaffer DV, Kane RS. **The influence of hydrogel modulus on the proliferation and differentiation of encapsulated neural stem cells.** *Biomaterials* 2009, **30:**4695-4699.

166. Balgude AP, Yu X, Szymanski A, Bellamkonda RV. **Agarose gel stiffness determines rate of DRG neurite extension in 3D cultures.** *Biomaterials* 2001, **22:**1077-1084.

167. Wong Po Foo CT, Lee JS, Mulyasasmita W, Parisi-Amon A, Heilshorn SC. **Two-component protein-engineered physical hydrogels for cell encapsulation.** *Proc Natl Acad Sci U S A* 2009, **106:**22067-22072.

168. Luo Y, Shoichet MS. **A photolabile hydrogel for guided three-dimensional cell growth and migration.** *Nat Mater* 2004, **3:**249-253.

169. Blewitt MJ, Willits RK. **The effect of soluble peptide sequences on neurite extension on 2D collagen substrates and within 3D collagen gels.** *Ann Biomed Eng* 2007, **35:**2159-2167.

170. Knight CG, Morton LF, Peachey AR, Tuckwell DS, Farndale RW, Barnes MJ. **The collagen-binding A-domains of integrins $\alpha_1\beta_1$ and $\alpha_2\beta_1$ recognize the same specific amino acid sequence, GFOGER, in native (triple-helical) collagens.** *J Biol Chem* 2000, **275:**35-40.

171. Fang M, Goldstein EL, Matich EK, Orr BG, Holl MM. **Type I collagen self-assembly: The roles of substrate and concentration.** *Langmuir* 2013, **29:**2330-2338.

172. Heino J. **The collagen family members as cell adhesion proteins.** *Bioessays* 2007, **29:**1001-1010.

173. Jokinen J, Dadu E, Nykvist P, Käpylä J, White DJ, Ivaska J, Vehviläinen P, Reunanen H, Larjava H, Häkkinen L, Heino J. **Integrin-mediated cell adhesion to type I collagen fibrils.** *J Biol Chem* 2004, **279:**31956-31963.

174. Kreutzberg GW. **Microglia: A sensor for pathological events in the CNS.** *Trends Neurosci* 1996, **19:**312-318.

175. Ransohoff RM, Perry VH. **Microglial physiology: Unique stimuli, specialized responses.** *Annu Rev Immunol* 2009, **27:**119-145.

176. Kettenmann H, Hanisch UK, Noda M, Verkhratsky A. **Physiology of microglia.** *Physiol Rev* 2011, **91:**461-553.

177. Tremblay MÈ, Stevens B, Sierra A, Wake H, Bessis A, Nimmerjahn A. **The role of microglia in the healthy brain.** *J Neurosci* 2011, **31:**16064-16069.

178. Nimmerjahn A, Kirchhoff F, Helmchen F. **Resting microglial cells are highly dynamic surveillants of brain parenchyma *in vivo*.** *Science* 2005, **308:**1314-1318.

179. Reynolds A, Laurie C, Mosley RL, Gendelman HE. **Oxidative stress and the pathogenesis of neurodegenerative disorders.** *Int Rev Neurobiol* 2007, **82:**297-325.

180. Agostinho P, Cunha RA, Oliveira C. **Neuroinflammation, oxidative stress and the pathogenesis of Alzheimer's disease.** *Curr Pharm Des* 2010, **16:**2766-2778.

181. Luo XG, Ding JQ, Chen SD. **Microglia in the aging brain: Relevance to neurodegeneration.** *Mol Neurodegener* 2010, **5:**12.

182. Liu B, Hong JS. **Role of microglia in inflammation-mediated neurodegenerative diseases: Mechanisms and strategies for therapeutic intervention.** *J Pharmacol Exp Ther* 2003, **304:**1-7.

183. Cernak I, Noble-Haeusslein LJ. **Traumatic brain injury: An overview of pathobiology with emphasis on military populations.** *J Cereb Blood Flow Metab* 2010, **30:**255-266.

184. Wani I, Parray FQ, Sheikh T, Wani RA, Amin A, Gul I, Nazir M. **Spectrum of abdominal organ injury in a primary blast type.** *World J Emerg Surg* 2009, **4:**46.

185. Smith JE. **The epidemiology of blast lung injury during recent military conflicts: A retrospective database review of cases presenting to deployed military hospitals, 2003-2009.** *Philos Trans R Soc Lond B Biol Sci* 2011, **366:**291-294.

186. Morley MG, Nguyen JK, Heier JS, Shingleton BJ, Pasternak JF, Bower KS. **Blast eye injuries: a review for first responders.** *Disaster Med Public Health Prep* 2010, **4:**154-160.

187. Cave KM, Cornish EM, Chandler DW. **Blast injury of the ear: Clinical update from the global war on terror.** *Mil Med* 2007, **172:**726-730.

188. Ruff RL, Ruff SS, Wang XF. **Improving sleep: Initial headache treatment in OIF/OEF veterans with blast-induced mild traumatic brain injury.** *J Rehabil Res Dev* 2009, **46:**1071-1084.

189. Lull ME, Block ML. **Microglial activation and chronic neurodegeneration.** *Neurotherapeutics* 2010, **7:**354-365.

190. Long JB, Bentley TL, Wessner KA, Cerone C, Sweeney S, Bauman RA. **Blast overpressure in rats: Recreating a battlefield injury in the laboratory.** *J Neurotrauma* 2009, **26:**827-840.

191. Bradford MM. **A rapid and sensitive method for the quantitation of microgram quantities of protein utilizing the principle of protein-dye binding.** *Anal Biochem* 1976, **72:**248-254.

192. Ennaceur A, Delacour J. **A new one-trial test for neurobiological studies of memory in rats. 1: Behavioral data.** *Behav Brain Res* 1988, **31:**47-59.

193. Belujon P, Grace AA. **Hippocampus, amygdala, and stress: Interacting systems that affect susceptibility to addiction.** *Ann N Y Acad Sci* 2011, **1216:**114-121.

194. Stetler RA, Gan Y, Zhang W, Liou AK, Gao Y, Cao G, Chen J. **Heat shock proteins: Cellular and molecular mechanisms in the central nervous system.** *Prog Neurobiol* 2010, **92:**184-211.

195. Taber KH, Warden DL, Hurley RA. **Blast-related traumatic brain injury: What is known?** *J Neuropsychiatry Clin Neurosci* 2006, **18:**141-145.

196. Gavett BE, Stern RA, Cantu RC, Nowinski CJ, McKee AC. **Mild traumatic brain injury: A risk factor for neurodegeneration.** *Alzheimers Res Ther* 2010, **2:**18.

197. Terrio H, Brenner LA, Ivins BJ, Cho JM, Helmick K, Schwab K, Scally K, Bretthauer R, Warden D. **Traumatic brain injury screening: Preliminary findings in a US Army Brigade Combat Team.** *J Head Trauma Rehabil* 2009, **24:**14-23.

198. Goldstein LE, Fisher AM, Tagge CA, Zhang XL, Velisek L, Sullivan JA, Upreti C, Kracht JM, Ericsson M, Wojnarowicz MW, Goletiani CJ, Maglakelidze GM, Casey N, Moncaster JA, Minaeva O, Moir RD, Nowinski CJ, Stern RA, Cantu RC, Geiling J, Blusztajn JK, Wolozin BL, Ikezu T, Stein TD, Budson AE, Kowall NW, Chargin D, Sharon A, Saman S, Hall GF, Moss WC, Cleveland RO, Tanzi RE, Stanton PK, McKee AC. **Chronic traumatic encephalopathy in blast-exposed military veterans and a blast neurotrauma mouse model.** *Sci Transl Med* 2012, **4:**134ra160.

199. Kamnaksh A, Kwon SK, Kovesdi E, Ahmed F, Barry ES, Grunberg NE, Long J, Agoston D. **Neurobehavioral, cellular, and molecular consequences of single and multiple mild blast exposure.** *Electrophoresis* 2012, **33:**3680-3692.

200. Kovesdi E, Kamnaksh A, Wingo D, Ahmed F, Grunberg NE, Long JB, Kasper CE, Agoston DV. **Acute minocycline treatment mitigates the symptoms of mild blast-induced traumatic brain injury.** *Front Neurol* 2012, **3:**111.

201. Park E, Eisen R, Kinio A, Baker AJ. **Electrophysiological white matter dysfunction and association with neurobehavioral deficits following low-level primary blast trauma.** *Neurobiol Dis* 2013, **52:**150-159.

202. Tweedie D, Rachmany L, Rubovitch V, Zhang Y, Becker KG, Perez E, Hoffer BJ, Pick CG, Greig NH. **Changes in mouse cognition and hippocampal gene expression observed in a mild physical- and blast-traumatic brain injury.** *Neurobiol Dis* 2013, **54:**1-11.

203. Readnower RD, Chavko M, Adeeb S, Conroy MD, Pauly JR, McCarron RM, Sullivan PG. **Increase in blood-brain barrier permeability, oxidative stress, and activated microglia in a rat model of blast-induced traumatic brain injury.** *J Neurosci Res* 2010, **88:**3530-3539.

204. Wang Y, Wei Y, Oguntayo S, Wilkins W, Arun P, Valiyaveettil M, Song J, Long JB, Nambiar MP. **Tightly coupled repetitive blast-induced traumatic brain injury: Development and characterization in mice.** *J Neurotrauma* 2011, **28:**2171-2183.

205. Agoston DV, Gyorgy A, Eidelman O, Pollard HB. **Proteomic biomarkers for blast neurotrauma: Targeting cerebral edema, inflammation, and neuronal death cascades.** *J Neurotrauma* 2009, **26:**901-911.

206. Svetlov SI, Larner SF, Kirk DR, Atkinson J, Hayes RL, Wang KK. **Biomarkers of blast-induced neurotrauma: Profiling molecular and cellular mechanisms of blast brain injury.** *J Neurotrauma* 2009, **26:**913-921.

207. Ho L, Zhao W, Dams-O'Connor K, Tang CY, Gordon W, Peskind ER, Yemul S, Haroutunian V, Pasinetti GM. **Elevated plasma MCP-1 concentration following traumatic brain injury as a potential "predisposition" factor associated with an increased risk for subsequent development of Alzheimer's disease.** *J Alzheimers Dis* 2012, **31:**301-313.

208. Valiyaveettil M, Alamneh YA, Miller SA, Hammamieh R, Arun P, Wang Y, Wei Y, Oguntayo S, Long JB, Nambiar MP. **Modulation of cholinergic pathways and inflammatory mediators in blast-induced traumatic brain injury.** *Chem Biol Interact* 2012, **203:**371-375.

209. Rhodes JK, Sharkey J, Andrews PJ. **The temporal expression, cellular localization, and inhibition of the chemokines MIP-2 and MCP-1 after traumatic brain injury in the rat.** *J Neurotrauma* 2009, **26:**507-525.

210. Kaur C, Singh J, Lim MK, Ng BL, Yap EP, Ling EA. **The response of neurons and microglia to blast injury in the rat brain.** *Neuropathol Appl Neurobiol* 1995, **21:**369-377.

211. Svetlov SI, Prima V, Glushakova O, Svetlov A, Kirk DR, Gutierrez H, Serebruany VL, Curley KC, Wang KK, Hayes RL. **Neuro-glial and systemic mechanisms of pathological responses in rat models of primary blast overpressure compared to "composite" blast.** *Front Neurol* 2012, **3:**15.

212. do Nascimento AL, Dos Santos NF, Campos Pelágio F, Aparecida Teixeira S, de Moraes Ferrari EA, Langone F. **Neuronal degeneration and gliosis time-course in the mouse hippocampal formation after pilocarpine-induced status epilepticus.** *Brain Res* 2012, **1470:**98-110.

213. Nagamoto-Combs K, Morecraft RJ, Darling WG, Combs CK. **Long-term gliosis and molecular changes in the cervical spinal cord of the rhesus monkey after traumatic brain injury.** *J Neurotrauma* 2010, **27:**565-585.

214. Schofield E, Kersaitis C, Shepherd CE, Kril JJ, Halliday GM. **Severity of gliosis in Pick's disease and frontotemporal lobar degeneration: Tau-positive glia differentiate these disorders.** *Brain* 2003, **126:**827-840.

215. Shapiro LA, Korn MJ, Ribak CE. **Newly generated dentate granule cells from epileptic rats exhibit elongated hilar basal dendrites that align along GFAP-immunolabeled processes.** *Neuroscience* 2005, **136:**823-831.

216. Choi K, Kim J, Kim GW, Choi C. **Oxidative stress-induced necrotic cell death via mitochondira-dependent burst of reactive oxygen species.** *Curr Neurovasc Res* 2009, **6:**213-222.

217. Sofroniew MV. **Reactive astrocytes in neural repair and protection.** *Neuroscientist* 2005, **11:**400-407.

218. Browne TC, McQuillan K, McManus RM, O'Reilly JA, Mills KH, Lynch MA. **IFN-γ production by amyloid β-specific Th1 cells promotes microglial activation and**

increases plaque burden in a mouse model of Alzheimer's disease. *J Immunol* 2013, **190:**2241-2251.

219. Liu Y, Hao W, Letiembre M, Walter S, Kulanga M, Neumann H, Fassbender K. **Suppression of microglial inflammatory activity by myelin phagocytosis: Role of p47-PHOX-mediated generation of reactive oxygen species.** *J Neurosci* 2006, **26:**12904-12913.

220. Takeuchi H, Wang J, Kawanokuchi J, Mitsuma N, Mizuno T, Suzumura A. **Interferon-γ induces microglial-activation-induced cell death: A hypothetical mechanism of relapse and remission in multiple sclerosis.** *Neurobiol Dis* 2006, **22:**33-39.

221. Diaz A, Limon D, Chavez R, Zenteno E, Guevara J. **Aβ25-35 injection into the temporal cortex induces chronic inflammation that contributes to neurodegeneration and spatial memory impairment in rats.** *J Alzheimers Dis* 2012, **30:**505-522.

222. Dinel AL, André C, Aubert A, Ferreira G, Layé S, Castanon N. **Cognitive and emotional alterations are related to hippocampal inflammation in a mouse model of metabolic syndrome.** *PLoS One* 2011, **6:**e24325.

223. Hauss-Wegrzyniak B, Dobrzanski P, Stoehr JD, Wenk GL. **Chronic neuroinflammation in rats reproduces components of the neurobiology of Alzheimer's disease.** *Brain Res* 1998, **780:**294-303.

224. Wang KC, Fan LW, Kaizaki A, Pang Y, Cai Z, Tien LT. **Neonatal lipopolysaccharide exposure induces long-lasting learning impairment, less anxiety-like response and hippocampal injury in adult rats.** *Neuroscience* 2013, **234:**146-157.

225. Zhang J, Zhen YF, Pu-Bu-Ci-Ren., Song LG, Kong WN, Shao TM, Li X, Chai XQ. **Salidroside attenuates beta amyloid-induced cognitive deficits *via* modulating oxidative stress and inflammatory mediators in rat hippocampus.** *Behav Brain Res* 2013, **244:**70-81.

226. Li G, Cheng H, Zhang X, Shang X, Xie H, Zhang X, Yu J, Han J. **Hippocampal neuron loss is correlated with cognitive deficits in SAMP8 mice.** *Neurol Sci* 2013, **34:**963-969.

227. Hicks RR, Smith DH, Lowenstein DH, Saint Marie R, McIntosh TK. **Mild experimental brain injury in the rat induces cognitive deficits associated with regional neuronal loss in the hippocampus.** *J Neurotrauma* 1993, **10:**405-414.

228. Witgen BM, Lifshitz J, Smith ML, Schwarzbach E, Liang SL, Grady MS, Cohen AS. **Regional hippocampal alteration associated with cognitive deficit following experimental brain injury: A systems, network and cellular evaluation.** *Neuroscience* 2005, **133:**1-15.

229. Cechetti F, Pagnussat AS, Worm PV, Elsner VR, Ben J, da Costa MS, Mestriner R, Weis SN, Netto CA. **Chronic brain hypoperfusion causes early glial activation and neuronal death, and subsequent long-term memory impairment.** *Brain Res Bull* 2012, **87:**109-116.

230. Stone HB, Coleman CN, Anscher MS, McBride WH. **Effects of radiation on normal tissue: consequences and mechanisms.** *Lancet Oncol* 2003, **4:**529-536.

231. Béhin A, Delattre JY. **Complications of radiation therapy on the brain and spinal cord.** *Semin Neurol* 2004, **24:**405-417.

232. Greene-Schloesser D, Moore E, Robbins ME. **Molecular pathways: radiation-induced cognitive impairment.** *Clin Cancer Res* 2013, **19:**2294-2300.

233. Warrington JP, Ashpole N, Csiszar A, Lee YW, Ungvari Z, Sonntag WE. **Whole brain radiation-induced vascular cognitive impairment: mechanisms and implications.** *J Vasc Res* 2013, **50:**445-457.

234. Baluchamy S, Zhang Y, Ravichandran P, Ramesh V, Sodipe A, Hall JC, Jejelowo O, Gridley DS, Wu H, Ramesh GT. **Differential oxidative stress gene expression profile in mouse brain after proton exposure.** *In Vitro Cell Dev Biol Anim* 2010, **46:**718-725.

235. Veeraraghavan J, Natarajan M, Herman TS, Aravindan N. **Low-dose γ-radiation-induced oxidative stress response in mouse brain and gut: Regulation by NFκB-MnSOD cross-signaling.** *Mutat Res* 2011, **718:**44-55.

236. Manda K, Ueno M, Anzai K. **Cranial irradiation-induced inhibition of neurogenesis in hippocampal dentate gyrus of adult mice: attenuation by melatonin pretreatment.** *J Pineal Res* 2009, **46:**71-78.

237. Infanger DW, Sharma RV, Davisson RL. **NADPH oxidases of the brain: distribution, regulation, and function.** *Antioxid Redox Signal* 2006, **8:**1583-1596.

238. Qin L, Crews FT. **NADPH oxidase and reactive oxygen species contribute to alcohol-induced microglial activation and neurodegeneration.** *J Neuroinflammation* 2012, **9:**5.

239. Bedard K, Krause KH. **The NOX family of ROS-generating NADPH oxidases: physiology and pathophysiology.** *Physiol Rev* 2007, **87:**245-313.

240. DeAngelis LM, Delattre JY, Posner JB. **Radiation-induced dementia in patients cured of brain metastases.** *Neurology* 1989, **39:**789-796.

241. Roman DD, Sperduto PW. **Neuropsychological effects of cranial radiation: current knowledge and future directions.** *Int J Radiat Oncol Biol Phys* 1995, **31:**983-998.

242. Johannesen TB, Lien HH, Hole KH, Lote K. **Radiological and clinical assessment of long-term brain tumour survivors after radiotherapy.** *Radiother Oncol* 2003, **69:**169-176.

243. Crossen JR, Garwood D, Glatstein E, Neuwelt EA. **Neurobehavioral sequelae of cranial irradiation in adults: a review of radiation-induced encephalopathy.** *J Clin Oncol* 1994, **12:**627-642.

244. Silber JH, Radcliffe J, Peckham V, Perilongo G, Kishnani P, Fridman M, Goldwein JW, Meadows AT. **Whole-brain irradiation and decline in intelligence: the influence of dose and age on IQ score.** *J Clin Oncol* 1992, **10:**1390-1396.

245. Li J, Bentzen SM, Li JL, Renschler M, Mehta MP. **Relationship between neurocognitive function and quality of life after whole-brain radiotherapy in patients with brain metastasis.** *Int J Radiat Oncol Biol Phys* 2008, **71:**64-70.

246. Shi L, Adams MM, Long A, Carter CC, Bennett C, Sonntag WE, Nicolle MM, Robbins M, D'Agostino R, Brunso-Bechtold JK. **Spatial learning and memory deficits after whole-brain irradiation are associated with changes in NMDA receptor subunits in the hippocampus.** *Radiat Res* 2006, **166:**892-899.

247. Brown WR, Thore CR, Moody DM, Robbins ME, Wheeler KT. **Vascular damage after fractionated whole-brain irradiation in rats.** *Radiat Res* 2005, **164:**662-668.

248. Raber J, Rola R, LeFevour A, Morhardt D, Curley J, Mizumatsu S, VandenBerg SR, Fike JR. **Radiation-induced cognitive impairments are associated with changes in indicators of hippocampal neurogenesis.** *Radiat Res* 2004, **162:**39-47.

249. Schnegg CI, Kooshki M, Hsu FC, Sui G, Robbins ME. **PPARδ prevents radiation-induced proinflammatory responses in microglia via transrepression of NF-κB and inhibition of the PKCα/MEK1/2/ERK1/2/AP-1 pathway.** *Free Radic Biol Med* 2012, **52:**1734-1743.

250. Fowler JF. **The linear-quadratic formula and progress in fractionated radiotherapy.** *Br J Radiol* 1989, **62:**679-694.

251. Chiang CS, McBride WH. **Radiation enhances tumor necrosis factor α production by murine brain cells.** *Brain Res* 1991, **566:**265-269.

252. Hwang SY, Jung JS, Kim TH, Lim SJ, Oh ES, Kim JY, Ji KA, Joe EH, Cho KH, Han IO. **Ionizing radiation induces astrocyte gliosis through microglia activation.** *Neurobiol Dis* 2006, **21:**457-467.

253. Schnegg CI, Greene-Schloesser D, Kooshki M, Payne VS, Hsu FC, Robbins ME. **The PPARδ agonist GW0742 inhibits neuroinflammation, but does not restore neurogenesis or prevent early delayed hippocampal-dependent cognitive impairment after whole-brain irradiation.** *Free Radic Biol Med* 2013, **61:**1-9.

254. Monje ML, Mizumatsu S, Fike JR, Palmer TD. **Irradiation induces neural precursor-cell dysfunction.** *Nat Med* 2002, **8:**955-962.

255. Zhao W, Diz DI, Robbins ME. **Oxidative damage pathways in relation to normal tissue injury.** *Br J Radiol* 2007, **80 Spec No 1:**S23-31.

256. Pendyala S, Natarajan V. **Redox regulation of Nox proteins.** *Respir Physiol Neurobiol* 2010, **174:**265-271.

257. Jaquet V, Scapozza L, Clark RA, Krause KH, Lambeth JD. **Small-molecule NOX inhibitors: ROS-generating NADPH oxidases as therapeutic targets.** *Antioxid Redox Signal* 2009, **11:**2535-2552.

258. Serrano F, Kolluri NS, Wientjes FB, Card JP, Klann E. **NADPH oxidase immunoreactivity in the mouse brain.** *Brain Res* 2003, **988:**193-198.

259. Surace MJ, Block ML. **Targeting microglia-mediated neurotoxicity: the potential of NOX2 inhibitors.** *Cell Mol Life Sci* 2012, **69:**2409-2427.

260. Jackman KA, Miller AA, De Silva TM, Crack PJ, Drummond GR, Sobey CG. **Reduction of cerebral infarct volume by apocynin requires pretreatment and is absent in Nox2-deficient mice.** *Br J Pharmacol* 2009, **156:**680-688.

261. Zekry D, Epperson TK, Krause KH. **A role for NOX NADPH oxidases in Alzheimer's disease and other types of dementia?** *IUBMB Life* 2003, **55:**307-313.

262. Green SP, Cairns B, Rae J, Errett-Baroncini C, Hongo JA, Erickson RW, Curnutte JT. **Induction of gp91-phox, a component of the phagocyte NADPH oxidase, in**

microglial cells during central nervous system inflammation. *J Cereb Blood Flow Metab* 2001, **21:**374-384.

263. Qin B, Cartier L, Dubois-Dauphin M, Li B, Serrander L, Krause KH. **A key role for the microglial NADPH oxidase in APP-dependent killing of neurons.** *Neurobiol Aging* 2006, **27:**1577-1587.

264. Drummond GR, Selemidis S, Griendling KK, Sobey CG. **Combating oxidative stress in vascular disease: NADPH oxidases as therapeutic targets.** *Nat Rev Drug Discov* 2011, **10:**453-471.

265. Rola R, Zou Y, Huang TT, Fishman K, Baure J, Rosi S, Milliken H, Limoli CL, Fike JR. **Lack of extracellular superoxide dismutase (EC-SOD) in the microenvironment impacts radiation-induced changes in neurogenesis.** *Free Radic Biol Med* 2007, **42:**1133-1145; discussion 1131-1132.

266. Fishman K, Baure J, Zou Y, Huang TT, Andres-Mach M, Rola R, Suarez T, Acharya M, Limoli CL, Lamborn KR, Fike JR. **Radiation-induced reductions in neurogenesis are ameliorated in mice deficient in CuZnSOD or MnSOD.** *Free Radic Biol Med* 2009, **47:**1459-1467.

267. Cullen DK, Wolf JA, Vernekar VN, Vukasinovic J, LaPlaca MC. **Neural tissue engineering and biohybridized microsystems for neurobiological investigation *in vitro* (Part 1).** *Crit Rev Biomed Eng* 2011, **39:**201-240.

268. Grinnell F. **Fibroblast biology in three-dimensional collagen matrices.** *Trends Cell Biol* 2003, **13:**264-269.

269. Kessler D, Dethlefsen S, Haase I, Plomann M, Hirche F, Krieg T, Eckes B. **Fibroblasts in mechanically stressed collagen lattices assume a "synthetic" phenotype.** *J Biol Chem* 2001, **276:**36575-36585.

270. Semenza GL. **Life with oxygen.** *Science* 2007, **318:**62-64.

271. Stamati K, Mudera V, Cheema U. **Evolution of oxygen utilization in multicellular organisms and implications for cell signalling in tissue engineering.** *J Tissue Eng* 2011, **2:**2041731411432365.

272. Ivanovic Z. **Hypoxia or in situ normoxia: The stem cell paradigm.** *J Cell Physiol* 2009, **219:**271-275.

273. Lewis MC, MacArthur BD, Malda J, Pettet G, Please CP. **Heterogeneous proliferation within engineered cartilaginous tissue: The role of oxygen tension.** *Biotechnol Bioeng* 2005, **91:**607-615.

274. Kellner K, Liebsch G, Klimant I, Wolfbeis OS, Blunk T, Schulz MB, Göpferich A. **Determination of oxygen gradients in engineered tissue using a fluorescent sensor.** *Biotechnol Bioeng* 2002, **80:**73-83.

275. Griffith LG, Swartz MA. **Capturing complex 3D tissue physiology *in vitro*.** *Nat Rev Mol Cell Biol* 2006, **7:**211-224.

276. Cross VL, Zheng Y, Choi NW, Verbridge SS, Sutermaster BA, Bonassar LJ, Fischbach C, Stroock AD. **Dense type I collagen matrices that support cellular remodeling and microfabrication for studies of tumor angiogenesis and vasculogenesis *in vitro*.** *Biomaterials* 2010, **31:**8596-8607.

277. Toborek M, Lee YW, Kaiser S, Hennig B. **Measurement of inflammatory properties of fatty acids in human endothelial cells.** *Methods Enzymol* 2002, **352:**198-219.

278. Cho HJ, Sajja VS, Vandevord PJ, Lee YW. **Blast induces oxidative stress, inflammation, neuronal loss and subsequent short-term memory impairment in rats.** *Neuroscience* 2013, **253:**9-20.

279. Pampaloni F, Reynaud EG, Stelzer EHK. **The third dimension bridges the gap between cell culture and live tissue.** *Nat Rev Mol Cell Biol* 2007, **8:**839-845.

280. Debnath J, Brugge JS. **Modelling glandular epithelial cancers in three-dimensional cultures.** *Nat Rev Cancer* 2005, **5:**675-688.

281. Fischbach C, Chen R, Matsumoto T, Schmelzle T, Brugge JS, Polverini PJ, Mooney DJ. **Engineering tumors with 3D scaffolds.** *Nat Methods* 2007, **4:**855-860.

282. Lee MY, Kumar RA, Sukumaran SM, Hogg MG, Clark DS, Dordick JS. **Three-dimensional cellular microarray for high-throughput toxicology assays.** *Proc Natl Acad Sci U S A* 2008, **105:**59-63.

283. Yoshii Y, Furukawa T, Waki A, Okuyama H, Inoue M, Itoh M, Zhang MR, Wakizaka H, Sogawa C, Kiyono Y, Yoshii H, Fujibayashi Y, Saga T. **High-throughput screening with nanoimprinting 3D culture for efficient drug development by mimicking the tumor environment.** *Biomaterials* 2015, **51:**278-289.

284. Cheema U, Brown RA, Alp B, MacRobert AJ. **Spatially defined oxygen gradients and vascular endothelial growth factor expression in an engineered 3D cell model.** *Cell Mol Life Sci* 2008, **65:**177-186.

285. Cheema U, Rong Z, Kirresh O, MacRobert AJ, Vadgama P, Brown RA. **Oxygen diffusion through collagen scaffolds at defined densities: implications for cell survival in tissue models.** *J Tissue Eng Regen Med* 2012, **6:**77-84.

286. Ardakani AG, Cheema U, Brown RA, Shipley RJ. **Quantifying the correlation between spatially defined oxygen gradients and cell fate in an engineered three-dimensional culture model.** *J R Soc Interface* 2014, **11:**20140501.

287. Streeter I, Cheema U. **Oxygen consumption rate of cells in 3D culture: The use of experiment and simulation to measure kinetic parameters and optimise culture conditions.** *Analyst* 2011, **136:**4013-4019.

288. Shen YI, Abaci HE, Krupsi Y, Weng LC, Burdick JA, Gerecht S. **Hyaluronic acid hydrogel stiffness and oxygen tension affect cancer cell fate and endothelial sprouting.** *Biomater Sci* 2014, **2:**655-665.

289. Verbridge SS, Choi NW, Zheng Y, Brooks DJ, Stroock AD, Fischbach C. **Oxygen-controlled three-dimensional cultures to analyze tumor angiogenesis.** *Tissue Eng Part A* 2010, **16:**2133-2141.

290. Almendros I, Montserrat JM, Torres M, González C, Navajas D, Farré R. **Changes in oxygen partial pressure of brain tissue in an animal model of obstructive apnea.** *Respir Res* 2010, **11:**3.

291. Liu KJ, Bacic G, Hoopes PJ, Jiang J, Du H, Ou LC, Dunn JF, Swartz HM. **Assessment of cerebral pO2 by EPR oximetry in rodents: effects of anesthesia, ischemia, and breathing gas.** *Brain Res* 1995, **685:**91-98.

292. Hou H, Grinberg OY, Taie S, Leichtweis S, Miyake M, Grinberg S, Xie H, Csete M, Swartz HM. **Electron paramagnetic resonance assessment of brain tissue oxygen tension in anesthetized rats.** *Anesth Analg* 2003, **96:**1467-1472, table of contents.

293. Koršič M, Jugović D, Kremžar B. **Intracranial pressure and biochemical indicators of brain damage: follow-up study.** *Croat Med J* 2006, **47:**246-252.

294. Ndubuizu O, LaManna JC. **Brain tissue oxygen concentration measurements.** *Antioxid Redox Signal* 2007, **9:**1207-1219.

295. Carreau A, El Hafny-Rahbi B, Matejuk A, Grillon C, Kieda C. **Why is the partial oxygen pressure of human tissues a crucial parameter? Small molecules and hypoxia.** *J Cell Mol Med* 2011, **15:**1239-1253.

296. Okazaki KM, Maltepe E. **Oxygen, epigenetics and stem cell fate.** *Regen Med* 2006, **1:**71-83.

297. Haw RT, Tong CK, Yew A, Lee HC, Phillips JB, Vidyadaran S. **A three-dimensional collagen construct to model lipopolysaccharide-induced activation of BV2 microglia.** *J Neuroinflammation* 2014, **11:**134.

298. Yamaguchi Y. **Lecticans: Organizers of the brain extracellular matrix.** *Cell Mol Life Sci* 2000, **57:**276-289.